THE EUROPEAN
PHYSICAL JOURNAL C

Regular Article - Experimental Physics

Measurements of the inclusive and differential production cross sections of a top-quark–antiquark pair in association with a Z boson at $\sqrt{s} = 13$ TeV with the ATLAS detector

ATLAS Collaboration⋆

CERN, 1211 Geneva 23, Switzerland

Abstract Measurements of both the inclusive and differential production cross sections of a top-quark–antiquark pair in association with a Z boson ($t\bar{t}Z$) are presented. The measurements are performed by targeting final states with three or four isolated leptons (electrons or muons) and are based on $\sqrt{s} = 13$ TeV proton–proton collision data with an integrated luminosity of 139 fb^{-1}, recorded from 2015 to 2018 with the ATLAS detector at the CERN Large Hadron Collider. The inclusive cross section is measured to be $\sigma_{t\bar{t}Z} = 0.99 \pm 0.05$ (stat.) ± 0.08 (syst.) pb, in agreement with the most precise theoretical predictions. The differential measurements are presented as a function of a number of kinematic variables which probe the kinematics of the $t\bar{t}Z$ system. Both absolute and normalised differential cross-section measurements are performed at particle and parton levels for specific fiducial volumes and are compared with theoretical predictions at different levels of precision, based on a χ^2/ndf and p value computation. Overall, good agreement is observed between the unfolded data and the predictions.

Contents

⋆ e-mail: atlas.publications@cern.ch

1 Introduction

Precise measurements of the properties of the top quark, the heaviest known elementary particle, are an important check of the internal consistency of the Standard Model (SM) of particle physics and could provide hints of possible new physics beyond the SM (BSM). The production cross sections of top-quark–antiquark pairs ($t\bar{t}$), single top quarks, as well as the top-quark mass, have been measured with a great level of precision [1–4]. The large centre-of-mass energy and luminosity of the Large Hadron Collider (LHC) enable precise and differential cross-section measurements for SM processes with small production rates, such as the associated production of a $t\bar{t}$ pair and a Z boson ($t\bar{t}Z$).

The $t\bar{t}Z$ production process is particularly interesting, as it provides direct access to the neutral coupling of the top quark to the electroweak (EW) gauge bosons [5,6]. Deviations of the coupling strength of the top quark to the Z boson (t–Z coupling) from its SM value might imply the existence of new effects in the EW symmetry breaking mechanism which could be probed in the context of effective field theory (EFT) [7]. Various BSM models predict large deviations

🖄 Springer

of the top quark's EW couplings from the SM value, which were probed by the previous generation of lepton colliders [8,9]. Precise measurements of the inclusive and differential cross sections of the $t\bar{t}Z$ process are, thus, of particular interest. Differential cross-section measurements can also offer sensitivity to differences among the predictions from various Monte Carlo (MC) generators and can, therefore, serve as an important input to the tuning of MC parameter values (MC tunes). Furthermore, the $t\bar{t}Z$ process is an irreducible background in several searches for BSM phenomena [10,11], as well as in measurements of important SM processes, such as $t\bar{t}$ production in association with a Higgs boson [12] or single top-quark production in association with a Z boson [13]. The ATLAS Collaboration measured the inclusive $t\bar{t}Z$ cross section using a subset of the LHC Run 2 data, collected in 2015 and 2016 [14] and a first differential measurement of the $t\bar{t}Z$ process was carried out by the CMS Collaboration using the 2016 and 2017 data sets [15].

Theoretical predictions of the $t\bar{t}Z$ cross section exist at next-to-leading order (NLO) with the resummation of soft gluon corrections computed at next-to-next-to-leading-logarithm (NNLL) precision [16,17] in perturbative quantum chromodynamics (QCD) with added EW corrections. Recently they have been matched to the complete set of NLO corrections of both QCD and EW origin [18,19] using the MADGRAPH5_AMC@NLO (MG5_AMC@NLO) framework [20].

This paper presents measurements of the inclusive and differential $t\bar{t}Z$ production cross section in final states with three or four isolated leptons (electrons or muons) with the ATLAS detector [21] at the LHC. The measurements were performed with $\sqrt{s} = 13$ TeV proton–proton (pp) collision data collected during Run 2 of the LHC (2015–2018) and corresponding to an integrated luminosity of 139 fb^{-1}. The Z boson is identified by targeting events featuring an oppositely charged electron (e) or muon (μ) pair. The detector signatures resulting from the hadronisation of final-state quarks from the decay of the $t\bar{t}$ system, in particular those from bottom (anti)quarks, are exploited by constructing target regions with different jet and b-jet multiplicities. The inclusive measurement follows an analysis strategy similar to the previous ATLAS $t\bar{t}Z$ measurement [14]. The production cross section is extracted by performing a simultaneous maximum-likelihood fit in the targeted analysis regions with the signal normalisation as the parameter of interest. In addition, a set of normalised and absolute differential measurements are presented as a function of different variables which probe the SM predictions for the kinematics of the $t\bar{t}Z$ system. Some of these variables are found to be sensitive to potential EFT signals [7], while others are more interesting in the context of MC tuning [22,23]. The differential measurements were performed at both particle and parton level in different fiducial volumes in order to correct for various acceptance effects.

For the first time, the $t\bar{t}Z$ cross section is measured with the full Run 2 data and includes differential measurements performed as functions of variables related to the $t\bar{t}$ system.

This paper is structured as follows. Section 2 provides a brief description of the ATLAS detector. In Sect. 3, the simulation of signal and background processes is discussed, followed by the definitions of the final-state objects at reconstruction, particle and parton levels in Sect. 4. The event selection, both online during data taking and offline after data taking, and the background estimation are discussed in Sects. 5 and 6, respectively. The sources of systematic uncertainties that affect the measurements are discussed in Sect. 7. The result of the inclusive cross-section measurement is presented in Sect. 8. Section 9 describes the differential variables and the unfolding procedure, followed by the results of the differential measurements. Conclusions are drawn in Sect. 10.

2 ATLAS detector

The ATLAS detector [21] at the LHC covers nearly the entire solid angle around the collision point.[1] It consists of an inner tracking detector surrounded by a thin superconducting solenoid, electromagnetic and hadronic calorimeters, and a muon spectrometer incorporating three sets of large superconducting toroidal magnets, each consisting of eight separate coils. The inner-detector system (ID) is immersed in a 2 T axial magnetic field and provides charged-particle tracking in the range $|\eta| < 2.5$.

The high-granularity silicon pixel detector covers the vertex region and typically provides four measurements per track, with the first hit typically being detected in the insertable B-layer (IBL) installed before Run 2 [24,25]. It is followed by the silicon microstrip tracker (SCT), which usually provides eight measurements per track. These silicon detectors are complemented by the transition radiation tracker (TRT), which enables radially extended track reconstruction up to $|\eta| = 2.5$. The TRT also provides electron identification information based on the fraction of hits above a higher energy-deposit threshold corresponding to transition radiation. Typically, around 30 TRT hits are measured in total.

The calorimeter system covers the pseudorapidity range $|\eta| < 4.9$. Within the region $|\eta| < 3.2$, electromag-

---

[1] ATLAS uses a right-handed coordinate system with its origin at the nominal interaction point (IP) in the centre of the detector and the z-axis along the beam pipe. The x-axis points from the IP to the centre of the LHC ring, and the y-axis points upwards. Cylindrical coordinates (r, ϕ) are used in the transverse plane, ϕ being the azimuthal angle around the z-axis. The pseudorapidity is defined in terms of the polar angle θ as $\eta = -\ln\tan(\theta/2)$. Angular distance is measured in units of $\Delta R \equiv \sqrt{(\Delta\eta)^2 + (\Delta\phi)^2}$.

netic calorimetry is provided by barrel and endcap high-granularity lead/liquid-argon (LAr) calorimeters, with an additional thin LAr presampler covering $|\eta| < 1.8$ to correct for energy loss in material upstream of the calorimeters. Hadronic calorimetry is provided by the steel/scintillator-tile calorimeter, segmented into three barrel structures within $|\eta| < 1.7$, and two copper/LAr hadronic endcap calorimeters. The solid angle coverage is extended with forward copper/LAr and tungsten/LAr calorimeter modules optimised for electromagnetic and hadronic measurements respectively.

The muon spectrometer (MS) comprises separate trigger and high-precision tracking chambers measuring the deflection of muons in a magnetic field generated by superconducting air-core toroids. The field integral of the toroids ranges between 2.0 and 6.0 T · m across most of the detector. A set of precision chambers covers the region $|\eta| < 2.7$ with three layers of monitored drift tubes, complemented by cathode-strip chambers in the forward region, where the background rates are highest. The muon trigger system covers the range $|\eta| < 2.4$ with resistive-plate chambers in the barrel, and thin-gap chambers in the endcap regions.

Interesting events are selected to be recorded by the first-level trigger system implemented in custom hardware, followed by selections made by algorithms implemented in software in the high-level trigger [26]. The first-level trigger accepts events from the 40 MHz bunch crossings at a rate below 100 kHz, which the high-level trigger reduces in order to record events to disk at about 1 kHz.

3 Data and simulated event samples

The analysis is performed on data from pp collisions at $\sqrt{s} = 13$ TeV delivered by the LHC and recorded by the ATLAS detector between 2015 and 2018. The bunch spacing for this data-taking period was 25 ns with an average number of pp interactions per bunch crossing ('pile-up') which varies by year and LHC beam conditions and was in the range from 10 to 70 for almost all events. After requirements on the stability of the beams, the operational status of all ATLAS detector components, and the quality of the recorded data, the total integrated luminosity of the data set corresponds to 139 fb^{-1}. This value is derived from the calibration of the luminosity scale using $x-y$ beam-separation scans, following a methodology similar to that detailed in Ref. [27], and using the LUCID-2 detector [28] for the baseline luminosity measurements.

The data were collected using a combination of single-electron and single-muon triggers, with requirements on the identification, isolation, and p_T of the leptons to maintain efficiency across the full momentum range while controlling the trigger rates [26]. For electrons the trigger thresholds were $p_T = 26$, 60 and 140 GeV, whereas for muons, the

thresholds were $p_T = 26$ and 50 GeV.[2] Identification and isolation requirements were applied to the triggers with the lower p_T thresholds [29–31].

Signal and background processes considered in this analysis were modelled using simulated MC samples. The effect of pile-up interactions was modelled by overlaying the hard-scattering event with simulated minimum-bias events generated with PYTHIA 8.186 [32] using the NNPDF 2.3lo set of parton distribution functions (PDFs) [33] and the A3 set of tuned MC parameters [34]. The simulated events were reweighted to match the pile-up conditions observed in the measured data. For processes featuring W boson, Z boson or top-quark production, the W, Z and top-quark masses were set to 80.4 GeV, 91.2 GeV [35] and 172.5 GeV, respectively. The decays of bottom and charm hadrons were simulated using the EVTGEN program [36]. The MC samples were either processed through a full simulation of the ATLAS detector based on GEANT4 [37,38] or a fast simulation (ATLFAST2) relying on parameterised showers in the calorimeter [39,40].

The $t\bar{t}Z$ signal process was modelled using the MG5_AMC@NLO 2.3.3 [41] generator together with EVTGEN 1.2.0, which provided a matrix element (ME) calculation at NLO in the strong coupling constant (α_s) with the NNPDF 3.0nlo [42] PDF set. The functional form of the renormalisation and factorisation scales (μ_r and μ_f) was set to $\mu_{r,f} = 0.5 \times \sum_i \sqrt{m_i^2 + p_{T,i}^2}$, where i runs over all final-state particles generated from the ME calculation. The $t\bar{t}\gamma^*$ contribution and the Z/γ^* interference were included with dilepton invariant masses ($m_{\ell\ell}$) down to 5 GeV. Top-quark decays were simulated at leading order (LO) using MAD-SPIN [43,44] to preserve all spin correlations. The events were interfaced with PYTHIA 8.210 [45] for the parton shower and hadronisation, using the A14 set of tuned parameters [46] and the NNPDF 2.3lo PDF set.

The SM theoretical prediction of the production cross section for the $t\bar{t}Z$ process, including all Z boson decay modes and taking into account the $t\bar{t}\gamma^*$ contribution and the Z/γ^* interference, is $\sigma_{t\bar{t}Z} = 0.88^{+0.09}_{-0.10}$ pb and includes NLO QCD+EW corrections [47]. This value is an off-shell extension of a cross-section calculation of $\sigma_{t\bar{t}Z} = 0.84^{+0.09}_{-0.10}$ pb, which was reported in Ref. [48] (based on Ref. [49]). The uncertainties are due to the QCD scales, the proton PDFs, and α_s.

The measured differential cross sections are compared with theoretical expectations obtained with different generators. Alternative $t\bar{t}Z$ samples were simulated with SHERPA 2.2.1 [50] generator at NLO QCD accuracy, using both inclusive and multi-leg set-ups. In both cases, dynamic

---

[2] Lower p_T thresholds of 24 GeV for electrons and 20 GeV for muons were applied for 2015 data.

μ_r and μ_f scales were used as in the nominal samples. The default SHERPA 2.2.1 parton shower was used together with the NNPDF 3.0nnlo PDF set [42]. The multi-leg sample was simulated using the MEPS@NLO prescription [51–54] with up to one additional parton at NLO and with a merging scale of 30 GeV. Another sample was generated with the same MG5_AMC@NLO and EVTGEN versions as the nominal sample but using a different MC program for the modelling of the parton-shower and hadronisation: HERWIG 7 [55,56] instead of PYTHIA 8. In addition, two alternative samples with the same settings as the nominal sample, but using a set of variations of the A14 tune's parameters (A14 eigentune variation Var3c [46]), were employed to evaluate the uncertainty associated with the amount of initial-state radiation (ISR).

The production of a single top quark or antiquark in association with a Z boson and one extra parton (tZq) was simulated using the MG5_AMC@NLO 2.3.3 generator at NLO QCD with the NNPDF 3.0nnlo PDF set. The events were interfaced with PYTHIA 8.230 using the A14 tune and the NNPDF 2.3lo PDF set. The tZq sample also includes off-shell Z decays to dilepton pairs with invariant masses in the range $m_{\ell\ell} > 30$ GeV. Single top-quark or top-antiquark production in association with both a W and a Z boson (tWZ) was simulated at NLO with MG5_AMC@NLO 2.2.2 and the NNPDF 3.0nnlo PDF set, using PYTHIA 8.235 for the parton-shower simulation. The interference between $t\bar{t}Z$ and tWZ was removed following a diagram removal approach referred to as the DR1 scheme [57].

Events featuring the production of a $t\bar{t}$ pair in association with a W or Higgs boson ($t\bar{t}W$ and $t\bar{t}H$) were generated using NLO QCD MEs in MG5_AMC@NLO 2.3.3 (for $t\bar{t}W$) or 2.6.0 (for $t\bar{t}H$) with the NNPDF 3.0nlo PDF set and showered with PYTHIA 8.210 or 8.230 using the A14 tune. MC samples featuring Higgs production in association with a W or Z boson ($H+W/Z$) were generated at LO with PYTHIA 8.186 using the A14 tune and the NNPDF 2.3lo PDF set.

Diboson processes featuring the production of three charged leptons and one neutrino or four charged leptons (WZ + jets or ZZ + jets, respectively) were simulated using the SHERPA 2.2.2 generator. In this set-up, multiple MEs were matched and merged with the SHERPA parton shower based on the Catani–Seymour dipole factorisation scheme [58,59] using the MEPS@NLO prescription [51–54]. The virtual QCD corrections for MEs at NLO accuracy were provided by the OPENLOOPS library [60,61]. Samples were generated using the NNPDF 3.0nnlo PDF set, along with the dedicated set of tuned parton-shower parameters developed by the SHERPA authors. The WZ/ZZ + jets events with up to one additional parton were simulated at NLO, whereas events with two or three partons were simulated at LO precision.

The production of three or four top quarks ($t\bar{t}t$ and $t\bar{t}t\bar{t}$) and the production of a $t\bar{t}$ pair with two W bosons ($t\bar{t}WW$) were simulated at LO using MG5_AMC@NLO 2.2.2 interfaced to PYTHIA 8.186 with the A14 tune and the NNPDF 2.3lo PDF set. Fully leptonic triboson processes (WWW, WWZ, WZZ and ZZZ) with up to six leptons in the final states were simulated with SHERPA 2.2.2 and the NNPDF 3.0nnlo PDF set. Final states with no additional partons were calculated at NLO, whereas final states with one, two or three additional partons, were calculated at leading order.

4 Object reconstruction

The following subsections describe the definitions of final-state objects at reconstruction (detector), particle, and parton levels, which are used to characterise the final-state event topologies and to define the phase-space regions for the cross-section measurements.

4.1 Reconstruction of detector-level objects

Electron candidates are reconstructed from clusters of energy deposits in the electromagnetic calorimeter that are matched to a track in the ID. They are required to satisfy $p_T > 7$ GeV, $|\eta| < 2.47$ and a 'Medium' likelihood-based identification requirement [62,63]. Electron candidates are excluded if their calorimeter clusters lie within the transition region between the barrel and the endcap of the electromagnetic calorimeter, $1.37 < |\eta| < 1.52$. The track associated with the electron must pass the requirements $|z_0 \sin(\theta)| < 0.5$ mm and $|d_0|/\sigma(d_0) < 5$, where z_0 describes the longitudinal impact parameter relative to the reconstructed primary vertex,[3] d_0 is the transverse impact parameter relative to the beam axis, and $\sigma(d_0)$ is the uncertainty on d_0.

Muon candidates are reconstructed from MS tracks matched to ID tracks in the pseudorapidity range of $|\eta| < 2.5$. They must satisfy $p_T > 7$ GeV along with the 'Medium' identification requirements defined in Refs. [64,65]. This criterion defines requirements on the number of hits in the different ID and MS subsystems and on the significance of the charge-to-momentum ratio q/p. In addition, the track associated with the muon candidate must have $|z_0 \sin(\theta)| < 0.5$ mm and $|d_0|/\sigma(d_0) < 3$.

Isolation criteria are applied to the selected electrons and muons. For electrons, the scalar sum of the p_T of tracks within a variable-size cone around the electron, excluding tracks originating from the electron itself, must be less than 6% of the electron p_T. The track isolation cone radius

---

[3] The primary vertex is defined as the vertex with the highest scalar sum of the squared transverse momenta of associated tracks with $p_T > 400$ MeV.

$\Delta R = \sqrt{(\Delta\eta)^2 + (\Delta\phi)^2}$ is given by the smaller of $\Delta R = 10\,\text{GeV}/p_\text{T}$ and $\Delta R = 0.2$. In addition, the sum of the transverse energy of the calorimeter topo-clusters[4] in a cone of $\Delta R = 0.2$ around the electron is required to be less than 6% of the electron p_T, excluding clusters originating from the electron itself. For muons, the scalar sum of the p_T of tracks within a variable-size cone around the muon, excluding its own track, must be less than 6% of the muon p_T, with the track isolation cone radius being given by the minimum of $\Delta R = 10\,\text{GeV}/p_\text{T}$ and $\Delta R = 0.3$.

Jets are reconstructed from topo-clusters, using the anti-k_t jet clustering algorithm [67] as implemented in the FAST-JET package [68], with a radius parameter of $R = 0.4$. They are calibrated through the application of a jet energy scale derived from 13 TeV data and simulation [69]. Only jet candidates with $p_\text{T} > 25\,\text{GeV}$ and $|\eta| < 2.5$ are considered in this analysis. To mitigate the impact of jets arising from additional pp collisions in a given bunch crossing, an additional selection criterion using a likelihood-based 'jet-vertex-tagging' (JVT) discriminant is applied to jets with $p_\text{T} < 120\,\text{GeV}$ and $|\eta| < 2.5$ [70].

Jets containing b-hadrons ('b-jets') are identified (tagged) by the MV2c10 b-tagging algorithm [71]. The algorithm uses a multivariate discriminant with quantities such as the impact parameters of associated tracks, and well-reconstructed secondary vertices. For the differential measurements, a selection that provides an 85% efficiency for identifying b-jets in simulated $t\bar{t}$ events, with rejection factors against light-flavour jets and c-jets of 28 and 2, respectively is used. Different calibrated b-tagging working points (WPs), corresponding to different b-jet selection efficiencies are used for the inclusive cross-section measurement. A method where exclusive bins in the b-tagging discriminant corresponding to different identification efficiencies is employed. In the following, this approach is referred to as pseudo-continuous b-tagging (PCBT).

Scale factors are applied as weights to MC events to correct for the mismodelling of efficiencies associated with the reconstruction, identification and trigger selection of electrons and muons, as well as the JVT and b-tagging requirements for jets. The b-tagging scale factors are derived from a pseudo-continuous calibration as outlined above.

The missing transverse momentum is defined as the negative vector sum of the transverse momenta of all selected and calibrated physics objects (electrons, photons, muons and jets). Low-momentum tracks from the primary vertex that are not associated with any of the reconstructed physics objects described previously are also included as a 'soft term' in the calculation [72]. The magnitude of the missing transverse momentum vector is denoted as E_T^miss.

Ambiguities can arise from the independent reconstruction of electron, muon and jet candidates in the detector. A sequential procedure (overlap removal) is applied to resolve these ambiguities and, thus, avoids a double counting of physics objects.[5] It is applied as follows. If an electron candidate and a and muon candidate share a track, the electron candidate is removed. Jet candidates within a distance of $\Delta R_{y,\phi} = \sqrt{(\Delta y)^2 + (\Delta\phi)^2} = 0.2$ from a remaining electron candidate are discarded. If multiple jets are found in this area, only the closest jet is removed. If the electron-jet distance is between 0.2 and 0.4, the electron candidate is removed. If the $\Delta R_{y,\phi}$ between any remaining jet and a muon candidate is less than 0.4, the muon candidate is removed if the jet has more than two associated tracks, otherwise the jet is discarded.

4.2 Particle- and parton-level objects and definitions of fiducial regions

In the measurements of differential $t\bar{t}Z$ cross sections, the measured spectra are corrected for detector effects to so-called particle and parton levels using an unfolding procedure.

Parton-level objects were obtained from the MC record of the $t\bar{t}Z$ event. The top quarks (antiquarks) and Z bosons were selected after final-state radiation and just before their corresponding decay, $t \to Wb$ or $Z \to \ell\ell$, respectively. The leptons originating from W and Z bosons were selected directly from the decay vertex of the parent bosons.

The parton-level fiducial volumes for final states with three or four leptons were defined as follows: the Z boson was required to decay into leptons, whereas the $t\bar{t}$ pair was required to decay via $t\bar{t} \to W^+bW^-\bar{b}$, with either one or both W bosons subsequently decaying leptonically.

The particular decay chains of interest are therefore:

$$Z \to \ell^+\ell^-,\ \ t \to W^+(\to \ell^+\nu_\ell) + b,\ \ \bar{t} \to W^-(\to q\bar{q}) + \bar{b}$$
$$\text{or}\ \ Z \to \ell^+\ell^-,\ \ t \to W^+(\to q\bar{q}) + b,\ \ \ \bar{t} \to W^-(\to \ell^-\bar{\nu}_\ell) + \bar{b}$$

for a three-lepton final state, and

$$Z \to \ell^+\ell^-,\ \ t \to W^+(\to \ell^+\nu_\ell) + b,\ \ \bar{t} \to W^-(\to \ell^-\bar{\nu}_\ell) + \bar{b}$$

---

[4] Topo-clusters are constructed from calorimeter cells that are combined using a topological clustering algorithm [66]. These objects provide a three-dimensional representation of energy depositions in the calorimeter and implement a nearest-neighbour noise suppression algorithm. The resulting clusters are classified as either electromagnetic or hadronic based on their shape, depth and energy density. Energy corrections are applied to the topo-clusters in order to calibrate them to the appropriate energy scale for their classification.

[5] The lepton candidates considered for the overlap removed are electrons selected with the 'Loose' identification [62,63] and muons selected with the 'Medium' identification requirement, but before placing isolation requirements on the leptons.

for a four-lepton final state. The two decay chains for the three-lepton final state differ only in terms of which of the top quark or antiquark decayed hadronically.

The invariant mass of the lepton pair originating from the Z boson has to be within a range of ± 15 GeV around the nominal Z boson mass (91.2 GeV) [35] to be sensitive to on-shell Z decays. Prompt τ-leptons from Z or W boson decays were not included in the parton-level fiducial volume, regardless of their subsequent decay into leptons or hadrons. No kinematic requirements were applied to the parton-level objects in order that the unfolded differential results at parton level can be more easily compared with fixed-order predictions.

Particle-level objects in simulated events were defined using quasi-stable particles with a mean lifetime greater than 30 ps originating from pp collisions. They were selected after hadronisation but before the interaction of these particles with the detector components or consideration of pile-up effects. Electrons and muons were required to not to have originated from a hadron in the MC generator event record, whether directly or through a τ-lepton decay. This ensures that they originated from the Z boson or the W bosons from top-quark decays, without requiring a direct match with the parent boson. The four-momenta of the bare leptons were modified ('dressed') by adding the four-momenta of all radiated photons within a cone of size $\Delta R = 0.1$, excluding photons from hadron decays, to take into account final-state photon radiation. Particle-level jets were reconstructed with the anti-k_t algorithm with a radius parameter of $R = 0.4$ applied to all stable particles, but excluding both the neutrinos originating from the Z boson or top quarks and the selected electrons, muons and photons used in the definition of the charged leptons. If b-hadrons with $p_T > 5$ GeV were found in the MC event record, they were clustered in the stable-particle jets with their energies set to a negligible positive value ('ghost-matching') [73]. Particle-level jets containing one or more of these b-hadrons were considered to originate from a b-quark. The particle-level missing transverse momentum was defined as the vector sum of the transverse momenta of all neutrinos found in the simulation history of the event, excluding those originating from hadron decay.

The particle-level fiducial volume for final states with three or four leptons was defined by applying the same p_T and $|\eta|$ requirements as those summarised for the detector-level selection in Tables 1 and 2, respectively. In addition, the same requirements were placed on the number of jets and b-jets, and the same requirements were placed on the opposite-sign–same-flavour (OSSF) lepton pair, along with the same invariant mass requirement for the Z-mass window as that used in the detector-level selection described in the

following section ($|m_{\ell\ell} - m_Z| < 10$ GeV).[6] For the particle-level fiducial volume for four-lepton final states, only one OSSF lepton pair was required within the Z-mass window – the remaining lepton pair was required only to be opposite-sign. Only one of the jets is required to have originated from a b-quark.

5 Event selection and signal regions

Only final states with exactly three or four isolated leptons (electrons or muons) and at least two jets, as defined in Sect. 4, are considered. All selected events are required to pass a single-electron or single-muon trigger. In addition, at least one reconstructed lepton with $p_T > 27$ GeV is required to be matched to the lepton reconstructed by the trigger algorithm and to be of the same flavour. Different signal regions are defined and optimised to achieve the best sensitivity to $t\bar{t}Z$ production with one or both top quarks decaying via $t \to bW \to b\ell\nu_\ell$. Furthermore, the regions are designed to contain a sufficient number of signal events in order to reduce the statistical uncertainties of the differential $t\bar{t}Z$ cross-section measurements. The signal regions are referred to as 'trilepton' (3ℓ) and 'tetralepton' (4ℓ) signal regions, depending on the number of reconstructed leptons, and are meant to target events with one or two prompt leptons, respectively from the $t\bar{t}$ decay.

5.1 Trilepton signal regions

A summary of the definitions of the trilepton signal regions is provided in Table 1. The requirement on the minimum transverse momentum of the leading, sub-leading and third lepton is 27, 20 and 20 GeV, respectively. The sum of the three lepton charges is required to be ± 1. The OSSF lepton pair with the invariant mass closest to the Z boson mass is considered to originate from the Z decay and its invariant mass (labelled as $m_{\ell\ell}^Z$) is required to be compatible with the mass of the Z boson ($|m_{\ell\ell}^Z - m_Z| < 10$ GeV). Furthermore, all OSSF lepton combinations are required to have $m_{OSSF} > 10$ GeV to remove contributions arising from low-mass resonances. Additional requirements are imposed on the total number of reconstructed jets (N_{jets}) and b-tagged jets ($N_{b\text{-jets}}$) in the event.

Different b-jet requirements are used for the inclusive and differential cross-section measurements. For the inclusive measurement, a combination of two orthogonal regions

---

[6] It should be noted that this invariant mass requirement is more stringent than the on-shell Z requirement used in defining the parton-level fiducial volumes in Sect. 4.2 and provides better background rejection. The requirement was therefore tightened for the detector-level selection, and the same range was then adopted for the particle-level definitions.

Table 1 The definitions of the trilepton signal regions: for the inclusive measurement, a combination of the regions with pseudo-continuous b-tagging 3ℓ-Z-$1b4j$-PCBT and 3ℓ-Z-$2b3j$-PCBT is used, whereas for the differential measurement only the region 3ℓ-Z-$2b3j$ with a fixed b-tagging WP is employed

Variable	3ℓ-Z-$1b4j$-PCBT inclusive	3ℓ-Z-$2b3j$-PCBT inclusive	3ℓ-Z-$2b3j$ differential
N_ℓ ($\ell = e, \mu$)	$= 3$		
	≥ 1 OSSF lepton pair with $\|m_{\ell\ell}^Z - m_Z\| < 10\,\text{GeV}$		
	for all OSSF combinations: $m_{\text{OSSF}} > 10\,\text{GeV}$		
p_T (ℓ_1, ℓ_2, ℓ_3)	$> 27, 20, 20\,\text{GeV}$		
N_{jets}	≥ 4	≥ 3	≥ 3
$N_{b\text{-jets}}$	$= 1@60\%$	$\geq 2@70\%$	$\geq 2@85\%$
	veto add. b-jets@70%		

Table 2 The definitions of the four tetralepton signal regions. The regions are defined to target different b-jet multiplicities and flavour combinations of the non-Z leptons ($\ell\ell^{\,\text{non-}Z}$)

Variable	4ℓ-SF-$1b$	4ℓ-SF-$2b$	4ℓ-DF-$1b$	4ℓ-DF-$2b$
$N_\ell(\ell = e, \mu)$	$= 4$			
	≥ 1 OSSF lepton pair with $\|m_{\ell\ell}^Z - m_Z\| < 10\,\text{GeV}$			
	for all OSSF combinations: $m_{\text{OSSF}} > 10\,\text{GeV}$			
p_T ($\ell_1, \ell_2, \ell_3, \ell_4$)	$> 27, 20, 10, 7\,\text{GeV}$			
$\ell\ell^{\,\text{non-}Z}$	e^+e^- or $\mu^+\mu^-$	e^+e^- or $\mu^+\mu^-$	$e^\pm \mu^\mp$	$e^\pm \mu^\mp$
E_T^{miss}	$> 100\,\text{GeV}$, if $\|m_{\ell\ell}^{\text{non-}Z} - m_Z\| \leq 10\,\text{GeV}$	$> 50\,\text{GeV}$, if $\|m_{\ell\ell}^{\text{non-}Z} - m_Z\| \leq 10\,\text{GeV}$	–	–
	$> 50\,\text{GeV}$, if $\|m_{\ell\ell}^{\text{non-}Z} - m_Z\| > 10\,\text{GeV}$	–		
N_{jets}	≥ 2	≥ 2	≥ 2	≥ 2
$N_{b\text{-jets}}$ @85%	$= 1$	≥ 2	$= 1$	≥ 2

which use different b-tagging WPs (PCBT, see Sect. 4) with 60% and 70% efficiency is employed. The tighter b-tagging WPs are used to suppress the WZ + jets background and reduce its impact on the overall precision of the measurement. The two regions, referred to as 3ℓ-Z-$1b4j$-PCBT and 3ℓ-Z-$2b3j$-PCBT, are kept distinct from one another during the fitting procedure used to perform the cross-section measurement. For the differential measurements, a looser, fixed WP corresponding to an 85% efficiency is used in order to increase the data statistics.

5.2 Tetralepton signal regions

The definitions of the tetralepton signal regions are summarised in Table 2. The requirement on the transverse momentum of the four leading leptons in all regions is 27, 20, 10 and 7 GeV, respectively. As in the case of the trilepton signal regions, all events are required to have at least one OSSF lepton pair with an invariant mass satisfying $\|m_{\ell\ell}^Z - m_Z\| < 10\,\text{GeV}$. Furthermore, the remaining leptons which are not associated with the Z boson (non-

Z) are required to have opposite charges, such that the sum of the four lepton charges is zero. As in the trilepton selection, a requirement that all OSSF lepton combinations satisfy $m_{\text{OSSF}} > 10\,\text{GeV}$ in order to suppress background contributions from low-mass resonances is applied.

The tetralepton signal regions are separated into different-flavour (DF) and same-flavour (SF) signal regions, according to the b-jet multiplicities and the flavour composition of the non-Z lepton pair. The ZZ + jets background is suppressed by setting requirements on the jet and b-jet multiplicities, as well as by applying cuts on E_T^{miss} and the invariant mass of the non-Z lepton pair ($m_{\ell\ell}^{\text{non-}Z}$) in the case of the SF regions. In the SF regions, events with $m_{\ell\ell}^{\text{non-}Z}$ close to the Z mass are accepted, but the E_T^{miss} requirement is increased to reduce the ZZ + jets background. If $m_{\ell\ell}^{\text{non-}Z}$ is not close to the Z mass, the E_T^{miss} cut is relaxed. For the inclusive cross-section measurement, the four tetralepton regions are included as separate bins in the fit, whereas for the differential measurements all the events are combined. Unlike the trilepton signal regions, the b-jets are all selected using a fixed 85% b-tagging efficiency WP. The tetralepton signal region selections are identical for the inclusive and differential measurements.

Table 3 Definitions of the control regions targeting the $WZ + $ jets, $WZ \to \ell\ell\ell\nu$ (left) and $ZZ + $ jets, $ZZ \to \ell\ell\ell\ell$ processes (right): the control regions are used to obtain normalisations of the light-flavour components of the $WZ/ZZ +$ jets backgrounds from data

Variable	3ℓ-WZ-CR	4ℓ-ZZ-CR
N_ℓ ($\ell = e, \mu$)	$= 3$	$= 4$
	1 OSSF lepton pair with	2 OSSF lepton pairs with
	$\|m_{\ell\ell} - m_Z\| < 10\,\text{GeV}$	$\|m_{\ell\ell} - m_Z\| < 10\,\text{GeV}$
p_T ($\ell_1, \ell_2, \ell_3, \ell_4$)	$> 27, 20, 20\,\text{GeV}$	$> 27, 20, 10, 7\,\text{GeV}$
N_jets	≥ 3	–
$N_{b\text{-jets}}$@85%	$= 0$	–
E_T^miss	–	$20\,\text{GeV} < E_\text{T}^\text{miss} < 40\,\text{GeV}$

6 Background estimation

Several processes can lead to background contaminations in the signal regions. The contributions from SM processes featuring the production of three or four prompt leptons[7] is discussed in Sect. 6.1, whereas the estimation of processes where at least one of the reconstructed leptons is a fake lepton is explained in Sect. 6.2.

6.1 Prompt lepton background

The dominant SM background processes in the trilepton and tetralepton regions are $WZ/ZZ +$ jets production with $WZ \to \ell\ell\ell\nu$ and $ZZ \to \ell\ell\ell\ell$ decays, respectively. The normalisations of these processes are obtained from data and measured in dedicated $WZ +$ jets and $ZZ +$ jets control regions (CRs) as defined in Table 3. The CRs are common to both the inclusive and the differential cross-section measurements. Invariant mass requirements on the OSSF lepton pairs are applied to select the Z bosons expected in both regions. A b-jet veto is applied in 3ℓ-WZ-CR to suppress the $t\bar{t}Z$ contribution and to ensure orthogonality with the trilepton signal region. In 4ℓ-ZZ-CR, no requirements are placed on the number of jets or b-jets. The invariant mass requirements on the two OSSF lepton pairs are sufficient to yield a very high $ZZ +$ jets purity in this region. Orthogonality with the tetralepton signal regions is ensured through the use of an E_T^miss requirement ($20\,\text{GeV} < E_\text{T}^\text{miss} < 40\,\text{GeV}$), where the lower bound is set so that the selected events are more similar kinematically to those in the signal regions. The $WZ +$ jets purity in 3ℓ-WZ-CR is approximately 80%, while the $ZZ +$ jets purity in 4ℓ-ZZ-CR is approximately 97%.

The event yields in these control regions are extrapolated to the signal regions in accord with simulation. As the control regions are mostly populated by WZ/ZZ plus light-flavour jet events, only the predictions from these light-flavour components in the signal regions are constrained by the observed data yields in the control regions. The $WZ/ZZ + b$- and c-jet[8] backgrounds are constrained to their MC predictions, but with additional normalisation uncertainties assigned (more details are provided in Sect. 7.3). Figure 1a and b show, respectively, the p_T and η distributions of the leading lepton for the $WZ +$ jets control region. The p_T distribution and the number of selected jets in the $ZZ +$ jets control region are shown in Fig. 2a and b. All distributions in the control regions are shown before the simultaneous fit to data is applied (pre-fit).

Another important background in the signal regions is tWZ production, which can lead to final states very similar to those of the $t\bar{t}Z$ signal. A relevant background process in the trilepton regions is tZq production, which contributes more for lower jet multiplicities. Other background processes, such as $t\bar{t} + W/H$, $t\bar{t}WW$, three/four top-quark production, $H + W/Z$ or triboson production can also contribute to the signal regions, but are significantly smaller than the other processes mentioned above.

The MC samples used to simulate these processes are described in Sect. 3. Besides the WZ/ZZ plus light-flavour jets background, for which control regions are employed to obtain the normalisation, the contributions from all SM processes leading to three or four prompt leptons are estimated entirely from MC simulation and normalised to their theoretical cross-section predictions.

6.2 Fake lepton background

Different types of objects, which are misidentified as leptons, are referred to as 'fake leptons' throughout the rest of the document. In the signal regions of this analysis, this background arises mainly from dileptonic $t\bar{t}$ decays where additional non-prompt leptons arise from heavy-flavour hadron decays.

To estimate the contribution of fake leptons in the signal regions, a fully data-driven method, called the 'matrix

---

[7] The term 'prompt' refers to leptons which are directly produced by the hard-scatter process or by the decays of heavy resonances such as W, Z or Higgs bosons.

[8] These backgrounds are defined by separating $WZ/ZZ +$ jets events into light-flavour jet, b-jet and c-jet components, depending on whether a b- or c-hadron is found in the MC event record of any of the selected jets.

(a)

(b)
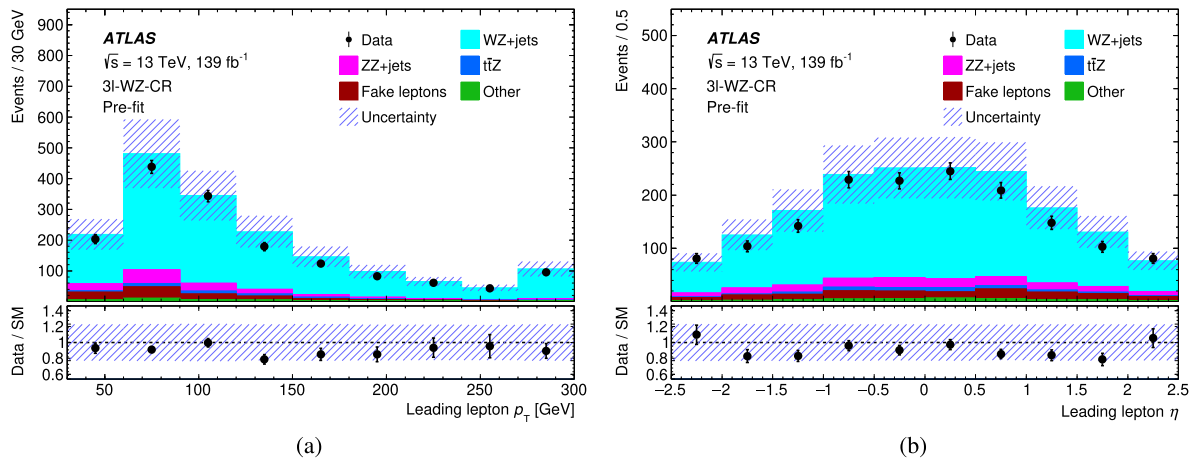
Fig. 1 Distribution of the **a** p_T and **b** η of the leading lepton in the $WZ + $ jets control region. The shaded band corresponds to the total uncertainty (systematic and statistical) of the total SM prediction. The lower panel shows the ratio of the data to the SM prediction. The results

and uncertainties are shown before the fit to data is performed. The category 'other' contains all processes mentioned in Sect. 3 which are not listed separately. Events with a leading lepton p_T above 300 GeV are included in the uppermost bin of **a**

(a)

(b)
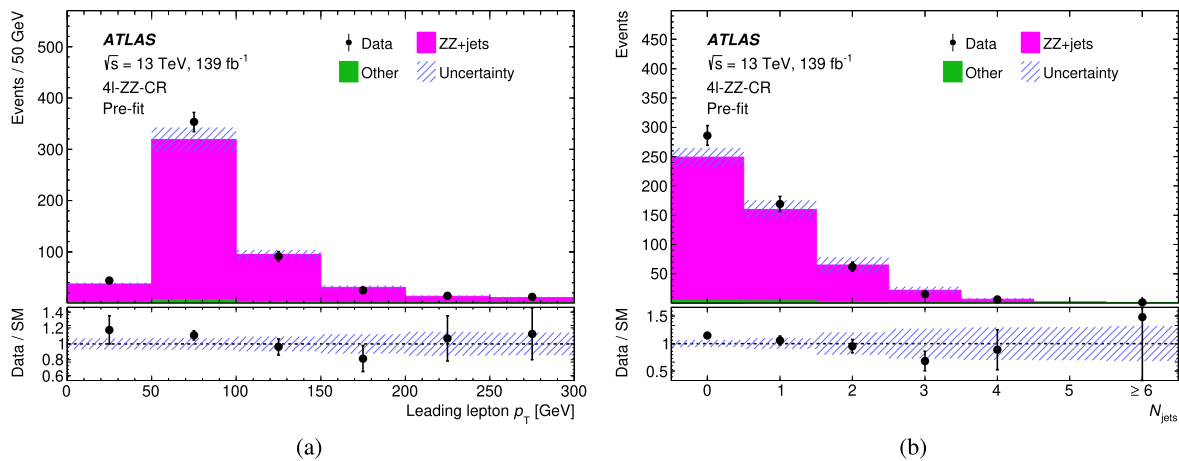
Fig. 2 Distribution of **a** the p_T of the leading lepton and **b** the number of selected jets in the $ZZ + $ jets control region. The shaded band corresponds to the total uncertainty (systematic and statistical) of the total SM prediction. The lower panel shows the ratio of the data to the SM

prediction. The results and uncertainties are shown before the fit to data is performed. The category 'other' contains all processes mentioned in Sect. 3 which are not listed separately. Events with a leading lepton p_T above 300 GeV are included in the uppermost bin of **a**

method' is employed. Descriptions of this technique can be found in Refs. [74,75]. It relies on the prompt and fake leptons having different probabilities of passing the identification, isolation and impact parameters requirements. The method uses data events selected with the same criteria as in the signal regions, but with looser lepton selections[9] than the ones defined in Sect. 4.

An alternative version of the matrix method is described in Ref. [76]. It evaluates the total number of fake electrons and muons entering the signal regions via the maximisation of a likelihood function. The likelihood function is constructed from a product of Poisson probability functions that represent the numbers of leptons passing different quality criteria for the signal regions. The observed number of leptons selected with the looser criteria and the probabilities (efficiencies) for fake or prompt leptons to satisfy the nominal lepton requirements are fixed, while the expectation values of the Poisson functions – the numbers of fake leptons in the signal regions – are obtained from the likelihood maximisa-

---

[9] Whereas 'Medium' electrons are used for the nominal selection, the identification WP is relaxed to 'LooseAndBLayerLH' [62] for the looser electron selection. No isolation requirements are applied for electrons and muons in the looser selection.

Table 4 The observed and expected numbers of events in the trilepton and tetralepton signal regions, as well as in the WZ/ZZ + jets control regions. The predictions are shown before the fit to data. The WZ and ZZ + jets backgrounds are listed separately for their light-flavour (l), b-jet and c-jet components. The category 'fake leptons' refers to the contributions from fake and non-prompt leptons. 'Other' includes the contributions from $H+W/Z$, $t\bar{t}WW$, three/four top-quark production and triboson processes. Background categories with event yields shown as '–' do not contribute significantly to a region. The indicated uncertainties consider statistical errors as well as all experimental and theoretical systematic uncertainties, except the normalisation uncertainties of the fitted background components

Region	3ℓ-Z-$1b4j$-PCBT	3ℓ-Z-$2b3j$-PCBT	4ℓ-SF-$1b$	4ℓ-SF-$2b$	4ℓ-DF-$1b$	4ℓ-DF-$2b$	3ℓ-WZ-CR	4ℓ-ZZ-CR
$t\bar{t}Z$	164 ± 14	210 ± 9	13.0 ± 1.6	23.3 ± 1.8	16.8 ± 1.4	22.5 ± 1.0	44 ± 11	0.7 ± 0.1
$WZ + l$	3.1 ± 2.3	0.3 ± 0.3	–	–	–	–	1160 ± 370	–
$WZ + b$	30 ± 18	16.0 ± 9.4	–	–	–	–	17 ± 10	–
$WZ + c$	12.5 ± 5.9	2.1 ± 1.0	–	–	–	–	230 ± 100	–
$ZZ + l$	0.3 ± 0.2	0.03 ± 0.03	1.8 ± 0.9	1.0 ± 0.5	0.5 ± 0.2	0.02 ± 0.01	116 ± 17	461 ± 37
$ZZ + b$	3.5 ± 1.8	2.2 ± 1.1	1.1 ± 0.7	2.8 ± 1.7	0.2 ± 0.1	0.08 ± 0.05	2.0 ± 1.0	14.3 ± 7.6
$ZZ + c$	0.8 ± 0.3	0.2 ± 0.1	1.0 ± 0.5	1.2 ± 0.6	0.2 ± 0.1	0.02 ± 0.01	13.7 ± 4.4	20.7 ± 7.5
tWZ	23.7 ± 4.2	19.3 ± 7.1	2.7 ± 0.5	2.0 ± 0.8	3.6 ± 1.1	2.1 ± 0.9	13.3 ± 1.2	0.2 ± 0.1
tZq	11.7 ± 5.0	29.3 ± 9.3	–	–	–	–	9.1 ± 3.5	–
$t\bar{t}+W/H$	5.8 ± 0.9	10.1 ± 2.2	0.5 ± 0.1	0.9 ± 0.1	0.6 ± 0.1	0.8 ± 0.1	1.8 ± 0.4	0.01 ± 0.01
Fake leptons	30 ± 15	14.6 ± 7.4	0.7 ± 0.6	0.9 ± 0.8	0.9 ± 0.8	0.3 ± 0.3	86 ± 43	7.7 ± 3.6
Other	0.7 ± 0.4	1.5 ± 0.7	0.7 ± 0.3	0.3 ± 0.1	0.7 ± 0.4	0.2 ± 0.1	12.4 ± 6.4	0.9 ± 0.6
SM total	286 ± 31	306 ± 21	21.3 ± 2.3	32.4 ± 3.0	23.4 ± 2.0	26.0 ± 1.5	1710 ± 390	505 ± 39
Data	272	343	19	33	33	32	1569	539

tion. This method offers a more robust fake-lepton estimation for statistically limited regions. For the differential measurements, the estimations are performed separately for each bin of the measured variables.

The probabilities of fake leptons to satisfy the nominal lepton requirements (fake-lepton efficiencies) are obtained from data. They are measured separately for electrons and muons in events with exactly two leptons with the same charge (same-sign) and at least one b-jet identified at the 85% efficiency WP. The measurements are performed after subtracting the contributions, estimated from MC events, of charge-misidentified electrons and prompt leptons in the same-sign region. It has been checked that the dominant fake lepton source in this region are heavy-flavour hadron decays, as in the signal regions. The fake-lepton efficiencies are approximately 10% for electrons and 15% for muons, with an increase to around 20% for muons with $p_T < 12$ GeV and > 35 GeV. The equivalent probabilities for prompt leptons (prompt-lepton efficiencies) are obtained from $Z \to \ell\ell$ simulation and the respective scale factors for electrons or muons. The prompt-lepton efficiencies are in most cases higher than 90% for both the electrons and muons. They increase for larger lepton p_T values and reach > 98 % for $p_T > 35$ GeV. Both the fake- and prompt-lepton efficiencies are parameterised as a function of p_T and $|\eta|$ of the respective lepton.

Systematic uncertainties are assigned to the fake-lepton estimates to account for differences in the relative contributions of the various fake-lepton sources between the signal regions and the regions used for the efficiency measurements. Further uncertainties arise from the subtraction of prompt and charge-misidentified leptons, as well as from the dependencies of the fake-lepton efficiencies on the number of jets/b-jets in the events. The method is also affected by statistical uncertainties arising from the limited number of events in the data sample used to evaluate the fake-lepton yields, as well as the statistical limitations of the efficiency measurements. Similarly to the nominal values, the uncertainties of the fake- and prompt-lepton efficiencies are binned in p_T and $|\eta|$ of the leptons and propagated to the fake-lepton estimation in the signal regions. The overall uncertainties are approximately 50% for both electrons and muons, but they can fluctuate for the differential measurements, depending on the variable and the kinematic region.

6.3 Pre-fit event yields in signal and control regions

To validate the SM background modelling explained in the previous sections, Table 4 presents a comparison between the total expected background prediction and the observed data events in the trilepton and tetralepton signal regions, as well as in the WZ + jets and ZZ + jets control regions. The event yields and uncertainties are shown before applying the fitting procedure. The statistical and all systematic uncertainties as explained in Sect. 7 are considered except the normalisation uncertainties of the processes which are free parameters in the fit. Within the uncertainties, agreement between data and the SM predictions is observed in nearly all regions.

7 Systematic uncertainties

The signal and background predictions in all signal regions are affected by several sources of experimental and theoretical systematic uncertainty. These are considered for both inclusive and differential measurements presented in Sects. 8 and 9. The uncertainties can be classified into the different categories which are described in the following subsections.

7.1 Detector-related uncertainties

The uncertainty in the combined 2015–2018 integrated luminosity is 1.7% [77], obtained using the LUCID-2 detector [28] for the primary luminosity measurements. This systematic uncertainty affects all processes modelled using MC simulations apart from the light-flavour components of the WZ/ZZ + jets backgrounds, whose normalisations are taken from data in control regions.

The uncertainty in the reweighting of the MC pile-up distribution to match the distribution in data is evaluated by varying the pile-up correction factors used to perform the reweighting.

Uncertainties associated with the lepton selection arise from the trigger, reconstruction, identification and isolation efficiencies, and the lepton momentum scale and resolution [63–65]. They are below 1% for the individual sources and have a total impact of 2–2.5% on the measurements. Uncertainties associated with the jet selection arise from the jet energy scale (JES), the JVT requirement and the jet energy resolution (JER). The JES and its uncertainties are derived by combining information from test-beam data, collision data and simulation [78]. The uncertainties in the JER and JVT increase at lower jet p_T. The overall effect of uncertainties related to jet selection and calibration is approximately 2%.

The efficiency of the flavour-tagging algorithm is measured for each jet flavour using control samples in data and in simulation. From these measurements, correction factors are derived to correct the tagging rates in the simulation. In the case of b-tagged jets, the correction factors and their uncertainties are estimated from data using dileptonic $t\bar{t}$ events [71]. In the case of c-jets, they are derived from jets arising from W boson decays in $t\bar{t}$ events [79]. In the case of light-flavour jets, the correction factors are derived using dijet events [80]. Sources of uncertainty affecting the b- and c-tagging efficiencies are evaluated as a function of jet p_T, including bin-to-bin correlations. The uncertainties in the efficiency for tagging light-flavour jets depend on the jet p_T and on η. An additional uncertainty is assigned to account for the extrapolation of the b-tagging efficiency measurement from the p_T region used to determine the correction factors to regions with higher p_T. The impact of flavour-tagging uncertainties on the measurements depends on the signal regions and is 2–3% in total.

7.2 Signal modelling uncertainties

Different sources of systematic uncertainty in the theoretical predictions of the $t\bar{t}Z$ process are considered. To evaluate the effect of μ_r and μ_f uncertainties, the scales used in the ME of the MG5_AMC@NLO + PYTHIA 8 samples are varied simultaneously, as well as individually, by factors of 2.0 and 0.5 relative to their nominal values. The uncertainty due to the ISR is estimated using a set of variations of the A14 tune's parameter values. Uncertainties associated with the choice of PDF set are evaluated according to the PDF4LHC prescription [81] using eigenvector variations from multiple NLO PDF sets, the effects of which are added in quadrature.

The systematic uncertainty due to the modelling of the parton shower, the hadronisation and the underlying event – called the parton-shower uncertainty in the following – is quantified by employing an alternative $t\bar{t}Z$ sample generated with MG5_AMC@NLO, but interfaced to HERWIG 7 instead of PYTHIA 8.

7.3 Background modelling uncertainties

The normalisation of the WZ + jets and ZZ + jets backgrounds with light-flavour jets are obtained from data, as discussed in Sect. 6.1. The WZ/ZZ + jets components with b- or c-jets are constrained to their MC predictions and normalisation uncertainties of 50% ($WZ/ZZ + b$) and 30% ($WZ/ZZ + c$) are assigned to them. These uncertainties are evaluated from data/MC comparisons in $Z + b/c$ events [82], but also take into account differences in the heavy-flavour jet fractions between Z + jets and WZ/ZZ + jets events. Modelling uncertainties of WZ/ZZ + jets related to the μ_r and μ_f scales and the PDF choice are obtained with the same prescription as for the signal. Uncertainties attributed to the resummation scale and CKKW matching scale [52,54] are evaluated from alternative WZ/ZZ + jets samples with variations of these scale choices.

Uncertainties related to the μ_r and μ_f scales and the PDF of the tWZ background are evaluated in the same way as for the $t\bar{t}Z$ and WZ/ZZ + jets samples. An additional uncertainty is assigned to the tWZ process to account for the interference between the $t\bar{t}Z$ and tWZ processes. It is evaluated by switching to an alternative diagram removal scheme (DR1 vs DR2) [57] and obtaining an uncertainty from the differences observed in the signal regions.

Scale and PDF uncertainties of the tZq background are obtained in the same way as for the previously described samples. In addition, a normalisation uncertainty of 30% is assigned, motivated by the measurements of this process presented in Refs. [83,84]. As for the $t\bar{t}Z$ signal, the uncertainty due to the ISR is evaluated using alternative samples with PYTHIA 8 A14 Var3c eigentune variations.
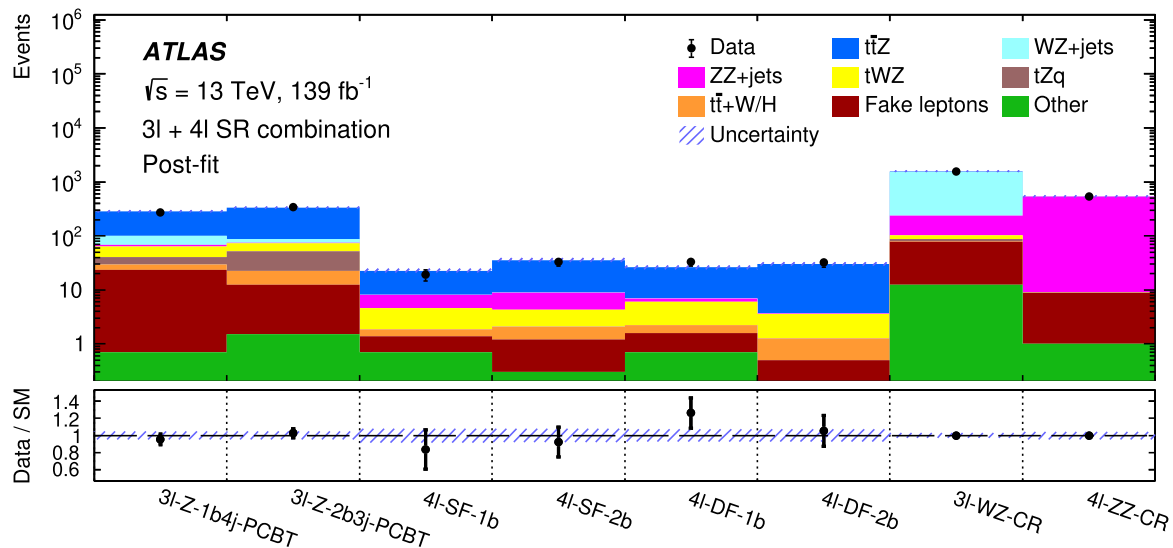
Fig. 3 The observed and expected event yields in the trilepton and tetralepton signal regions, as well as the $WZ/ZZ +$ jets control regions, after the combined fit. The bottom panel shows the ratio of data to the total SM prediction. The size of the combined statistical and systematic uncertainty in the sum of the fitted signal and backgrounds is indicated by the blue hatched band

For the fake-lepton background, statistical as well as systematic uncertainties are considered as explained in Sect. 6. They are evaluated for each signal region independently and applied as normalisation uncertainties of the total fake-lepton background contribution in each region.

For the $t\bar{t}H$ background, a normalisation uncertainty of approximately 10% due to the choice of QCD scales and PDF is used [48]. For processes giving smaller backgrounds, namely $H+W/Z$, $t\bar{t}W$, $t\bar{t}WW$, triboson and three/four top-quark production, a conservative overall normalisation uncertainty of 50% is applied.

8 Results of the inclusive cross-section measurement

The ratio of the measured value of the inclusive $t\bar{t}Z$ production cross section to its corresponding SM prediction ($\mu_{t\bar{t}Z}$) is obtained from a simultaneous fit to the numbers of events in the trilepton and tetralepton signal regions (as defined in Tables 1, 2), as well as the $WZ +$ jets and $ZZ +$ jets control regions (defined in Table 3). For trilepton events, only the dedicated regions for the inclusive measurement are included in the fit. The fit is based on the profile-likelihood technique, with a likelihood function as a product of Poisson probability functions given by the observed event yields in the signal and control regions. The value of $\mu_{t\bar{t}Z}$ as well as the normalisations of the light-flavour components of the $WZ/ZZ +$ jets backgrounds are treated as free parameters in the fit. The systematic uncertainties described in Sect. 7 are included in the fit as nuisance parameters constrained by Gaussian

functions. None of the uncertainty parameters is found to be significantly constrained or pulled by the fit. The calculation of confidence intervals and hypothesis testing is performed using a modified frequentist method as implemented in the RooStats framework [85–87].

Within their uncertainties, the fitted normalisations of the light-flavour components of the $WZ +$ jets and $ZZ +$ jets backgrounds are compatible with unity, but can vary by up to 10% from their initial value. The observed and expected total event yields in the signal regions and the $WZ/ZZ +$ jets control regions after the combined fit (post-fit) are shown in Fig. 3 and detailed in Table 5. The strong anti-correlation between the $WZ + l$ and $WZ + c$ backgrounds results in a smaller total uncertainty of the fitted SM background expectation in 3ℓ-WZ-CR compared with the uncertainties of the individual $WZ + l$ and $WZ + c$ components.

Comparisons between data and the post-fit SM predictions for some selected variables which offer sensitivity to the quality of the background modelling in the signal regions are also presented. The number of selected jets with $p_T > 25$ GeV in signal region 3ℓ-Z-$1b4j$-PCBT is shown in Fig. 4a. The p_T of the leading lepton in 3ℓ-Z-$2b3j$-PCBT is given in Fig. 4b. Figure 5a depicts the number of selected jets and Fig. 5b the p_T of the leading lepton in the combination of the four tetralepton regions. Figure 6a shows the p_T and Fig. 6b the rapidity (y) of the reconstructed Z boson in the combination of the trilepton and tetralepton regions.

Table 6 summarises the measured $\mu_{t\bar{t}Z}$ parameters obtained from the individual fits in the trilepton and tetralepton regions, as well as the value from the combined $3\ell + 4\ell$ fit.

Table 5 The observed and expected numbers of events in the trilepton and tetralepton signal regions, as well as the WZ/ZZ + jets control regions, after the combined fit. The definitions of the background categories are the same as in Table 4. Categories with event yields shown as '–' do not contribute significantly to a region. The indicated uncertainties consider all experimental and theoretical systematic uncertainties as well as the statistical errors. As systematic uncertainties might be correlated between different processes, the individual uncertainties do not necessarily add up in quadrature to the uncertainty of the total SM prediction

Region	3ℓ-Z-$1b4j$-PCBT	3ℓ-Z-$2b3j$-PCBT	4ℓ-SF-$1b$	4ℓ-SF-$2b$	4ℓ-DF-$1b$	4ℓ-DF-$2b$	3ℓ-WZ-CR	4ℓ-ZZ-CR
$t\bar{t}Z$	185 ± 16	247 ± 20	14.5 ± 1.7	26.9 ± 2.5	19.3 ± 1.8	26.7 ± 2.3	45 ± 11	0.8 ± 0.1
$WZ + l$	2.4 ± 1.8	0.2 ± 0.3	–	–	–	–	1068 ± 110	–
$WZ + b$	20 ± 11	10.8 ± 6.1	–	–	–	–	11.2 ± 6.3	–
$WZ + c$	10.8 ± 4.8	1.8 ± 0.8	–	–	–	–	207 ± 87	–
$ZZ + l$	0.3 ± 0.2	0.02 ± 0.02	1.7 ± 0.7	0.9 ± 0.5	0.5 ± 0.1	0.02 ± 0.01	121 ± 15	496 ± 26
$ZZ + b$	3.0 ± 1.6	2.0 ± 1.0	0.9 ± 0.6	2.5 ± 1.5	0.2 ± 0.1	0.07 ± 0.07	1.8 ± 0.9	12.9 ± 7.1
$ZZ + c$	0.7 ± 0.2	0.1 ± 0.1	0.9 ± 0.5	1.1 ± 0.6	0.2 ± 0.1	0.02 ± 0.01	13.0 ± 4.1	19.8 ± 7.1
tWZ	23.8 ± 4.0	20.5 ± 7.0	2.7 ± 0.4	2.2 ± 0.8	3.8 ± 1.1	2.3 ± 0.9	13.2 ± 1.2	0.2 ± 0.1
tZq	10.8 ± 4.5	29.7 ± 9.0	–	–	–	–	8.6 ± 3.2	–
$t\bar{t} + W/H$	5.8 ± 0.9	10.1 ± 2.2	0.5 ± 0.1	0.9 ± 0.1	0.6 ± 0.1	0.8 ± 0.1	1.8 ± 0.4	0.01 ± 0.01
Fake leptons	23 ± 11	11.0 ± 5.3	0.7 ± 0.3	0.9 ± 0.4	0.9 ± 0.5	0.3 ± 0.1	65 ± 31	7.9 ± 3.1
Other	0.7 ± 0.4	1.5 ± 0.7	0.7 ± 0.3	0.2 ± 0.1	0.7 ± 0.4	0.2 ± 0.1	12.4 ± 6.3	1.0 ± 0.5
SM total	286 ± 13	334 ± 15	22.5 ± 1.8	35.6 ± 2.7	26.1 ± 1.9	30.3 ± 2.2	1569 ± 43	539 ± 23
Data	272	343	19	33	33	32	1569	539
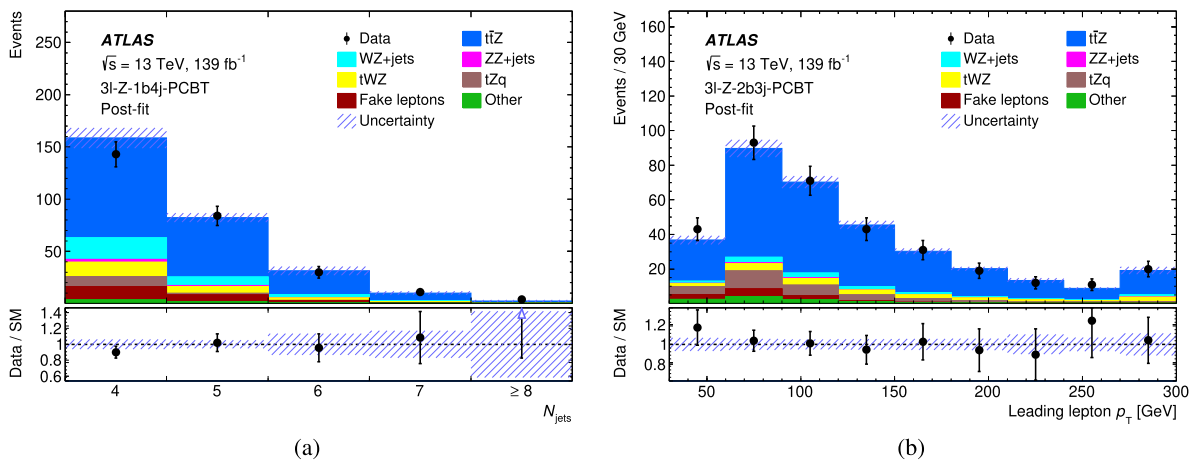
Fig. 4 Post-fit distributions of **a** N_{jets} in 3ℓ-Z-$1b4j$-PCBT and **b** the p_{T} of the leading lepton in 3ℓ-Z-$2b3j$-PCBT. The shaded band includes all sources of statistical and systematic uncertainty after the combined fit. The lower panel shows the ratio of data to the total SM prediction. The uppermost bins include all events above the x-axis ranges. The blue triangular marker in the lower panel of **a** points to the position of a data point which lies slightly beyond the y-axis range shown

The values obtained from the fit in the different regions are compatible within their uncertainties. The 3ℓ-channel events represent the dominant contribution to the combined result, and the individual 3ℓ result can be seen to differ only slightly from that using the combined selections. The total systematic uncertainties in the 4ℓ channel are smaller than those in the 3ℓ channel, but the overall precision is poorer in the 4ℓ channel due to the limited number of data events.

The measured $\mu_{t\bar{t}Z}$ value and its uncertainty based on the fit results from the combined trilepton and tetralepton channels are converted to a cross-section measurement. The value corresponds to the phase-space region where the invariant mass of the decay products of the Z boson lies between 70 and 110 GeV. The cross section is measured to be

$$\sigma(pp \rightarrow t\bar{t}Z) = 0.99 \pm 0.05 \,(\text{stat.}) \pm 0.08 \,(\text{syst.}) \text{ pb}.$$

The result agrees with the SM prediction of $0.84^{+0.09}_{-0.10}$ pb at NLO QCD and EW accuracy [48,49] and more recent calculations including NNLL corrections or the complete set (QCD and EW) of NLO corrections [16,17].

(a)

(b)
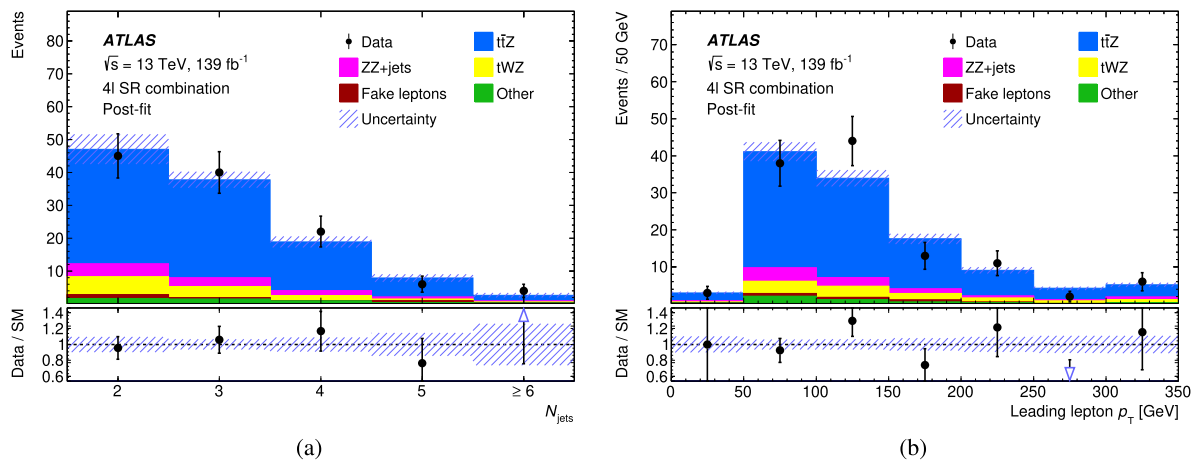
Fig. 5 Post-fit distributions of **a** N_{jets} and **b** the p_T of the leading lepton in the combination of the tetralepton signal regions. The shaded band includes all sources of statistical and systematic uncertainty after the combined fit. The lower panel shows the ratio of data to the total SM prediction. The uppermost bins include all events above the x-axis ranges. The blue triangular markers in the lower panels point to the positions of data points which lie slightly beyond the y-axis range shown

(a)

(b)
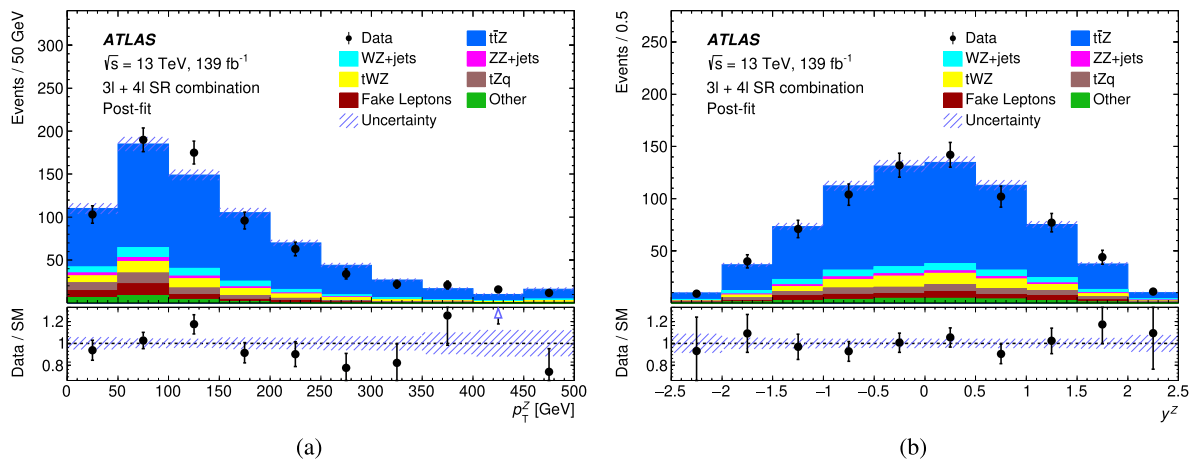
Fig. 6 Post-fit distributions of the **a** p_T and **b** rapidity of the Z boson in the combination of the trilepton and tetralepton regions. The shaded band includes all sources of statistical and systematic uncertainty after the combined fit. The lower panel shows the ratio of data to the total SM prediction. The uppermost bins include all events above the x-axis ranges. The blue triangular marker in the lower panel of **a** points to the position of a data point which lies slightly beyond the y-axis range shown

The contributions from the relevant uncertainties of the measured cross section are summarised in Table 7. For this table, the uncertainties are grouped into several type-related categories and are shown together with the total uncertainty. As none of the uncertainties show significant asymmetries, they are symmetrised. The dominant uncertainty sources can be attributed to the $t\bar{t}Z$ parton shower, the modelling of the tWZ background, and jet flavour-tagging. It should be noted that the uncertainty in the cross section due to the systematic uncertainty on the luminosity is larger than the 1.7% mentioned in Sect. 7.1, as the luminosity affects both signal and background normalisation.

Table 6 Measured $\mu_{t\bar{t}Z}$ parameters obtained from the fits in the different lepton channels. The uncertainties include statistical and systematic sources. The uncertainty of the theoretical prediction of the $t\bar{t}Z$ cross section (see Sect. 3) is not considered for the $\mu_{t\bar{t}Z}$ values

Channel	$\mu_{t\bar{t}Z}$
Trilepton	1.17 ± 0.07 (stat.) $^{+0.12}_{-0.11}$ (syst.)
Tetralepton	1.21 ± 0.15 (stat.) $^{+0.11}_{-0.10}$ (syst.)
Combination ($3\ell + 4\ell$)	1.19 ± 0.06 (stat.) ± 0.10 (syst.)

Table 7 List of relative uncertainties of the measured inclusive $t\bar{t}Z$ cross section from the combined fit. The uncertainties are symmetrised for presentation and grouped into the categories described in the text. The quadrature sum of the individual uncertainties is not equal to the total uncertainty due to correlations introduced by the fit

Uncertainty	$\Delta\sigma_{t\bar{t}Z}/\sigma_{t\bar{t}Z}$ [%]
$t\bar{t}Z$ parton shower	3.1
tWZ modelling	2.9
b-tagging	2.9
WZ/ZZ + jets modelling	2.8
tZq modelling	2.6
Lepton	2.3
Luminosity	2.2
Jets + E_T^{miss}	2.1
Fake leptons	2.1
$t\bar{t}Z$ ISR	1.6
$t\bar{t}Z$ μ_f and μ_r scales	0.9
Other backgrounds	0.7
Pile-up	0.7
$t\bar{t}Z$ PDF	0.2
Total systematic	8.4
Data statistics	5.2
Total	10

9 Differential cross-section measurements

9.1 Description of the observables and reconstruction of the $t\bar{t}$ system

A set of ten observables were selected for the differential cross-section measurements which probe the kinematics of the $t\bar{t}Z$ system. The definitions of these variables are summarised in Table 8. With the exception of the number of reconstructed jets (N_{jets}), which is unfolded to particle level only, all distributions are unfolded to both particle and parton level. Two of the variables, namely the transverse momentum and the absolute value of the rapidity of the Z boson (p_T^Z and $|y^Z|$), which are sensitive to $t\bar{t}Z$ generator modelling and various BSM effects, are defined identically for the trilepton and tetralepton selections. The differential measurements for these variables are therefore performed using an inclusive selection denoted by $3\ell + 4\ell$.

The jet multiplicity is a natural variable to use to probe the modelling of QCD radiation and hadronisation in MC generators. It is measured separately for the trilepton and tetralepton selections due to the different number of final-state quarks from the decay of the $t\bar{t}$ system in the two channels. The transverse momentum of the lepton which is not associated with the Z boson ($p_T^{\ell,\text{non-}Z}$) in the trilepton signal regions provides a good test of the modelling of the p_T of

the top quark (antiquark) and its decay products in the MC generator.

The absolute azimuthal separation and rapidity difference between the Z boson and the leptonic top quark ($|\Delta\phi(Z, t_{lep})|$ and $|\Delta y(Z, t_{lep})|$) in the trilepton signal regions, as well as the absolute azimuthal separation between the Z boson and the $t\bar{t}$ system ($|\Delta\phi(t\bar{t}, Z)|$) in the tetralepton regions, provide direct probes of the $t\bar{t}Z$ vertex. These variables therefore offer sensitivity to a number of BSM effects which could modify the coupling between the Z boson and the top quark.

The absolute azimuthal separation between the two leptons associated with the top quarks ($|\Delta\phi(\ell_t^+, \ell_{\bar{t}}^-)|$) in tetralepton events provides sensitivity to BSM effects modifying the spin correlations between the two top quarks. The transverse momentum of the $t\bar{t}$ system ($p_T^{t\bar{t}}$) is sensitive to the MC modelling of the hard-scattering process as well as the modelling of the QCD radiation in the parton shower.

In order to construct the $|\Delta\phi(Z, t_{lep})|$ and $|\Delta y(Z, t_{lep})|$ variables in the trilepton regions, the full four-vector of the leptonic top quark from the $t\bar{t}$ system (t_{lep}) is required.[10] For both detector- and particle-level quantities the reconstructed E_T^{miss} (both its magnitude and azimuthal angle), is first attributed to the neutrino from the associated W boson decay. The SM value of the W boson mass [35] is then used to determine the z-component of the neutrino momentum by analytically solving the corresponding quadratic equation. In many cases the solution is ambiguous. For those, both real solutions are considered. For cases in which the discriminant of the quadratic equation is negative, the p_T of the neutrino is set to the particular value which yields a single solution. In order to form the final top-quark candidate, the reconstructed leptonically decaying W boson candidate – or candidates in the case of two neutrino solutions – is added, via a four-vector sum, to the closer (in ΔR) of the two reconstructed jets in the event with the highest output from the b-tagging algorithm (MV2c10). At particle level, the two jets which are ghost-matched to a b-hadron (as described in Sect. 4.2) are considered. In the case of only a single such ghost-matched jet, that jet is selected to form the top-quark candidate. Events with two distinct neutrino solutions will have two possible top-quark candidates, so the one with an invariant mass of the W-b system more consistent with a top-quark decay is chosen.

In the tetralepton channel the $t\bar{t}$ system is reconstructed in the transverse plane only. The underlying assumption is that the two neutrinos from the $t\bar{t}$ decay represent the dominant source of missing transverse momentum in the event; the value of the reconstructed E_T^{miss} can, therefore, be taken to be a reasonable proxy for the vector sum of the neutrino momenta in the transverse plane. Such a partial reconstruc-

---

[10] The leptonic top quark is defined as the top quark or antiquark which decays via $t \to Wb$, $W \to \ell\nu$.

Table 8 Summary of the variables used for the differential measurements. Some variables are considered for the trilepton or tetralepton signal regions only, as indicated. The jet multiplicity is measured for the two topologies separately, whereas for the variables related only to the kinematics of the Z boson (p_T^Z and $|y^Z|$), the trilepton and tetralepton regions are combined

Variable	Definition
$3\ell + 4\ell$	
p_T^Z	Transverse momentum of the Z boson
$|y^Z|$	Absolute value of the rapidity of the Z boson
3ℓ	
N_{jets}	Number of selected jets with $p_T > 25\,\text{GeV}$ and $|\eta| < 2.5$
$p_T^{\ell,\text{non-}Z}$	Transverse momentum of the lepton which is not associated with the Z boson
$|\Delta\phi(Z, t_{\text{lep}})|$	Azimuthal separation between the Z boson and the top quark (antiquark) featuring the $W \to \ell\nu$ decay
$|\Delta y(Z, t_{\text{lep}})|$	Absolute rapidity difference between the Z boson and the top quark (antiquark) featuring the $W \to \ell\nu$ decay
4ℓ	
N_{jets}	Number of selected jets with $p_T > 25\,\text{GeV}$ and $|\eta| < 2.5$
$|\Delta\phi(\ell_t^+, \ell_{\bar{t}}^-)|$	Azimuthal separation between the two leptons from the $t\bar{t}$ system
$|\Delta\phi(t\bar{t}, Z)|$	Azimuthal separation between the Z boson and the $t\bar{t}$ system
$p_T^{t\bar{t}}$	Transverse momentum of the $t\bar{t}$ system

tion avoids the need to determine the full kinematics of both neutrinos separately, while still allowing the reconstruction of the $p_T^{t\bar{t}}$ and $|\Delta\phi(t\bar{t}, Z)|$ variables for the differential measurements. The selection of the two b-tagged jets is performed analogously to the trilepton case. At detector level, the two reconstructed jets with the highest b-tagging score are selected. At particle level, the two jets ghost-matched to a b-hadron are selected; in the case of only one ghost-matched jet, the jet with the highest p_T of those remaining is selected as the second b-jet.

9.2 Unfolding procedure

To measure the differential cross-section distributions at particle and parton levels in the specific fiducial phase-spaces defined in Sect. 4.2, an iterative Bayesian unfolding procedure is used [88]. It relies on the Bayesian probability formula starting from a given prior of the particle- or parton-level distribution and iteratively updating it with the posterior distribution. The unfolding is performed using the RooUnfold package [89]. The differential $t\bar{t}Z$ cross sections are calculated using the following equation:

$$\frac{d\sigma_{t\bar{t}Z}}{dX^i} = \frac{1}{\mathcal{L} \cdot \mathcal{B} \cdot \Delta X^i \cdot \epsilon_{\text{eff}}^i} \cdot \sum_j [\mathcal{M}^{-1}]_{ij}$$
$$\cdot f_{\text{acc}}^j \cdot \left(N_{\text{obs}}^j - N_{\text{bkg}}^j\right),$$

where X denotes the variable used for the differential measurement (with the bin-width ΔX), the index i indicates the bin at particle (or parton) level and j the detector-level bin.

The migration matrix $\mathcal{M}$ quantifies the detector response and can be derived from the bin-to-bin migrations of events from particle or parton level to detector level in the nominal $t\bar{t}Z$ simulation for each of the considered differential variables. Its inverse, $\mathcal{M}^{-1}$, is determined through the iterative unfolding procedure. For each j, N_{obs}^j denotes the number of observed data events, and N_{bkg}^j is the expected background contribution. The various background contributions are estimated in the same way as for the inclusive measurement (see Sect. 6). In this case, the $WZ/ZZ+l$ backgrounds are corrected by normalisation parameters obtained from an inclusive fit based on the combined $3\ell + 4\ell$ channels. A statistics-only version of the fit was performed solely for the extraction of the normalisation parameters in this case. The acceptance corrections, f_{acc}^j, account for events that are generated outside the fiducial phase-space but pass the detector-level selection, whereas the efficiency correction terms, ϵ_{eff}^i, correct for events that are in the fiducial phase-space but are not reconstructed in the detector. In either case, the term 'fiducial' refers to the corresponding type of unfolding being performed – either to parton or particle level. The integrated luminosity is denoted by $\mathcal{L}$. The branching ratio $\mathcal{B}$ is that of the $t\bar{t}Z$ system to final states with three or four charged electrons or muons, originating directly from either the Z boson decay or the decay of the W bosons from the $t\bar{t}$ system, and is used to extrapolate the measurements to cover all $t\bar{t}$ and Z decays. The branching ratio correction is only applied for the parton-level measurements and corresponds to the decay channels applicable for the fiducial region based on the particular variable involved (see Table 8). The values for $\mathcal{B}$, calculated using inputs taken from Ref. [35], are 0.0193 (3ℓ), 0.0030 (4ℓ), and 0.0223 ($3\ell + 4\ell$).

Figure 7 shows the particle- and parton-level migration matrices that are used for the differential cross-section mea-
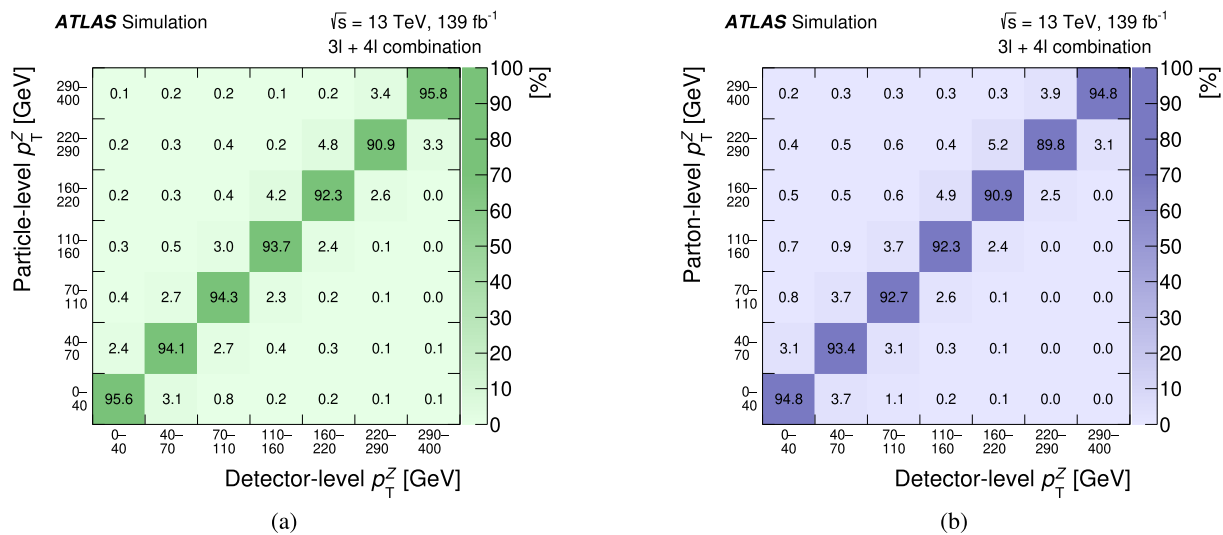
Fig. 7 The migration matrices for the p_T of the Z boson in the combination of the trilepton and tetralepton regions. The matrices quantify the migrations from **a** particle or **b** parton level to detector level. The quoted values are expressed as a percentage. The matrices are normalised such that the sum of any given row is 100%, although small differences may be present due to rounding
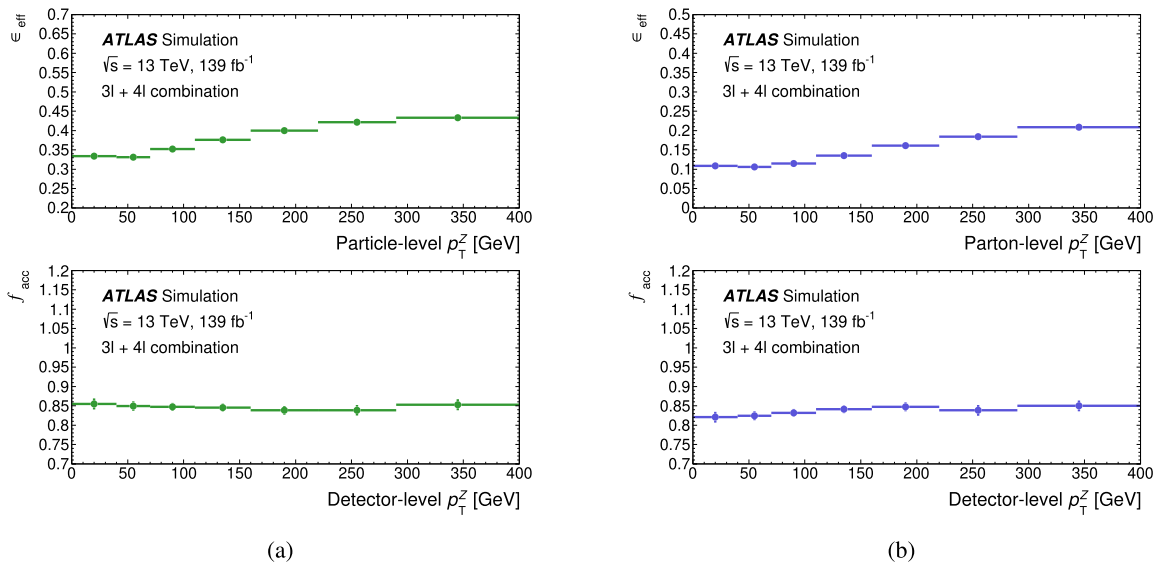
Fig. 8 The efficiency (ϵ_{eff}) and acceptance (f_{acc}) correction factors for the **a** particle-level and **b** parton-level measurements as a function of the p_T of the Z boson in the combination of the trilepton and tetralep-ton regions. The error bars represent the MC statistical uncertainties per bin based on the nominal signal sample

surements depending on the p_T of the Z boson. The matrices are normalised such that the sum of entries in each row is equal to one. The entries in the matrices represent the fraction of events at either particle or parton level in a y-axis bin that are reconstructed at detector level in an x-axis bin. Thus, the fraction of events in the diagonal elements shows the quality of the resolution for a specific variable. In the case of p_T^Z, these fractions lie between 90 and 96% for both particle and parton level. For some of the other variables which do not depend only on the Z boson reconstruction (e.g. N_{jets},

$p_T^{t\bar{t}}$), the migrations between bins can be significantly larger and reach a level of 20–25%. Figure 8 depicts the corresponding correction factors as a function of p_T^Z: ϵ_{eff} increases for larger p_T^Z due to higher lepton reconstruction efficiencies for increasing transverse momenta. It lies between 33 and 43% at particle level and between 10 and 22% at parton level. The values of f_{acc} are in all bins higher than 80% for both particle and parton level and show no notable dependence on p_T^Z.

The choice of binning is determined separately for each variable by performing a multi-dimensional scan in order to

(a)

(b)

(c)

(d)
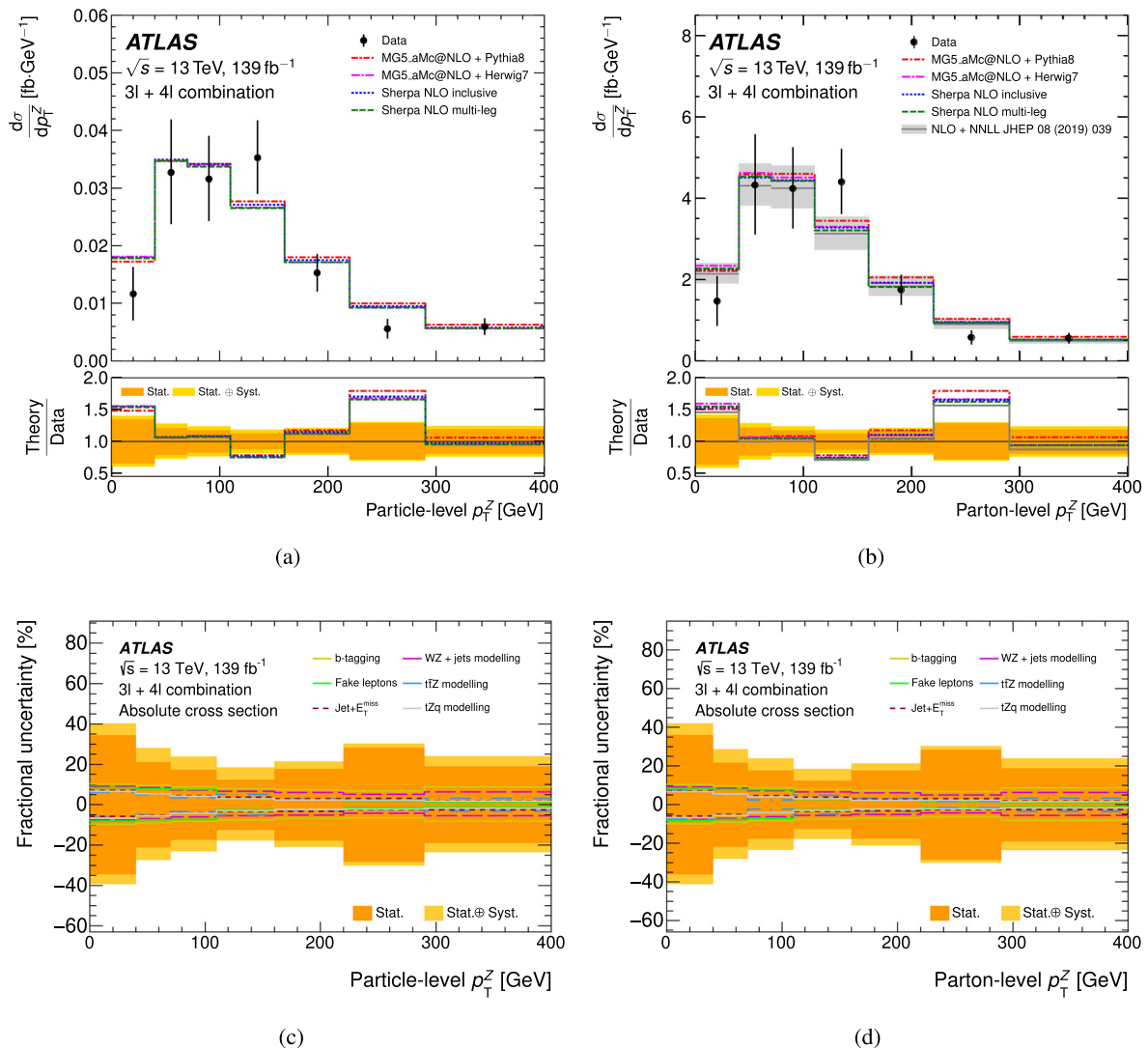
Fig. 9 Absolute differential $t\bar{t}Z$ cross sections measured at **a** particle level and **b** parton level as a function of the transverse momentum of the reconstructed Z boson. **c, d** Show the relative contributions from different categories of systematic uncertainties per bin. The large difference between the y-axis scales in **a** and **b** is a result of different efficiency and acceptance corrections between the particle- and parton-level measurements, together with the branching ratio correction of $\mathcal{B} = 0.0223$ for the combined $3\ell + 4\ell$ channels, which is applied only for the parton-level result

strike a reasonable balance between three partially competing aspects: retaining a large number of bins; limiting the relative impact from statistical uncertainties of the measured data; and ensuring large values ($> 50\%$) for the diagonal elements of the matrices associated with the bin migrations between particle/parton and detector level. As a result, the binning for the differential measurements differs from that shown in Figs. 4, 5 and 6. The stability of the unfolding procedure is determined by constructing pseudo-data sets by randomly sampling events from the nominal $t\bar{t}Z$ MC sample, such that the pseudo-data sets contain approximately the same number of events as in the measured data. So-called 'pull tests'

are performed as part of the binning optimisation to verify that the unfolding is stable for the selected number and range of bins. In addition, linear re-weightings are applied to the pseudo-data to test the ability of the unfolding procedure to correct the pseudo-data back to their underlying true spectra, obtained from the MC event record. The number of iterations used in the iterative Bayesian unfolding is also optimised with pseudo-experiments: for each iteration, a χ^2 per degree-of-freedom (ndf) is calculated by comparing the bin contents of the unfolded pseudo-data with those from the previous iteration. In the case of the first iteration, the unfolded pseudo-data are instead compared with the corresponding generator-level
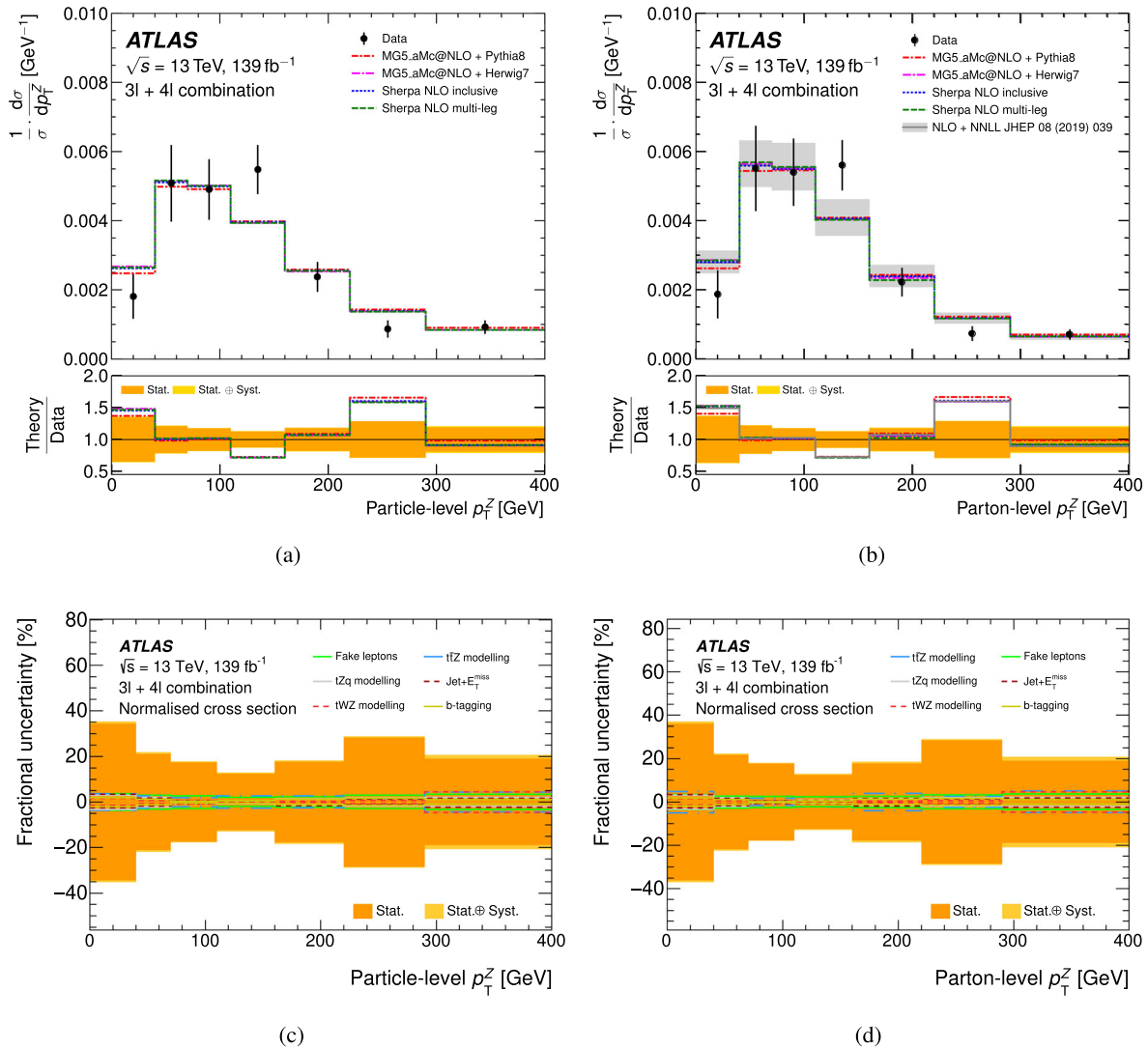
Fig. 10 Normalised differential $t\bar{t}Z$ cross sections measured at **a** particle level and **b** parton level as a function of the transverse momentum of the reconstructed Z boson. **c**, **d** Show the relative contributions from different categories of systematic uncertainties per bin

distribution. Iterations are performed until the χ^2/ndf value of a given distribution stabilises at a constant value while the statistical uncertainty returned from the unfolding procedure is kept as low as possible. For all variables, the number of iterations used lies between two and five. Systematic uncertainties are propagated to the unfolded distributions by varying the detector-level distributions within the uncertainties and repeating the unfolding procedure.

The normalised differential cross sections are obtained by dividing the distributions by the integrated fiducial cross sections, which are computed by adding up the contributions from all bins. The evaluation of systematic uncertainties is performed after the normalisation is done and it is on the same prescriptions employed for the absolute differential measurements.

9.3 Results of the differential measurements

The measured differential $t\bar{t}Z$ cross sections unfolded to particle and parton levels for the p_{T} of the reconstructed Z boson are presented in Fig. 9.

The results are displayed in the seven p_{T} bin ranges used when performing the unfolding, with any additional contributions beyond 400 GeV included in the uppermost bin. The relative contributions from statistical and systematic uncertainties in each bin are shown in the theory-to-data ratio panels of the upper figures, where the net effect corresponds to a sum in quadrature of the two. In the lower figures, the same relative contributions are shown as well as a decomposition of the systematic uncertainties into various cate-

gories.[11] The black data points in the upper figures correspond to the measured unfolded data and error bars representing the sum in quadrature of statistical and systematic uncertainties. The total uncertainty of this measurement is between 20 and 40%, depending on the bin, with the dominant uncertainty arising from the limited number of data events. Other significant sources of systematic uncertainty are associated with $t\bar{t}Z$ modelling and b-tagging. Figure 10 shows the same set of results for the normalised distributions for this variable. The uncertainties on the normalised cross sections are notably smaller (15–35%) than those of the absolute cross sections because several systematic uncertainties cancel out. The differential cross sections measured in data are compared with the NLO QCD predictions from different $t\bar{t}Z$ generators, as described in Sect. 3. The predictions are shown for MG5_AMC@NLO interfaced to PYTHIA 8 (red) or HERWIG 7 (magenta), as well as for SHERPA 2.2.1 inclusive (blue) and multi-leg (green). For the p_T^Z measurement, the different generators provide very similar predictions.

Results for the other observables described in Table 8 are presented in Figures 11, 12, 13, 14 and 15. For these variables, only the absolute parton-level differential measurements are shown, with the exception of N_{jets}, which is unfolded only to particle level. Additional differential $t\bar{t}Z$ predictions at NLO, NLO + NNLL or approximate next-to-next-to-leading-order (nNLO) precision – including EW corrections – are shown in grey for the parton-level results for most of the observables. The calculations were carried out in similar fashion to that described in Ref. [18], but specifically performed in the context of this analysis in order to provide predictions for the measured observables and to match the number and ranges of bins for the different variables.[12] These additional parton-level predictions are not provided for two of the observables, namely $p_T^{\ell,\text{non-}Z}$ and $|\Delta\phi(\ell_t^+, \ell_{\bar{t}}^-)|$, since the decays of the $t\bar{t}$ pair and the Z boson were not included in the theoretical calculations.

In order to test the overall compatibility between the unfolded measurements and the various predictions, a χ^2/ndf and corresponding p value is evaluated for each of the differential measurements, separately for the parton level and particle level as well as for the absolute and normalised cases.

---

[11] Unlike the presentation of the uncertainties shown in Table 7, the category '$t\bar{t}Z$ modelling' contains the sum in quadrature of all individual modelling uncertainties associated with the $t\bar{t}Z$ signal: parton shower, μ_{f}, μ_{r} scales, PDF and ISR.

[12] The precision of the calculations depends on the particular variable and can be provided at either NLO, NLO + NNLL or nNLO. The orders of the calculations are indicated on the plots. Their uncertainties include the contributions from scale variations, PDF uncertainties and MC statistics, which are added linearly to follow a conservative approach for the evaluation of the total uncertainty.
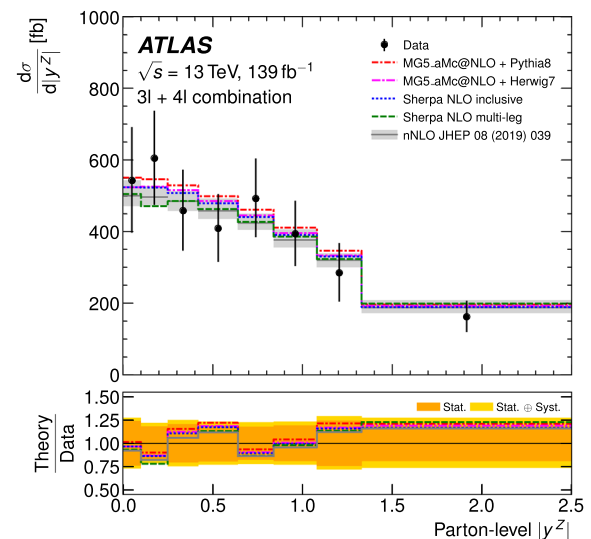
(a)
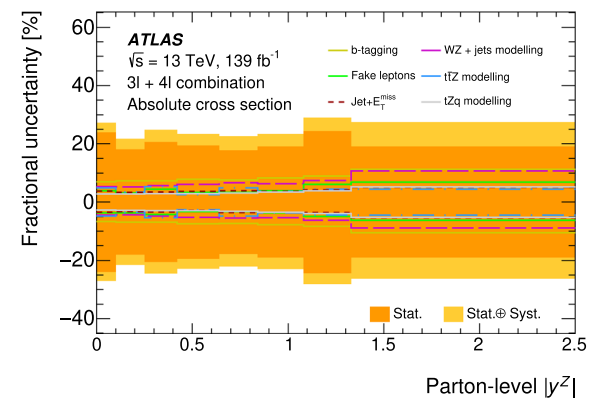
(b)

Fig. 11 **a** Absolute differential $t\bar{t}Z$ cross sections and **b** the relative contributions from different categories of systematic uncertainties per bin measured at parton level as a function of the absolute rapidity of the Z boson

The χ^2 value is defined as:

$$\chi^2 = \sum_{i=1}^{N_{\text{bins}}} \sum_{j=1}^{N_{\text{bins}}} (n_i - \mu_i)(n_j - \mu_j)[C^{-1}]_{ij},$$

where n_i and μ_i correspond to the content in bin i of the distributions from the unfolded data and the given prediction, respectively, and $[C^{-1}]_{ij}$ to the element in row i and column j of the inverse of the covariance matrix for the particular variable. The values, n_i and μ_i, are, therefore, notational shorthands for $d\sigma_{t\bar{t}Z}/dX^i$, or $1/\sigma \cdot d\sigma_{t\bar{t}Z}/dX^i$ in the normalised case.

A given p value can be interpreted as the probability of obtaining a value of χ^2 greater or equal to the quoted value for a particular number of degrees of freedom, where the
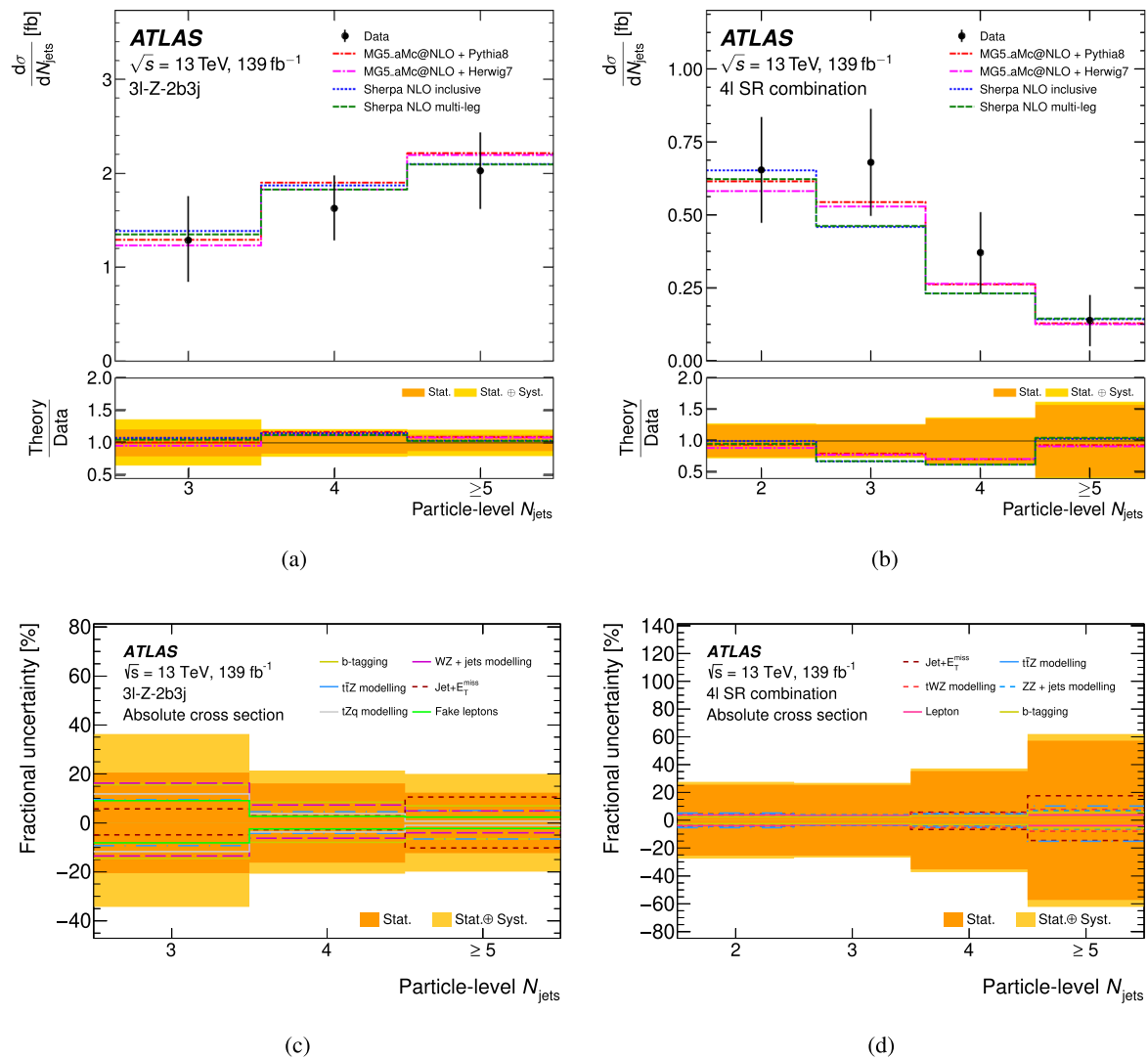
Fig. 12 Absolute differential $t\bar{t}Z$ cross section measured at particle level as a function of N_{jets} with $p_{\mathrm{T}} > 25$ GeV for **a** the trilepton and **b** the tetralepton event selection. **c**, **d** Show the relative contributions from different categories of systematic uncertainties per bin

latter is equal to the number of bins (N_{bins}) in the case of the absolute measurements and $N_{\mathrm{bins}} - 1$ for the normalised measurements.

The construction of the covariance matrix is based on the approach described in Ref. [90], and it includes both the statistical and systematic uncertainties. The latter include detector-related uncertainties as well as those related to the modelling of the signal and various background processes. While all sources of uncertainty related to the measurements are incorporated in the covariance matrix elements, uncertainties in the theoretical predictions, themselves, are omitted, and their impact is, therefore, not reflected in the quoted χ^2 and corresponding p values.

For a given variable, the elements of the covariance matrix, C_{ij}, are evaluated using a bootstrap technique, whereby 150,000 Poisson-fluctuated distributions are produced, each corresponding to a pre-unfolded distribution for a given pseudo-experiment. For the detector-related uncertainties, Gaussian-distributed shifts are added coherently to each of the Poisson-fluctuated bin contents, with each shift corresponding to a particular uncertainty source. The shifts are applied as a multiplicative scale relative to the particular bin content, and with the amount and direction of each shift dictated by the corresponding uncertainty source.

Each of the varied distributions is subsequently unfolded using the nominal acceptance and efficiency corrections, as well as the nominal migration matrix – those derived from the nominal MG5_AMC@NLO + PYTHIA 8 signal sample. Gaussian-distributed shifts are then added coherently to the post-unfolding distributions for each of the signal- and background-modelling uncertainty sources. These shifts are also determined and applied as relative variations for each

(a)

(b)

(c)

(d)
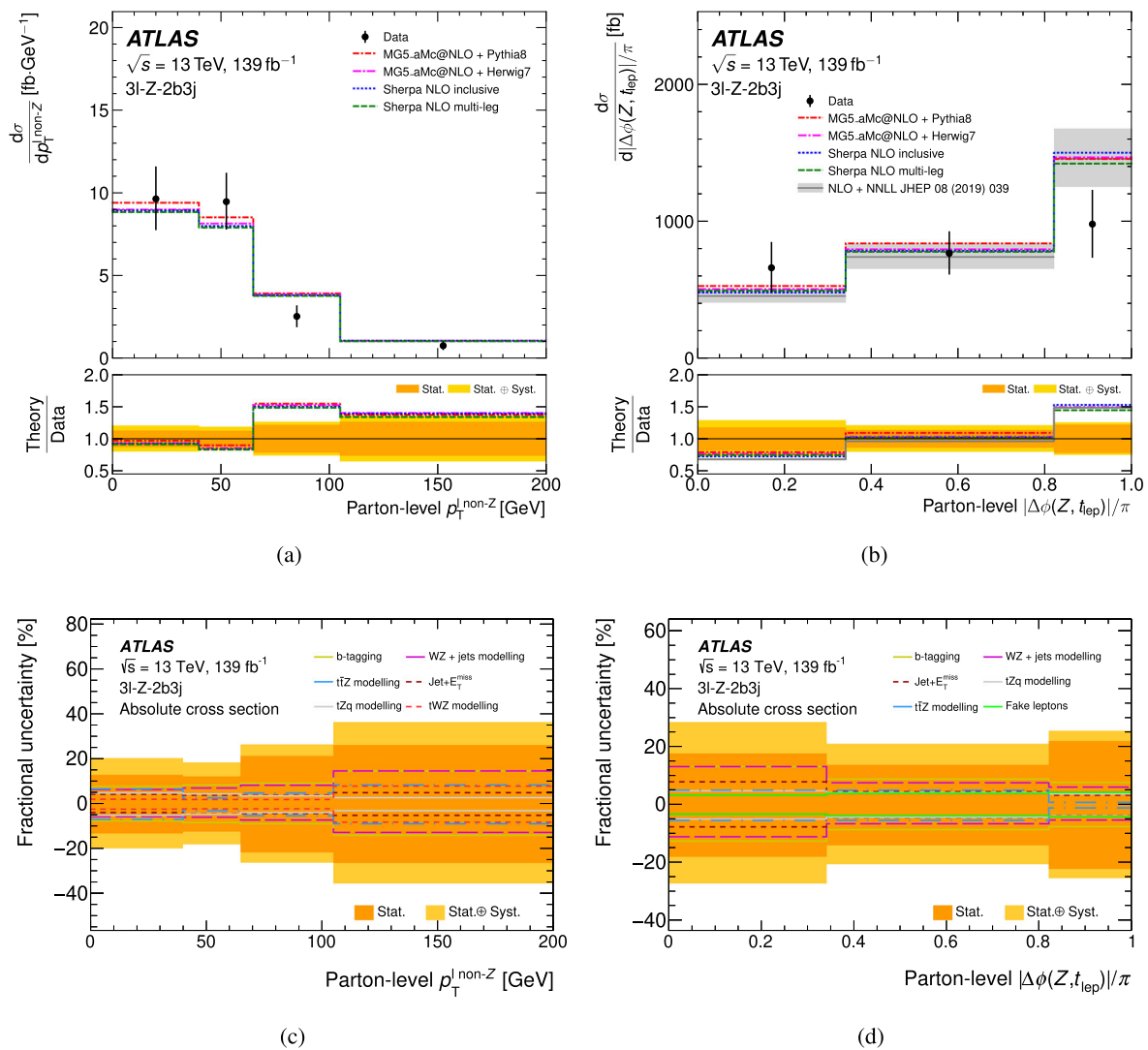
Fig. 13 Absolute differential $t\bar{t}Z$ cross sections measured at parton level as a function of **a** $p_T^{\ell,\text{non-}Z}$ and **b** the azimuthal separation ($\Delta\phi$) between the Z boson and the reconstructed top quark. **c**, **d** Show the relative contributions from different categories of systematic uncertainties per bin

particular source. The relative variations in this case are defined according to the difference between the generated and the unfolded cross section of a given alternative signal or background model, using nominal corrections in the unfolding.

The resulting changes to the unfolded distributions are, then, used to determine the elements of the covariance matrix for that particular variable. The covariance matrices for the normalised measurements are constructed in an analogous fashion. In this case, the distributions are normalised to unity after all effects are included. In order to avoid performing the unfolding on distributions with negative bin contents, that can arise due to the effects of systematic uncertainties and the subtraction of backgrounds, any such bin contents are set to zero prior to the unfolding.

The uncertainties reflected in the elements, C_{ij}, initially evaluated as relative values, are then multiplied by the differential cross-section values from the measured data in each particular bin in order to yield absolute uncertainties.

In general, each of the individual sources contributing to the full covariance matrix will contribute to the off-diagonal terms, including even those from the limited data sample size where non-diagonal contributions arise from correlations between the bins introduced during the unfolding process.

The correlations between the bins in the absolute differential measurements for the trilepton and combined channels are sizeable – in many cases in the 20–55% range – and positive. In the case of the tetralepton channel, where statistical uncertainties are more dominant, the correlations are generally below 20% in absolute value. The correlations in the case

(a)

(b)

(c)

(d)
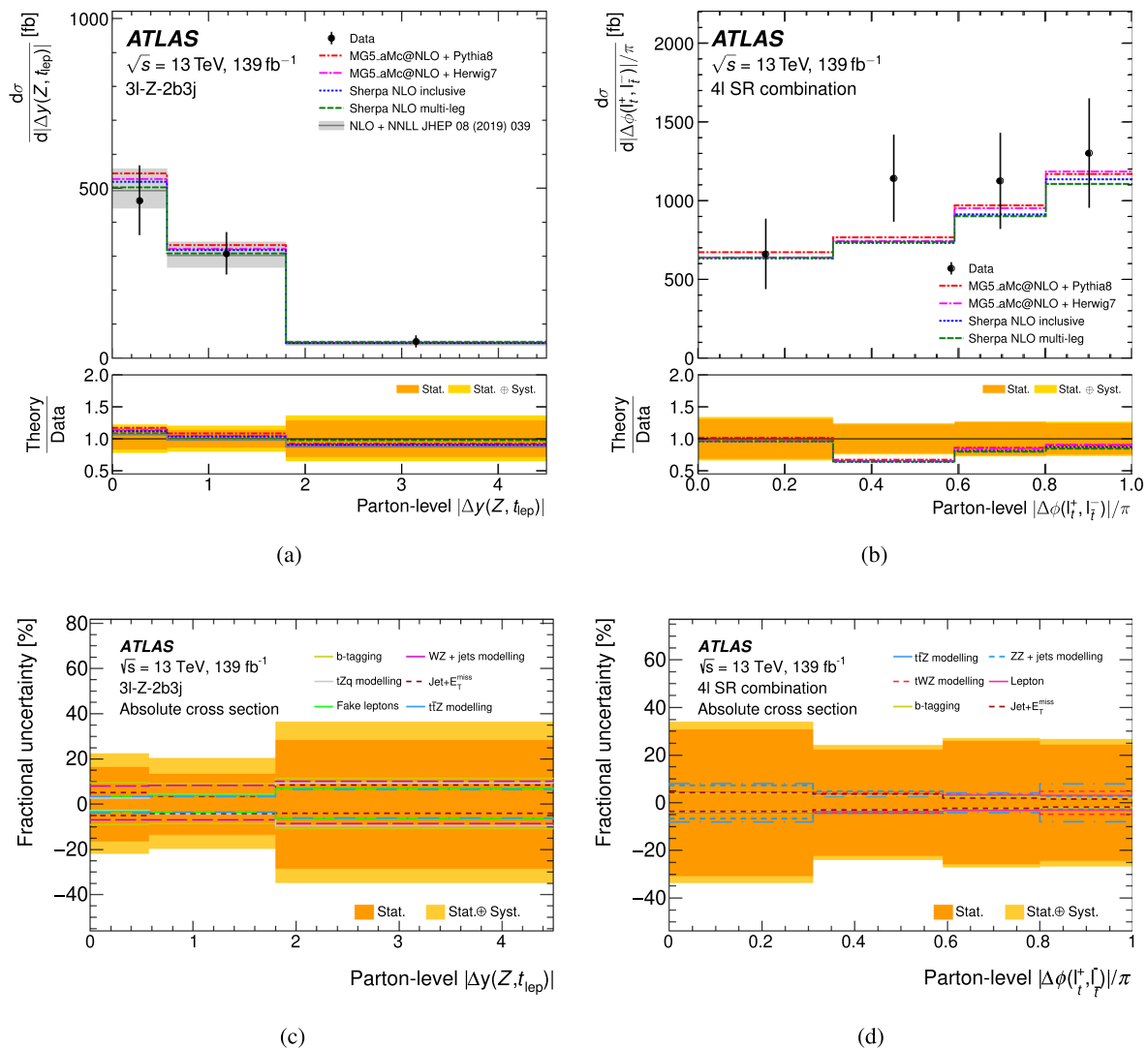
Fig. 14 Absolute differential $t\bar{t}Z$ cross sections measured at parton level as a function of **a** the rapidity difference ($|\Delta y|$) between the Z boson and the reconstructed top quark and **b** the azimuthal separation ($\Delta\phi$) between the two leptons associated with the top-quark pair. **c**, **d** Show the relative contributions from different categories of systematic uncertainties per bin

of the normalised measurements are generally negative and reach absolute values even larger than in the absolute cross-section measurements, with the most extreme case being a value of $\rho = -0.76$ between the first and second bin of the $|\Delta y(Z, t_{\text{lep}})|$ variable in the trilepton channel. For the Z-related variables in the combined channel, the effect of the larger data sample is partially balanced by the increase in the number of bins, such that the correlations in the absolute measurements for p_{T}^Z and $|y^Z|$ are also positive, but lie in the 15–45% range. In the normalised measurements for these two variables, the correlations are also mostly negative but are smaller in magnitude than for other variables (strictly $|\rho| < 40\%$, but in most cases $|\rho| < 20\%$).

Table 9 summarises the evaluated χ^2/ndf and p values used to quantify the compatibility between the measured unfolded data and the various predictions. For the parton-

level measurements, the values for the additional theory predictions at NLO, NLO+NNLL or nNLO are also shown for those variables for which predictions are available [18].

Overall, the unfolded spectra from the measured data are compatible with the various predictions for most of the variables considered. For the p_{T}^Z variable in the combined $3\ell + 4\ell$ channel, as well as for $p_{\text{T}}^{\ell, \text{non-}Z}$ and $|\Delta\phi(Z, t_{\text{lep}})|$ in the trilepton channel, slightly lower p values are obtained for several predictions, but in all cases they are found to be greater than 0.05. For the p_{T}^Z variable in the combined channel, the slightly poorer agreement is driven in large part by the sixth bin ($220\,\text{GeV} \leq p_{\text{T}}^Z < 290\,\text{GeV}$). For this variable, however, the p value is larger (0.17) for the additional NLO+NNLL prediction in the absolute differential measurement. For the $|\Delta\phi(t\bar{t}, Z)|$ variable in the tetralepton channel, for which the data exhibit a greater relative fraction of
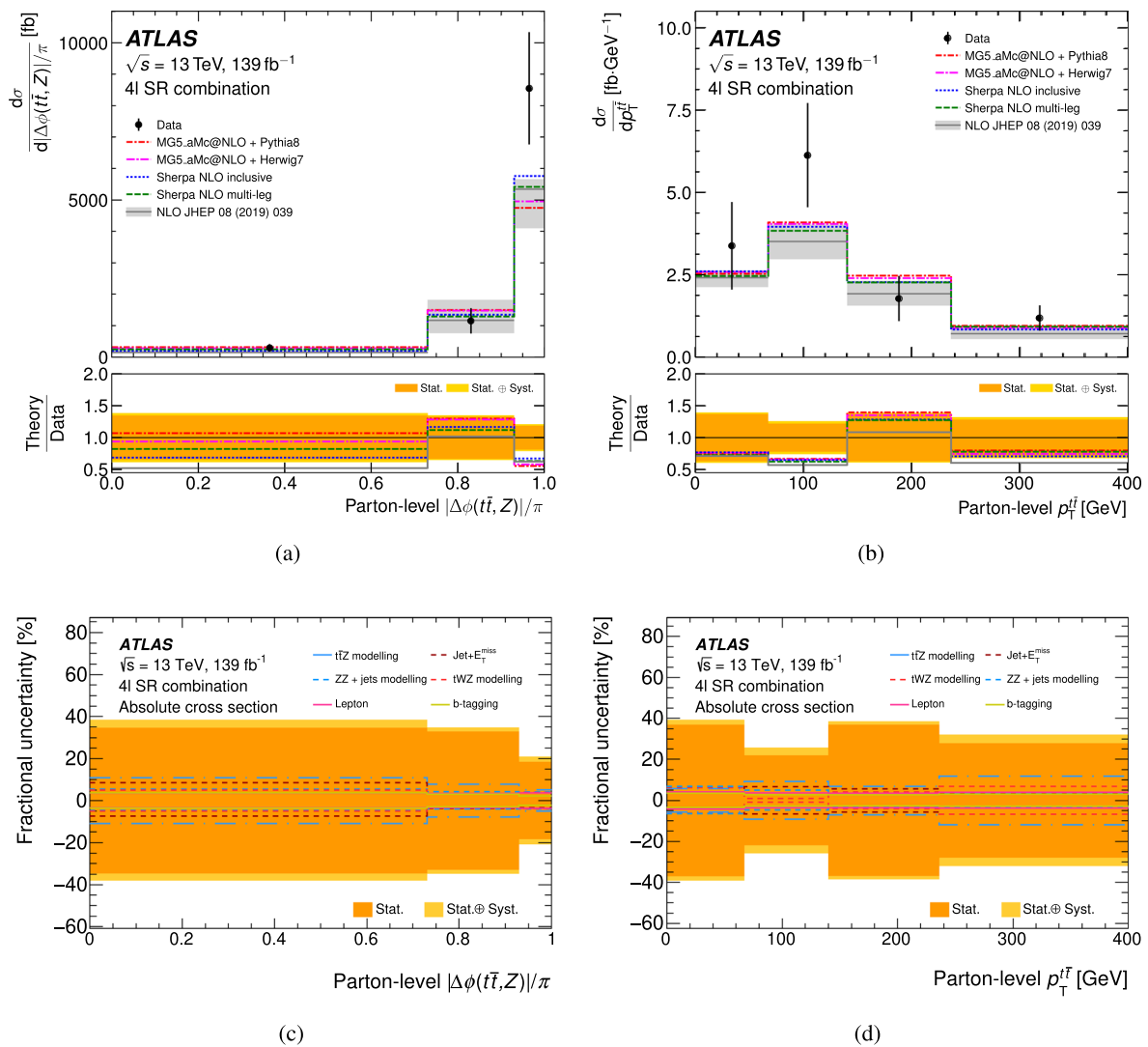
Fig. 15 Absolute differential $t\bar{t}Z$ cross sections measured at parton level as a function of **a** the azimuthal separation ($\Delta\phi$) between the Z boson and the reconstructed $t\bar{t}$ system and **b** the p_{T} of the $t\bar{t}$ system. **c**, **d** Show the relative contributions from different categories of systematic uncertainties per bin

events with larger azimuthal separation between the Z boson and the $t\bar{t}$ system, a slightly better level of agreement is observed for the SHERPA predictions compared with those from MG5_AMC@NLO. As the statistical uncertainties of the measured data are almost always significantly larger than the differences between the predictions, no definite conclusion about the overall compatibility for these observables can be made. The effect of the uncertainties in the fixed-order parton-level theoretical predictions in the rightmost column of Table 9 was evaluated. This was done by adding terms of the form $\delta\mu_i\delta\mu_j$ to the covariance matrix, where $\delta\mu_{i(j)}$ is the sum in quadrature of the uncertainties associated with the scale and PDF choice for bin $i(j)$. The bin contents of the theoretical predictions were, therefore, considered to be 100% correlated. The inclusion of these uncertainties leads to a relative increase of 20–50% in the p values for the variables

$|\Delta\phi(Z, t_{\mathrm{lep}})|$, $|\Delta\phi(t\bar{t}, Z)|$, and $p_{\mathrm{T}}^{t\bar{t}}$ relative to those quoted in Table 9. For the variables $|\Delta y(Z, t_{\mathrm{lep}})|$, p_{T}^Z, and $|y^Z|$, the impact is negligible.

A difference between the measured inclusive cross section quoted in Sect. 8 and the cross section based on the integrated absolute parton-level spectra in the combined $3\ell + 4\ell$ channel is observed. The two measurements differ both in terms of the method used and in their selection due to the use of different b-tagging WPs (refer to Table 1). Approximately 67% of selected data events are common to both measurements. The compatibility between the two cross-section measurements is evaluated using pseudo-experiments taking into account the correlation between uncertainties, including all sources of statistical and systematic effects, and it is found to be at the level of two standard deviations.

Table 9 Summary of the tests of compatibility between the unfolded differential measurements and the various predictions. Quoted are the χ^2/ndf and corresponding p values incorporating all bins for the given variable and based on the assumption that all sources of uncertainty are Gaussian-distributed. The values associated with the additional theory predictions (last column) are included where applicable. These additional predictions are obtained in Ref. [18], with their precisions depending on the particular variable: NLO for $|\Delta\phi(t\bar{t}, Z)|$ and $p_T^{t\bar{t}}$; NLO+NNLL for $|\Delta\phi(Z, t_{\text{lep}})|$, $|\Delta y(Z, t_{\text{lep}})|$ and p_T^Z; and nNLO for $|y^Z|$

Variable	Particle	Parton	Absolute	Normalised	Figure	MG5_AMC@NLO 2.3.3 + PYTHIA 8		MG5_AMC@NLO 2.3.3 + HERWIG 7		SHERPA 2.2.1 NLO multi-leg		SHERPA 2.2.1 NLO inclusive		Additional theory	
						χ^2/ndf	p value	χ^2/ndf	p value	χ^2/ndf	p value	χ^2/ndf	p value	χ^2/ndf	p value
$3\ell + 4\ell$															
p_T^Z	✓		✓		9a	12.8/7	0.08	12.0/7	0.10	11.6/7	0.11	12.1/7	0.10	–	–
p_T^Z		✓	✓		9b	12.8/7	0.08	11.7/7	0.11	11.2/7	0.13	11.3/7	0.13	10.4/7	0.17
p_T^Z	✓			✓	10a	11.0/6	0.09	10.8/6	0.09	10.6/6	0.10	10.7/6	0.10	–	–
p_T^Z		✓		✓	10b	11.0/6	0.09	10.8/6	0.10	10.7/6	0.10	10.6/6	0.10	10.5/6	0.11
$|y^Z|$		✓	✓		11a	2.8/8	0.95	2.9/8	0.94	4.0/8	0.85	2.7/8	0.95	2.9/8	0.94
3ℓ															
N_{jets}	✓		✓		12a	0.8/3	0.85	0.6/3	0.90	0.3/3	0.95	0.5/3	0.92	–	–
$p_T^{\ell,\text{non-}Z}$		✓	✓		13a	7.6/4	0.11	8.8/4	0.07	8.3/4	0.08	8.6/4	0.07	–	–
$|\Delta\phi(Z, t_{\text{lep}})|$		✓	✓		13b	5.5/3	0.14	5.8/3	0.12	5.2/3	0.16	6.9/3	0.07	6.6/3	0.09
$|\Delta y(Z, t_{\text{lep}})|$		✓	✓		14a	0.9/3	0.82	0.7/3	0.88	0.2/3	0.98	0.5/3	0.92	0.3/3	0.96
4ℓ															
N_{jets}	✓		✓		12b	1.4/4	0.84	1.7/4	0.79	2.8/4	0.59	2.8/4	0.59	–	–
$|\Delta\phi(\ell_t^+, \ell_{\bar{t}}^-)|$		✓	✓		14b	2.1/4	0.72	2.3/4	0.69	2.7/4	0.62	2.6/4	0.63	–	–
$|\Delta\phi(t\bar{t}, Z)|$		✓	✓		15a	5.2/3	0.16	4.7/3	0.19	3.5/3	0.32	3.4/3	0.33	4.9/3	0.18
$p_T^{t\bar{t}}$		✓	✓		15b	3.5/4	0.47	3.6/4	0.47	3.5/4	0.48	3.5/4	0.47	4.6/4	0.33

10 Conclusions

Inclusive and differential measurements of the production cross section of a $t\bar{t}$ pair in association with a Z boson are presented. The full $\sqrt{s} = 13$ TeV pp collision data set collected by the ATLAS detector during Run 2 of the LHC between 2015 and 2018, corresponding to 139 fb^{-1}, was used for this analysis. Only final states with three or four isolated charged leptons (electrons or muons) were considered for the measurements. The measured inclusive cross section of the $t\bar{t}Z$ process is $\sigma_{t\bar{t}Z} = 0.99 \pm 0.05$ (stat.) ± 0.08 (syst.) pb, in agreement with the SM prediction. The dominant sources of systematic uncertainty in this measurement are associated with the $t\bar{t}Z$ parton-shower modelling, b-tagging, and modelling of the tWZ background.

Absolute and normalised differential cross sections were measured as functions of nine different observables sensitive to the MC modelling of the $t\bar{t}Z$ process and to potential BSM effects. The differential cross-section measurements were performed at particle and parton levels in specific fiducial volumes. The unfolded spectra from the measured data are compared with the predictions of different NLO QCD $t\bar{t}Z$ MC generators and theoretical predictions at NLO, NLO + NNLL and nNLO precision, based on a χ^2/ndf and p value compatibility test. For most of the considered observables, good agreement between data and the predictions is observed. The differences between the various predictions are determined to be smaller than the uncertainties of the unfolded data. For the variables $p_{\rm T}^Z$, $p_{\rm T}^{\ell,{\rm non-}Z}$, $|\Delta\phi(Z, t_{\rm lep})|$ and $|\Delta\phi(t\bar{t}, Z)|$, the observed and predicted differential results show slightly poorer agreement, but p values > 0.05 are obtained in all cases.

References

1. ATLAS Collaboration, Measurements of top-quark pair differential and double-differential cross-sections in the ℓ+jets channel with pp collisions at $\sqrt{s} = 13$ TeV using the ATLAS detector. Eur. Phys. J. C **79**, 1028 (2019). https://doi.org/10.1140/epjc/s10052-019-7525-6. arXiv:1908.07305 [hep-ex] (**Erratum: Eur. Phys. J. C 80 (2020) 1092**)
2. CMS Collaboration, Measurement of $t\bar{t}$ normalised multi-differential cross sections in pp collisions at $\sqrt{s} = 13$ TeV, and simultaneous determination of the strong coupling strength, top quark pole mass, and parton distribution functions. Eur. Phys. J. C **80**, 658 (2020). https://doi.org/10.1140/epjc/s10052-020-7917-7. arXiv:1904.05237 [hep-ex]
3. ATLAS and CMS Collaborations, Combinations of single-top-quark production cross-section measurements and $|f_{LV} V_{tb}|$ determinations at $\sqrt{s} = 7$ and 8 TeV with the ATLAS and

CMS experiments. JHEP **05**, 088 (2019). https://doi.org/10.1007/JHEP05(2019)088. arXiv:1902.07158 [hep-ex]

4. ATLAS Collaboration, Measurement of the top quark mass in the $t\bar{t} \to$ dilepton channel from $\sqrt{s} = 8$ TeV ATLAS data. Phys. Lett. B **761**, 350 (2016). https://doi.org/10.1016/j.physletb.2016.08.042. arXiv:1606.02179 [hep-ex]

5. A. Buckley et al., Constraining top quark effective theory in the LHC Run II era. JHEP **04**, 015 (2016). https://doi.org/10.1007/JHEP04(2016)015. arXiv:1512.03360 [hep-ph]

6. J.A. Dror, M. Farina, E. Salvioni, J. Serra, Strong tW scattering at the LHC. JHEP **01**, 071 (2016). https://doi.org/10.1007/JHEP01(2016)071. arXiv:1511.03674 [hep-ph]

7. O.B. Bylund, F. Maltoni, I. Tsinikos, E. Vryonidou, C. Zhang, Probing top quark neutral couplings in the standard model effective field theory at NLO QCD. JHEP **05**, 052 (2016). https://doi.org/10.1007/JHEP05(2016)052. arXiv:1601.08193 [hep-ph]

8. S. Schael et al., Precision electroweak measurements on the Z resonance. Phys. Rep. **427**, 257 (2006). https://doi.org/10.1016/j.physrep.2005.12.006. arXiv:hep-ex/0509008

9. F. Richard, Present and future constraints on top EW couplings (2014). arXiv:1403.2893 [hep-ph]

10. ATLAS Collaboration, Search for new phenomena in events with same-charge leptons and b-jets in pp collisions at $\sqrt{s} = 13$ TeV with the ATLAS detector. JHEP **12**, 039 (2018). https://doi.org/10.1007/JHEP12(2018)039. arXiv:1807.11883 [hep-ex]

11. ATLAS Collaboration, Search for squarks and gluinos in final states with same-sign leptons and jets using 139 fb^{-1} of data collected with the ATLAS detector. JHEP **06**, 046 (2020). https://doi.org/10.1007/JHEP06(2020)046. arXiv:1909.08457 [hep-ex]

12. ATLAS Collaboration, Observation of Higgs boson production in association with a top quark pair at the LHC with the ATLAS detector. Phys. Lett. B **784**, 173 (2018). https://doi.org/10.1016/j.physletb.2018.07.035. arXiv:1806.00425 [hep-ex]

13. ATLAS Collaboration, Observation of the associated production of a top quark and a Z boson in pp collisions at $\sqrt{s} = 13$ TeV with the ATLAS detector. JHEP **07**, 124 (2020). https://doi.org/10.1007/JHEP07(2020)124. arXiv:2002.07546 [hep-ex]

14. ATLAS Collaboration, Measurement of the $t\bar{t}Z$ and $t\bar{t}W$ cross sections in proton–proton collisions at $\sqrt{s} = 13$ TeV with the ATLAS detector. Phys. Rev. D **99**, 072009 (2019). https://doi.org/10.1103/PhysRevD.99.072009. arXiv:1901.03584 [hep-ex]

15. CMS Collaboration, Measurement of top quark pair production in association with a Z boson in proton-proton collisions at $\sqrt{s} = 13$ TeV. JHEP **03**, 056 (2020). https://doi.org/10.1007/JHEP03(2020)056. arXiv:1907.11270 [hep-ex]

16. A. Broggio, A. Ferroglia, G. Ossola, B.D. Pecjak, R.D. Sameshima, Associated production of a top pair and a Z boson at the LHC to NNLL accuracy. JHEP **04**, 105 (2017). https://doi.org/10.1007/JHEP04(2017)105. arXiv:1702.00800 [hep-ph]

17. A. Kulesza, L. Motyka, D. Schwartländer, T. Stebel, V. Theeuwes, Associated production of a top quark pair with a heavy electroweak gauge boson at $NLO + NNLL$ accuracy. Eur. Phys. J. C **79**, 249 (2019). https://doi.org/10.1140/epjc/s10052-019-6746-z. arXiv:1812.08622 [hep-ph]

18. A. Broggio et al., Top-quark pair hadroproduction in association with a heavy boson at NLO+NNLL including EW corrections. JHEP **08**, 039 (2019). https://doi.org/10.1007/JHEP08(2019)039 arXiv:1907.04343 [hep-ph], We express particular thanks to the authors of for providing additional custom theoretical predictions for comparison with the differential measurements

19. A. Kulesza, L. Motyka, D. Schwartländer, T. Stebel, V. Theeuwes, Associated top quark pair production with a heavy boson: differential cross sections at NLO+NNLL accuracy. Eur. Phys. J. C **80**, 428 (2020). https://doi.org/10.1140/epjc/s10052-020-7987-6. arXiv:2001.03031 [hep-ph]

20. R. Frederix et al., The automation of next-to-leading order electroweak calculations. JHEP **07**, 185 (2018). https://doi.org/10.1007/JHEP07(2018)185. arXiv:1804.10017 [hep-ph]

21. ATLAS Collaboration, The ATLAS experiment at the CERN large hadron collider. JINST **3**, S08003 (2008). https://doi.org/10.1088/1748-0221/3/08/S08003

22. ATLAS Collaboration, Studies on top-quark Monte Carlo modelling with Sherpa and MG5_aMC@NLO, ATL-PHYS-PUB-2017-007, (2017). https://cds.cern.ch/record/2261938

23. ATLAS Collaboration, Improvements in $t\bar{t}$ modelling using NLO+PS Monte Carlo generators for Run 2, ATL-PHYS-PUB-2018-009 (2018). https://cds.cern.ch/record/2630327

24. ATLAS Collaboration, ATLAS Insertable B-Layer Technical Design Report, ATLAS-TDR-19; CERN-LHCC-2010-013, (2010). https://cds.cern.ch/record/1291633, Addendum: ATLAS-TDR-19-ADD-1; CERN-LHCC-2012-009, 2012. https://cds.cern.ch/record/1451888

25. B. Abbott et al., Production and integration of the ATLAS Insertable B-Layer. JINST **13**, T05008 (2018). https://doi.org/10.1088/1748-0221/13/05/T05008. arXiv:1803.00844 [physics.ins-det]

26. ATLAS Collaboration, Performance of the ATLAS trigger system in 2015. Eur. Phys. J. C **77**, 317 (2017). https://doi.org/10.1140/epjc/s10052-017-4852-3. arXiv:1611.09661 [hep-ex]

27. ATLAS Collaboration, Luminosity determination in pp collisions at $\sqrt{s} = 8$ TeV using the ATLAS detector at the LHC. Eur. Phys. J. C **76** 653 (2016). https://doi.org/10.1140/epjc/s10052-016-4466-1. arXiv:1608.03953 [hep-ex]

28. G. Avoni et al., The new LUCID-2 detector for luminosity measurement and monitoring in ATLAS. JINST **13**, P07017 (2018). https://doi.org/10.1088/1748-0221/13/07/P07017

29. ATLAS Collaboration, 2015 start-up trigger menu and initial performance assessment of the ATLAS trigger using Run-2 data, ATL-DAQ-PUB-2016-001 (2016). https://cds.cern.ch/record/2136007

30. ATLAS Collaboration, Trigger Menu in 2016, ATL-DAQ-PUB-2017-001 (2017). https://cds.cern.ch/record/2242069

31. ATLAS Collaboration, Trigger Menu in 2017, ATL-DAQ-PUB-2018-002 (2018). https://cds.cern.ch/record/2625986

32. T. Sjöstrand, S. Mrenna, P. Skands, A brief introduction to PYTHIA 8.1. Comput. Phys. Commun. **178**, 852 (2008). https://doi.org/10.1016/j.cpc.2008.01.036. arXiv:0710.3820 [hep-ph]

33. R.D. Ball et al., Parton distributions with LHC data. Nucl. Phys. B **867**, 244 (2013). https://doi.org/10.1016/j.nuclphysb.2012.10.003. arXiv:1207.1303 [hep-ph]

34. ATLAS Collaboration, The Pythia 8 A3 tune description of ATLAS minimum bias and inelastic measurements incorporating the Donnachie–Landshoff diffractive model, ATL-PHYS-PUB-2016-017 (2016). https://cds.cern.ch/record/2206965

35. Particle Data Group, Review of Particle Physics. PTEP **8**, 083C01 (2020). https://doi.org/10.1093/ptep/ptaa104

36. D.J. Lange, The EvtGen particle decay simulation package. Nucl. Instrum. Methods A **462**, 152 (2001). https://doi.org/10.1016/S0168-9002(01)00089-4

37. ATLAS Collaboration, The ATLAS Simulation Infrastructure. Eur. Phys. J. C **70**, 823 (2010). https://doi.org/10.1140/epjc/s10052-010-1429-9. arXiv:1005.4568 [physics.ins-det]

38. GEANT4 Collaboration, S. Agostinelli et al., Geant4: a simulation toolkit. Nucl. Instrum. Methods A **506**, 250 (2003). https://doi.org/10.1016/S0168-9002(03)01368-8

39. ATLAS Collaboration, The simulation principle and performance of the ATLAS fast calorimeter simulation FastCaloSim, ATL-PHYS-PUB-2010-013 (2010). https://cds.cern.ch/record/1300517

40. ATLAS Collaboration, The new Fast Calorimeter Simulation in ATLAS, ATL-SOFT-PUB-2018-002 (2018). https://cds.cern.ch/record/2630434

41. J. Alwall et al., The automated computation of tree-level and next-to-leading order differential cross sections, and their matching to parton shower simulations. JHEP **07**, 079 (2014). https://doi.org/10.1007/JHEP07(2014)079. arXiv:1405.0301 [hep-ph]

42. R.D. Ball et al., Parton distributions for the LHC run II. JHEP **04**, 040 (2015). https://doi.org/10.1007/JHEP04(2015)040. arXiv:1410.8849 [hep-ph]

43. S. Frixione, E. Laenen, P. Motylinski, B.R. Webber, Angular correlations of lepton pairs from vector boson and top quark decays in Monte Carlo simulations. JHEP **04**, 081 (2007). https://doi.org/10.1088/1126-6708/2007/04/081. arXiv:hep-ph/0702198

44. P. Artoisenet, R. Frederix, O. Mattelaer, R. Rietkerk, Automatic spin-entangled decays of heavy resonances in Monte Carlo simulations. JHEP **03**, 015 (2013). https://doi.org/10.1007/JHEP03(2013)015. arXiv:1212.3460 [hep-ph]

45. T. Sjöstrand et al., An introduction to PYTHIA 8.2. Comput. Phys. Commun. **191**, 159 (2015). https://doi.org/10.1016/j.cpc.2015.01.024. arXiv:1410.3012 [hep-ph]

46. ATLAS Collaboration, ATLAS Pythia 8 tunes to 7 TeV data, ATL-PHYS-PUB-2014-021 (2014). https://cds.cern.ch/record/1966419

47. ATLAS Collaboration, Modelling of the $t\bar{t}H$ and $t\bar{t}V(V = W, Z)$ processes for $\sqrt{s} = 13$ TeV ATLAS analyses, ATL-PHYS-PUB-2016-005 (2016). https://cds.cern.ch/record/2120826

48. D. de Florian et al., Handbook of LHC Higgs cross sections: 4. Deciphering the Nature of the Higgs Sector (2016). https://doi.org/10.23731/CYRM-2017-002. arXiv:1610.07922 [hep-ph]

49. S. Frixione, V. Hirschi, D. Pagani, H.-S. Shao, M. Zaro, Electroweak and QCD corrections to top-pair hadroproduction in association with heavy bosons. JHEP **06**, 184 (2015). https://doi.org/10.1007/JHEP06(2015)184. arXiv:1504.03446 [hep-ph]

50. E. Bothmann et al., Event generation with Sherpa 2.2. SciPost Phys. **7**, 034 (2019). https://doi.org/10.21468/SciPostPhys.7.3.034. arXiv:1905.09127 [hep-ph]

51. S. Höche, F. Krauss, M. Schönherr, F. Siegert, A critical appraisal of NLO+PS matching methods. JHEP **09**, 049 (2012). https://doi.org/10.1007/JHEP09(2012)049. arXiv:1111.1220 [hep-ph]

52. S. Höche, F. Krauss, M. Schönherr, F. Siegert, QCD matrix elements + parton showers. The NLO case. JHEP **04**, 027 (2013). https://doi.org/10.1007/JHEP04(2013)027. arXiv:1207.5030 [hep-ph]

53. S. Catani, F. Krauss, R. Kuhn, B.R. Webber, QCD Matrix Elements + Parton Showers. JHEP **11**, 063 (2001). https://doi.org/10.1088/1126-6708/2001/11/063. arXiv:hep-ph/0109231

54. S. Höche, F. Krauss, S. Schumann, F. Siegert, QCD matrix elements and truncated showers. JHEP **05**, 053 (2009). https://doi.org/10.1088/1126-6708/2009/05/053. arXiv:0903.1219 [hep-ph]

55. M. Bähr et al., Herwig++ physics and manual. Eur. Phys. J. C **58**, 639 (2008). https://doi.org/10.1140/epjc/s10052-008-0798-9. arXiv:0803.0883 [hep-ph]

56. J. Bellm et al., Herwig 7.0/Herwig++ 3.0 release note. Eur. Phys. J. C **76**, 196 (2016). https://doi.org/10.1140/epjc/s10052-016-4018-8. arXiv:1512.01178 [hep-ph]

57. F. Demartin, B. Maier, F. Maltoni, K. Mawatari, M. Zaro, tWH associated production at the LHC. Eur. Phys. J. C **77**, 34 (2017). https://doi.org/10.1140/epjc/s10052-017-4601-7. arXiv:1607.05862 [hep-ph]

58. T. Gleisberg, S. Höche, Comix, a new matrix element generator. JHEP **12**, 039 (2008). https://doi.org/10.1088/1126-6708/2008/12/039. arXiv:0808.3674 [hep-ph]

59. S. Schumann, F. Krauss, A parton shower algorithm based on Catani–Seymour dipole factorisation. JHEP **03**, 038 (2008). https://doi.org/10.1088/1126-6708/2008/03/038. arXiv:0709.1027 [hep-ph]

60. F. Cascioli, P. Maierhöfer, S. Pozzorini, Scattering amplitudes with open loops. Phys. Rev. Lett. **108**, 111601 (2012). https://doi.org/10.1103/PhysRevLett.108.111601. arXiv:1111.5206 [hep-ph]

61. A. Denner, S. Dittmaier, L. Hofer, Collier: a fortran-based complex one-loop library in extended regularizations. Comput. Phys. Commun. **212**, 220 (2017). https://doi.org/10.1016/j.cpc.2016.10.013. arXiv:1604.06792 [hep-ph]

62. ATLAS Collaboration, Electron reconstruction and identification in the ATLAS experiment using the 2015 and 2016 LHC proton–proton collision data at $\sqrt{s} = 13$ TeV. Eur. Phys. J. C **79**, 639 (2019). https://doi.org/10.1140/epjc/s10052-019-7140-6. arXiv:1902.04655 [hep-ex]

63. ATLAS Collaboration, Electron and photon performance measurements with the ATLAS detector using the 2015–2017 LHC proton–proton collision data. JINST **14**, P12006 (2019). https://doi.org/10.1088/1748-0221/14/12/P12006. arXiv:1908.00005 [hep-ex]

64. ATLAS Collaboration, Muon reconstruction performance of the ATLAS detector in proton–proton collision data at $\sqrt{s} = 13$ TeV. Eur. Phys. J. C **76**, 292 (2016). https://doi.org/10.1140/epjc/s10052-016-4120-y. arXiv:1603.05598 [hep-ex]

65. ATLAS Collaboration, Muon reconstruction and identification efficiency in ATLAS using the full Run 2 pp collision data set at $\sqrt{s} = 13$ TeV (2020). arXiv:2012.00578 [hep-ex]

66. ATLAS Collaboration, Topological cell clustering in the ATLAS calorimeters and its performance in LHC Run 1. Eur. Phys. J. C **77**, 490 (2017). https://doi.org/10.1140/epjc/s10052-017-5004-5. arXiv:1603.02934 [hep-ex]

67. M. Cacciari, G.P. Salam, G. Soyez, The anti-k_t jet clustering algorithm. JHEP **04**, 063 (2008). https://doi.org/10.1088/1126-6708/2008/04/063. arXiv:0802.1189 [hep-ph]

68. M. Cacciari, G.P. Salam, G. Soyez, FastJet user manual. Eur. Phys. J. C **72**, 1896 (2012). https://doi.org/10.1140/epjc/s10052-012-1896-2. arXiv:1111.6097 [hep-ph]

69. ATLAS Collaboration, Jet energy scale measurements and their systematic uncertainties in proton–proton collisions at $\sqrt{s} = 13$ TeV with the ATLAS detector. Phys. Rev. D **96** 072002 (2017). https://doi.org/10.1103/PhysRevD.96.072002. arXiv:1703.09665 [hep-ex]

70. ATLAS Collaboration, Performance of pile-up mitigation techniques for jets in pp collisions at $\sqrt{s} = 8$ TeV using the ATLAS detector. Eur. Phys. J. C **76**, 581 (2016). https://doi.org/10.1140/epjc/s10052-016-4395-z. arXiv:1510.03823 [hep-ex]

71. ATLAS Collaboration, ATLAS b-jet identification performance and efficiency measurement with $t\bar{t}$ events in pp collisions at $\sqrt{s} = 13$ TeV. Eur. Phys. J. C **79**, 970 (2019). https://doi.org/10.1140/epjc/s10052-019-7450-8. arXiv:1907.05120 [hep-ex]

72. ATLAS Collaboration, Performance of missing transverse momentum reconstruction with the ATLAS detector using proton–proton collisions at $\sqrt{s} = 13$ TeV. Eur. Phys. J. C **78**, 903 (2018). https://doi.org/10.1140/epjc/s10052-018-6288-9. arXiv:1802.08168 [hep-ex]

73. M. Cacciari, G.P. Salam, G. Soyez, The catchment area of jets. JHEP **04**, 005 (2008). https://doi.org/10.1088/1126-6708/2008/04/005. arXiv:0802.1188 [hep-ph]

74. ATLAS Collaboration, Estimation of non-prompt and fake lepton backgrounds in final states with top quarks produced in proton–proton collisions at $\sqrt{s} = 8$ TeV with the ATLAS Detector, ATLAS-CONF-2014-058 (2014). https://cds.cern.ch/record/1951336

75. ATLAS Collaboration, Search for supersymmetry at $\sqrt{s} = 8$ TeV in final states with jets and two same-sign leptons or three leptons with the ATLAS detector. JHEP **06**, 035 (2014). https://doi.org/10.1007/JHEP06(2014)035. arXiv:1404.2500 [hep-ex]

76. E.W. Varnes, A Poisson likelihood approach to fake lepton estimation with the matrix method (2016). arXiv:1606.06817 [hep-ex]

77. ATLAS Collaboration, Luminosity determination in pp collisions at $\sqrt{s} = 13$ TeV using the ATLAS detector at the LHC, ATLAS-CONF-2019-021 (2019). https://cds.cern.ch/record/2677054

78. ATLAS Collaboration, Jet energy scale and resolution measured in proton–proton collisions at $\sqrt{s} = 13$ TeV with the ATLAS detector (2020). arXiv:2007.02645 [hep-ex]

79. ATLAS Collaboration, Measurement of b-tagging efficiency of c-jets in $t\bar{t}$ events using a likelihood approach with the ATLAS detector, ATLAS-CONF-2018-001 (2018). https://cds.cern.ch/record/2306649

80. ATLAS Collaboration, Calibration of light-flavour b-jet mistagging rates using ATLAS proton–proton collision data at $\sqrt{s} = 13$ TeV, ATLAS-CONF-2018-006 (2018). https://cds.cern.ch/record/2314418

81. J. Butterworth et al., PDF4LHC recommendations for LHC Run II. J. Phys. G **43**, 023001 (2016). https://doi.org/10.1088/0954-3899/43/2/023001. arXiv:1510.03865 [hep-ph]

82. ATLAS Collaboration, Measurements of the production cross-section for a Z boson in association with b-jets in proton–proton collisions at $\sqrt{s} = 13$ TeV with the ATLAS detector. JHEP **07**, 044 (2020). https://doi.org/10.1007/JHEP07(2020)044. arXiv:2003.11960 [hep-ex]

83. ATLAS Collaboration, Measurement of the production cross-section of a single top quark in association with a Z boson in proton–proton collisions at 13 TeV with the ATLAS detector. Phys. Lett. B **780**, 557 (2018). https://doi.org/10.1016/j.physletb.2018.03.023. arXiv:1710.03659 [hep-ex]

84. CMS Collaboration, Measurement of the associated production of a single top quark and a Z boson in pp collisions at $\sqrt{s} = 13$ TeV. Phys. Lett. B **779**, 358 (2018). https://doi.org/10.1016/j.physletb.2018.02.025. arXiv:1712.02825 [hep-ex]

85. G. Cowan, K. Cranmer, E. Gross, O. Vitells, Asymptotic formulae for likelihood-based tests of new physics. Eur. Phys. J. C **71**, 1554 (2011). https://doi.org/10.1140/epjc/s10052-011-1554-0. arXiv:1007.1727 [physics.data-an]. https://doi.org/10.1140/epjc/s10052-013-2501-z (**Erratum: Eur. Phys. J. C 73 (2013) 2501**)

86. A.L. Read, Presentation of search results: the CL_S technique. J. Phys. G **28**, 2693 (2002). https://doi.org/10.1088/0954-3899/28/10/313

87. W. Verkerke, D. Kirkby, The RooFit toolkit for data modeling (2003). arXiv:physics/0306116 [physics.data-an]

88. G. D'Agostini, A multidimensional unfolding method based on Bayes' theorem. Nucl. Instrum. Methods A **362**, 487 (1995). https://doi.org/10.1016/0168-9002(95)00274-X. issn: 0168-9002

89. T. Adye, Unfolding algorithms and tests using RooUnfold. Proceedings, 2011 Workshop on Statistical Issues Related to Discovery Claims in Search Experiments and Unfolding (CERN, Geneva, Switzerland, 17th–20th Jan. 2011) 313, https://doi.org/10.5170/CERN-2011-006.313. arXiv:1105.1160 [physics.data-an]

90. ATLAS Collaboration, Measurements of top-quark pair single- and double-differential cross-sections in the all-hadronic channel in pp collisions at $\sqrt{s} = 13$ TeV using the ATLAS detector. JHEP **01**, 033 (2021). https://doi.org/10.1007/JHEP01(2021)033. arXiv:2006.09274 [hep-ex]

91. ATLAS Collaboration, ATLAS Computing Acknowledgements, ATL-SOFT-PUB-2020-001. https://cds.cern.ch/record/2717821

ATLAS Collaboration

G. Aad[102], B. Abbott[128], D. C. Abbott[103], A. Abed Abud[36], K. Abeling[53], D. K. Abhayasinghe[94], S. H. Abidi[167], O. S. AbouZeid[40], N. L. Abraham[156], H. Abramowicz[161], H. Abreu[160], Y. Abulaiti[6], B. S. Acharya[67a,67b,n], B. Achkar[53], L. Adam[100], C. Adam Bourdarios[5], L. Adamczyk[84a], L. Adamek[167], J. Adelman[121], A. Adiguzel[12c,ac], S. Adorni[54], T. Adye[143], A. A. Affolder[145], Y. Afik[160], C. Agapopoulou[65], M. N. Agaras[38], A. Aggarwal[119], C. Agheorghiesei[27c], J. A. Aguilar-Saavedra[139a,139f,ab], A. Ahmad[36], F. Ahmadov[80], W. S. Ahmed[104], X. Ai[18], G. Aielli[74a,74b], S. Akatsuka[86], M. Akbiyik[100], T. P. A. Åkesson[97], E. Akilli[54], A. V. Akimov[111], K. Al Khoury[65], G. L. Alberghi[23a,23b], J. Albert[176], M. J. Alconada Verzini[161], S. Alderweireldt[36], M. Aleksa[36], I. N. Aleksandrov[80], C. Alexa[27b], T. Alexopoulos[10], A. Alfonsi[120], F. Alfonsi[23a,23b], M. Alhroob[128], B. Ali[141], S. Ali[158], M. Aliev[166], G. Alimonti[69a], C. Allaire[36], B. M. M. Allbrooke[156], B. W. Allen[131], P. P. Allport[21], A. Aloisio[70a,70b], F. Alonso[89], C. Alpigiani[148], E. Alunno Camelia[74a,74b], M. Alvarez Estevez[99], M. G. Alviggi[70a,70b], Y. Amaral Coutinho[81b], A. Ambler[104], L. Ambroz[134], C. Amelung[36], D. Amidei[106], S. P. Amor Dos Santos[139a], S. Amoroso[46], C. S. Amrouche[54], F. An[79], C. Anastopoulos[149], N. Andari[144], T. Andeen[11], J. K. Anders[20], S. Y. Andrean[45a,45b], A. Andreazza[69a,69b], V. Andrei[61a], C. R. Anelli[176], S. Angelidakis[9], A. Angerami[39], A. V. Anisenkov[122a,122b], A. Annovi[72a], C. Antel[54], M. T. Anthony[149], E. Antipov[129], M. Antonelli[51], D. J. A. Antrim[18], F. Anulli[73a], M. Aoki[82], J. A. Aparisi Pozo[174], M. A. Aparo[156], L. Aperio Bella[46], N. Aranzabal[36], V. Araujo Ferraz[81a], R. Araujo Pereira[81b], C. Arcangeletti[51], A. T. H. Arce[49], J.-F. Arguin[110], S. Argyropoulos[52], J.-H. Arling[46], A. J. Armbruster[36], A. Armstrong[171], O. Arnaez[167], H. Arnold[120], Z. P. Arrubarrena Tame[114], G. Artoni[134], H. Asada[117], K. Asai[126], S. Asai[163], T. Asawatavonvanich[165], N. A. Asbah[59], E. M. Asimakopoulou[172], L. Asquith[156], J. Assahsah[35d], K. Assamagan[29], R. Astalos[28a], R. J. Atkin[33a], M. Atkinson[173], N. B. Atlay[19], H. Atmani[65], P. A. Atmasiddha[106], K. Augsten[141], V. A. Austrup[182], G. Avolio[36], M. K. Ayoub[15a], G. Azuelos[110,aj], D. Babal[28a], H. Bachacou[144], K. Bachas[162], F. Backman[45a,45b], P. Bagnaia[73a,73b], H. Bahrasemani[152], A. J. Bailey[174], V. R. Bailey[173], J. T. Baines[143], C. Bakalis[10], O. K. Baker[183], P. J. Bakker[120], E. Bakos[16], D. Bakshi Gupta[8], S. Balaji[157], R. Balasubramanian[120], E. M. Baldin[122a,122b], P. Balek[180], F. Balli[144], W. K. Balunas[134], J. Balz[100], E. Banas[85], M. Bandieramonte[138], A. Bandyopadhyay[19], Sw. Banerjee[181,i], L. Barak[161], W. M. Barbe[38], E. L. Barberio[105], D. Barberis[55a,55b], M. Barbero[102], G. Barbour[95], T. Barillari[115], M-S. Barisits[36], J. Barkeloo[131], T. Barklow[153], R. Barnea[160],

B. M. Barnett[143], R. M. Barnett[18], Z. Barnovska-Blenessy[60a], A. Baroncelli[60a], G. Barone[29], A. J. Barr[134], L. Barranco Navarro[45a,45b], F. Barreiro[99], J. Barreiro Guimarães da Costa[15a], U. Barron[161], S. Barsov[137], F. Bartels[61a], R. Bartoldus[153], G. Bartolini[102], A. E. Barton[90], P. Bartos[28a], A. Basalaev[46], A. Basan[100], A. Bassalat[65,ag], M. J. Basso[167], R. L. Bates[57], S. Batlamous[35e], J. R. Batley[32], B. Batool[151], M. Battaglia[145], M. Bauce[73a,73b], F. Bauer[144,*], P. Bauer[24], H. S. Bawa[31], A. Bayirli[12c], J. B. Beacham[49], T. Beau[135], P. H. Beauchemin[170], F. Becherer[52], P. Bechtle[24], H. C. Beck[53], H. P. Beck[20,p], K. Becker[178], C. Becot[46], A. Beddall[12d], A. J. Beddall[12a], V. A. Bednyakov[80], M. Bedognetti[120], C. P. Bee[155], T. A. Beermann[182], M. Begalli[81b], M. Begel[29], A. Behera[155], J. K. Behr[46], F. Beisiegel[24], M. Belfkir[5], A. S. Bell[95], G. Bella[161], L. Bellagamba[23b], A. Bellerive[34], P. Bellos[9], K. Beloborodov[122a,122b], K. Belotskiy[112], N. L. Belyaev[112], D. Benchekroun[35a], N. Benekos[10], Y. Benhammou[161], D. P. Benjamin[6], M. Benoit[29], J. R. Bensinger[26], S. Bentvelsen[120], L. Beresford[134], M. Beretta[51], D. Berge[19], E. Bergeaas Kuutmann[172], N. Berger[5], B. Bergmann[141], L. J. Bergsten[26], J. Beringer[18], S. Berlendis[7], G. Bernardi[135], C. Bernius[153], F. U. Bernlochner[24], T. Berry[94], P. Berta[100], A. Berthold[48], I. A. Bertram[90], O. Bessidskaia Bylund[182], N. Besson[144], S. Bethke[115], A. Betti[42], A. J. Bevan[93], J. Beyer[115], S. Bhatta[155], D. S. Bhattacharya[177], P. Bhattarai[26], V. S. Bhopatkar[6], R. Bi[138], R. M. Bianchi[138], O. Biebel[114], D. Biedermann[19], R. Bielski[36], K. Bierwagen[100], N. V. Biesuz[72a,72b], M. Biglietti[75a], T. R. V. Billoud[141], M. Bindi[53], A. Bingul[12d], C. Bini[73a,73b], S. Biondi[23a,23b], C. J. Birch-sykes[101], M. Birman[180], T. Bisanz[36], J. P. Biswal[3], D. Biswas[181,i], A. Bitadze[101], C. Bittrich[48], K. Bjørke[133], T. Blazek[28a], I. Bloch[46], C. Blocker[26], A. Blue[57], U. Blumenschein[93], G. J. Bobbink[120], V. S. Bobrovnikov[122a,122b], S. S. Bocchetta[97], D. Bogavac[14], A. G. Bogdanchikov[122a,122b], C. Bohm[45a], V. Boisvert[94], P. Bokan[172,53], T. Bold[84a], A. E. Bolz[61b], M. Bomben[135], M. Bona[93], J. S. Bonilla[131], M. Boonekamp[144], C. D. Booth[94], A. G. Borbély[57], H. M. Borecka-Bielska[91], L. S. Borgna[95], A. Borisov[123], G. Borissov[90], D. Bortoletto[134], D. Boscherini[23b], M. Bosman[14], J. D. Bossio Sola[104], K. Bouaouda[35a], J. Boudreau[138], E. V. Bouhova-Thacker[90], D. Boumediene[38], A. Boveia[127], J. Boyd[36], D. Boye[33c], I. R. Boyko[80], A. J. Bozson[94], J. Bracinik[21], N. Brahimi[60c,60d], G. Brandt[182], O. Brandt[32], F. Braren[46], B. Brau[103], J. E. Brau[131], W. D. Breaden Madden[57], K. Brendlinger[46], R. Brener[160], L. Brenner[36], R. Brenner[172], S. Bressler[180], B. Brickwedde[100], D. L. Briglin[21], D. Britton[57], D. Britzger[115], I. Brock[24], R. Brock[107], G. Brooijmans[39], W. K. Brooks[146d], E. Brost[29], P. A. Bruckman de Renstrom[85], B. Brüers[46], D. Bruncko[28b], A. Bruni[23b], G. Bruni[23b], M. Bruschi[23b], N. Bruscino[73a,73b], L. Bryngemark[153], T. Buanes[17], Q. Buat[155], P. Buchholz[151], A. G. Buckley[57], I. A. Budagov[80], M. K. Bugge[133], O. Bulekov[112], B. A. Bullard[59], T. J. Burch[121], S. Burdin[91], C. D. Burgard[120], A. M. Burger[129], B. Burghgrave[8], J. T. P. Burr[46], C. D. Burton[11], J. C. Burzynski[103], V. Büscher[100], E. Buschmann[53], P. J. Bussey[57], J. M. Butler[25], C. M. Buttar[57], J. M. Butterworth[95], P. Butti[36], W. Buttinger[143], C. J. Buxo Vazquez[107], A. Buzatu[158], A. R. Buzykaev[122a,122b], G. Cabras[23a,23b], S. Cabrera Urbán[174], D. Caforio[56], H. Cai[138], V. M. M. Cairo[153], O. Cakir[4a], N. Calace[36], P. Calafiura[18], G. Calderini[135], P. Calfayan[66], G. Callea[57], L. P. Caloba[81b], A. Caltabiano[74a,74b], S. Calvente Lopez[99], D. Calvet[38], S. Calvet[38], T. P. Calvet[102], M. Calvetti[72a,72b], R. Camacho Toro[135], S. Camarda[36], D. Camarero Munoz[99], P. Camarri[74a,74b], M. T. Camerlingo[75a,75b], D. Cameron[133], C. Camincher[36], S. Campana[36], M. Campanelli[95], A. Camplani[40], V. Canale[70a,70b], A. Canesse[104], M. Cano Bret[78], J. Cantero[129], T. Cao[161], Y. Cao[173], M. D. M. Capeans Garrido[36], M. Capua[41a,41b], R. Cardarelli[74a], F. Cardillo[174], G. Carducci[41a,41b], I. Carli[142], T. Carli[36], G. Carlino[70a], B. T. Carlson[138], E. M. Carlson[168a,176], L. Carminati[69a,69b], R. M. D. Carney[153], S. Caron[119], E. Carquin[146d], S. Carrá[46], G. Carratta[23a,23b], J. W. S. Carter[167], T. M. Carter[50], M. P. Casado[14,f], A. F. Casha[167], E. G. Castiglia[183], F. L. Castillo[174], L. Castillo Garcia[14], V. Castillo Gimenez[174], N. F. Castro[139a,139e], A. Catinaccio[36], J. R. Catmore[133], A. Cattai[36], V. Cavaliere[29], V. Cavasinni[72a,72b], E. Celebi[12b], F. Celli[134], K. Cerny[130], A. S. Cerqueira[81a], A. Cerri[156], L. Cerrito[74a,74b], F. Cerutti[18], A. Cervelli[23a,23b], S. A. Cetin[12b], Z. Chadi[35a], D. Chakraborty[121], J. Chan[181], W. S. Chan[120], W. Y. Chan[91], J. D. Chapman[32], B. Chargeishvili[159b], D. G. Charlton[21], T. P. Charman[93], M. Chatterjee[20], C. C. Chau[34], S. Che[127], S. Chekanov[6], S. V. Chekulaev[168a], G. A. Chelkov[80,ae], B. Chen[79], C. Chen[60a], C. H. Chen[79], H. Chen[15c], H. Chen[29], J. Chen[60a], J. Chen[39], J. Chen[26], S. Chen[136], S. J. Chen[15c], X. Chen[15b], Y. Chen[60a], Y.-H. Chen[46], H. C. Cheng[63a], H. J. Cheng[15a], A. Cheplakov[80], E. Cheremushkina[123], R. Cherkaoui El Moursli[35e], E. Cheu[7], K. Cheung[64], T. J. A. Chevalérias[144], L. Chevalier[144], V. Chiarella[51], G. Chiarelli[72a], G. Chiodini[68a], A. S. Chisholm[21], A. Chitan[27b], I. Chiu[163], Y. H. Chiu[176], M. V. Chizhov[80], K. Choi[11], A. R. Chomont[73a,73b], Y. Chou[103], Y. S. Chow[120], L. D. Christopher[33f], M. C. Chu[63a], X. Chu[15a,15d],

J. Chudoba[140], J. J. Chwastowski[85], L. Chytka[130], D. Cieri[115], K. M. Ciesla[85], V. Cindro[92], I. A. Cioară[27b], A. Ciocio[18], F. Cirotto[70a,70b], Z. H. Citron[180,j], M. Citterio[69a], D. A. Ciubotaru[27b], B. M. Ciungu[167], A. Clark[54], P. J. Clark[50], S. E. Clawson[101], C. Clement[45a,45b], Y. Coadou[102], M. Cobal[67a,67c], A. Coccaro[55b], J. Cochran[79], R. Coelho Lopes De Sa[103], H. Cohen[161], A. E. C. Coimbra[36], B. Cole[39], A. P. Colijn[120], J. Collot[58], P. Conde Muiño[139a,139h], S. H. Connell[33c], I. A. Connelly[57], S. Constantinescu[27b], F. Conventi[70a,ak], A. M. Cooper-Sarkar[134], F. Cormier[175], K. J. R. Cormier[167], L. D. Corpe[95], M. Corradi[73a,73b], E. E. Corrigan[97], F. Corriveau[104,z], M. J. Costa[174], F. Costanza[5], D. Costanzo[149], G. Cowan[94], J. W. Cowley[32], J. Crane[101], K. Cranmer[125], R. A. Creager[136], S. Crépé-Renaudin[58], F. Crescioli[135], M. Cristinziani[24], V. Croft[170], G. Crosetti[41a,41b], A. Cueto[5], T. Cuhadar Donszelmann[171], H. Cui[15a,15d], A. R. Cukierman[153], W. R. Cunningham[57], S. Czekierda[85], P. Czodrowski[36], M. M. Czurylo[61b], M. J. Da Cunha Sargedas De Sousa[60b], J. V. Da Fonseca Pinto[81b], C. Da Via[101], W. Dabrowski[84a], F. Dachs[36], T. Dado[47], S. Dahbi[33f], T. Dai[106], C. Dallapiccola[103], M. Dam[40], G. D'amen[29], V. D'Amico[75a,75b], J. Damp[100], J. R. Dandoy[136], M. F. Daneri[30], M. Danninger[152], V. Dao[36], G. Darbo[55b], O. Dartsi[5], A. Dattagupta[131], T. Daubney[46], S. D'Auria[69a,69b], C. David[168b], T. Davidek[142], D. R. Davis[49], I. Dawson[149], K. De[8], R. De Asmundis[70a], M. De Beurs[120], S. De Castro[23a,23b], N. De Groot[119], P. de Jong[120], H. De la Torre[107], A. De Maria[15c], D. De Pedis[73a], A. De Salvo[73a], U. De Sanctis[74a,74b], M. De Santis[74a,74b], A. De Santo[156], J. B. De Vivie De Regie[65], D. V. Dedovich[80], A. M. Deiana[42], J. Del Peso[99], Y. Delabat Diaz[46], D. Delgove[65], F. Deliot[144], C. M. Delitzsch[7], M. Della Pietra[70a,70b], D. Della Volpe[54], A. Dell'Acqua[36], L. Dell'Asta[74a,74b], M. Delmastro[5], C. Delporte[65], P. A. Delsart[58], S. Demers[183], M. Demichev[80], G. Demontigny[110], S. P. Denisov[123], L. D'Eramo[121], D. Derendarz[85], J. E. Derkaoui[35d], F. Derue[135], P. Dervan[91], K. Desch[24], K. Dette[167], C. Deutsch[24], M. R. Devesa[30], P. O. Deviveiros[36], F. A. Di Bello[73a,73b], A. Di Ciaccio[74a,74b], L. Di Ciaccio[5], W. K. Di Clemente[136], C. Di Donato[70a,70b], A. Di Girolamo[36], G. Di Gregorio[72a,72b], A. Di Luca[76a,76b], B. Di Micco[75a,75b], R. Di Nardo[75a,75b], K. F. Di Petrillo[59], R. Di Sipio[167], C. Diaconu[102], F. A. Dias[120], T. Dias Do Vale[139a], M. A. Diaz[146a], F. G. Diaz Capriles[24], J. Dickinson[18], M. Didenko[166], E. B. Diehl[106], J. Dietrich[19], S. Díez Cornell[46], C. Diez Pardos[151], A. Dimitrievska[18], W. Ding[15b], J. Dingfelder[24], S. J. Dittmeier[61b], F. Dittus[36], F. Djama[102], T. Djobava[159b], J. I. Djuvsland[17], M. A. B. Do Vale[147], M. Dobre[27b], D. Dodsworth[26], C. Doglioni[97], J. Dolejsi[142], Z. Dolezal[142], M. Donadelli[81c], B. Dong[60c], J. Donini[38], A. D'onofrio[15c], M. D'Onofrio[91], J. Dopke[143], A. Doria[70a], M. T. Dova[89], A. T. Doyle[57], E. Drechsler[152], E. Dreyer[152], T. Dreyer[53], A. S. Drobac[170], D. Du[60b], T. A. du Pree[120], Y. Duan[60d], F. Dubinin[111], M. Dubovsky[28a], A. Dubreuil[54], E. Duchovni[180], G. Duckeck[114], O. A. Ducu[27b,36], D. Duda[115], A. Dudarev[36], A. C. Dudder[100], E. M. Duffield[18], M. D'uffizi[101], L. Duflot[65], M. Dührssen[36], C. Dülsen[182], M. Dumancic[180], A. E. Dumitriu[27b], M. Dunford[61a], S. Dungs[47], A. Duperrin[102], H. Duran Yildiz[4a], M. Düren[56], A. Durglishvili[159b], D. Duschinger[48], B. Dutta[46], D. Duvnjak[1], G. I. Dyckes[136], M. Dyndal[36], S. Dysch[101], B. S. Dziedzic[85], M. G. Eggleston[49], T. Eifert[8], G. Eigen[17], K. Einsweiler[18], T. Ekelof[172], H. El Jarrari[35e], V. Ellajosyula[172], M. Ellert[172], F. Ellinghaus[182], A. A. Elliot[93], N. Ellis[36], J. Elmsheuser[29], M. Elsing[36], D. Emeliyanov[143], A. Emerman[39], Y. Enari[163], M. B. Epland[49], J. Erdmann[47], A. Ereditato[20], P. A. Erland[85], M. Errenst[182], M. Escalier[65], C. Escobar[174], O. Estrada Pastor[174], E. Etzion[161], G. Evans[139a], H. Evans[66], M. O. Evans[156], A. Ezhilov[137], F. Fabbri[57], L. Fabbri[23a,23b], V. Fabiani[119], G. Facini[178], R. M. Fakhrutdinov[123], S. Falciano[73a], P. J. Falke[24], S. Falke[36], J. Faltova[142], Y. Fang[15a], Y. Fang[15a], G. Fanourakis[44], M. Fanti[69a,69b], M. Faraj[67a,67c], A. Farbin[8], A. Farilla[75a], E. M. Farina[71a,71b], T. Farooque[107], S. M. Farrington[50], P. Farthouat[36], F. Fassi[35e], P. Fassnacht[36], D. Fassouliotis[9], M. Faucci Giannelli[50], W. J. Fawcett[32], L. Fayard[65], O. L. Fedin[137,o], W. Fedorko[175], A. Fehr[20], M. Feickert[173], L. Feligioni[102], A. Fell[149], C. Feng[60b], M. Feng[49], M. J. Fenton[171], A. B. Fenyuk[123], S. W. Ferguson[43], J. Ferrando[46], A. Ferrari[172], P. Ferrari[120], R. Ferrari[71a], D. E. Ferreira de Lima[61b], A. Ferrer[174], D. Ferrere[54], C. Ferretti[106], F. Fiedler[100], A. Filipčič[92], F. Filthaut[119], K. D. Finelli[25], M. C. N. Fiolhais[139a,139c,a], L. Fiorini[174], F. Fischer[114], J. Fischer[100], W. C. Fisher[107], T. Fitschen[21], I. Fleck[151], P. Fleischmann[106], T. Flick[182], B. M. Flierl[114], L. Flores[136], L. R. Flores Castillo[63a], F. M. Follega[76a,76b], N. Fomin[17], J. H. Foo[167], G. T. Forcolin[76a,76b], B. C. Forland[66], A. Formica[144], F. A. Förster[14], A. C. Forti[101], E. Fortin[102], M. G. Foti[134], D. Fournier[65], H. Fox[90], P. Francavilla[72a,72b], S. Francescato[73a,73b], M. Franchini[23a,23b], S. Franchino[61a], D. Francis[36], L. Franco[5], L. Franconi[20], M. Franklin[59], G. Frattari[73a,73b], A. N. Fray[93], P. M. Freeman[21], B. Freund[110], W. S. Freund[81b], E. M. Freundlich[47], D. C. Frizzell[128], D. Froidevaux[36], J. A. Frost[134], M. Fujimoto[126], C. Fukunaga[164], E. Fullana Torregrosa[174], T. Fusayasu[116], J. Fuster[174],
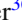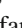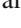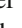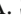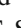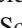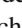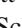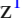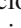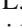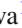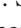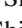
A. Gabrielli[23a,23b], A. Gabrielli[36], S. Gadatsch[54], P. Gadow[115], G. Gagliardi[55a,55b], L. G. Gagnon[110], G. E. Gallardo[134], E. J. Gallas[134], B. J. Gallop[143], R. Gamboa Goni[93], K. K. Gan[127], S. Ganguly[180], J. Gao[60a], Y. Gao[50], Y. S. Gao[31,l], F. M. Garay Walls[146a], C. García[174], J. E. García Navarro[174], J. A. García Pascual[15a], C. Garcia-Argos[52], M. Garcia-Sciveres[18], R. W. Gardner[37], N. Garelli[153], S. Gargiulo[52], C. A. Garner[167], V. Garonne[133], S. J. Gasiorowski[148], P. Gaspar[81b], A. Gaudiello[55a,55b], G. Gaudio[71a], P. Gauzzi[73a,73b], I. L. Gavrilenko[111], A. Gavrilyuk[124], C. Gay[175], G. Gaycken[46], E. N. Gazis[10], A. A. Geanta[27b], C. M. Gee[145], C. N. P. Gee[143], J. Geisen[97], M. Geisen[100], C. Gemme[55b], M. H. Genest[58], C. Geng[106], S. Gentile[73a,73b], S. George[94], T. Geralis[44], L. O. Gerlach[53], P. Gessinger-Befurt[100], G. Gessner[47], M. Ghasemi Bostanabad[176], M. Ghneimat[151], A. Ghosh[65], A. Ghosh[78], B. Giacobbe[23b], S. Giagu[73a,73b], N. Giangiacomi[167], P. Giannetti[72a], A. Giannini[70a,70b], G. Giannini[14], S. M. Gibson[94], M. Gignac[145], D. T. Gil[84b], B. J. Gilbert[39], D. Gillberg[34], G. Gilles[182], N. E. K. Gillwald[46], D. M. Gingrich[3,aj], M. P. Giordani[67a,67c], P. F. Giraud[144], G. Giugliarelli[67a,67c], D. Giugni[69a], F. Giuli[74a,74b], S. Gkaitatzis[162], I. Gkialas[9,g], E. L. Gkougkousis[14], P. Gkountoumis[10], L. K. Gladilin[113], C. Glasman[99], J. Glatzer[14], P. C. F. Glaysher[46], A. Glazov[46], G. R. Gledhill[131], I. Gnesi[41b,b], M. Goblirsch-Kolb[26], D. Godin[110], S. Goldfarb[105], T. Golling[54], D. Golubkov[123], A. Gomes[139a,139b], R. Goncalves Gama[53], R. Gonçalo[139a,139c], G. Gonella[131], L. Gonella[21], A. Gongadze[80], F. Gonnella[21], J. L. Gonski[39], S. González de la Hoz[174], S. Gonzalez Fernandez[14], R. Gonzalez Lopez[91], C. Gonzalez Renteria[18], R. Gonzalez Suarez[172], S. Gonzalez-Sevilla[54], G. R. Gonzalvo Rodriguez[174], L. Goossens[36], N. A. Gorasia[21], P. A. Gorbounov[124], H. A. Gordon[29], B. Gorini[36], E. Gorini[68a,68b], A. Gorišek[92], A. T. Goshaw[49], M. I. Gostkin[80], C. A. Gottardo[119], M. Gouighri[35b], A. G. Goussiou[148], N. Govender[33c], C. Goy[5], I. Grabowska-Bold[84a], E. C. Graham[91], J. Gramling[171], E. Gramstad[133], S. Grancagnolo[19], M. Grandi[156], V. Gratchev[137], P. M. Gravila[27f], F. G. Gravili[68a,68b], C. Gray[57], H. M. Gray[18], C. Grefe[24], K. Gregersen[97], I. M. Gregor[46], P. Grenier[153], K. Grevtsov[46], C. Grieco[14], N. A. Grieser[128], A. A. Grillo[145], K. Grimm[31,k], S. Grinstein[14,v], J.-F. Grivaz[65], S. Groh[100], E. Gross[180], J. Grosse-Knetter[53], Z. J. Grout[95], C. Grud[106], A. Grummer[118], J. C. Grundy[134], L. Guan[106], W. Guan[181], C. Gubbels[175], J. Guenther[77], A. Guerguichon[65], J. G. R. Guerrero Rojas[174], F. Guescini[115], D. Guest[77], R. Gugel[100], A. Guida[46], T. Guillemin[5], S. Guindon[36], J. Guo[60c], W. Guo[106], Y. Guo[60a], Z. Guo[102], R. Gupta[46], S. Gurbuz[12c], G. Gustavino[128], M. Guth[52], P. Gutierrez[128], C. Gutschow[95], C. Guyot[144], C. Gwenlan[134], C. B. Gwilliam[91], E. S. Haaland[133], A. Haas[125], C. Haber[18], H. K. Hadavand[8], A. Hadef[100], M. Haleem[177], J. Haley[129], J. J. Hall[149], G. Halladjian[107], G. D. Hallewell[102], K. Hamano[176], H. Hamdaoui[35e], M. Hamer[24], G. N. Hamity[50], K. Han[60a], L. Han[15c], L. Han[60a], S. Han[18], Y. F. Han[167], K. Hanagaki[82,t], M. Hance[145], D. M. Handl[114], M. D. Hank[37], R. Hankache[135], E. Hansen[97], J. B. Hansen[40], J. D. Hansen[40], M. C. Hansen[24], P. H. Hansen[40], E. C. Hanson[101], K. Hara[169], T. Harenberg[182], S. Harkusha[108], P. F. Harrison[178], N. M. Hartman[153], N. M. Hartmann[114], Y. Hasegawa[150], A. Hasib[50], S. Hassani[144], S. Haug[20], R. Hauser[107], M. Havranek[141], C. M. Hawkes[21], R. J. Hawkings[36], S. Hayashida[117], D. Hayden[107], C. Hayes[106], R. L. Hayes[175], C. P. Hays[134], J. M. Hays[93], H. S. Hayward[91], S. J. Haywood[143], F. He[60a], Y. He[165], M. P. Heath[50], V. Hedberg[97], A. L. Heggelund[133], N. D. Hehir[93], C. Heidegger[52], K. K. Heidegger[52], W. D. Heidorn[79], J. Heilman[34], S. Heim[46], T. Heim[18], B. Heinemann[46,ah], J. G. Heinlein[136], J. J. Heinrich[131], L. Heinrich[36], J. Hejbal[140], L. Helary[46], A. Held[125], S. Hellesund[133], C. M. Helling[145], S. Hellman[45a,45b], C. Helsens[36], R. C. W. Henderson[90], L. Henkelmann[32], A. M. Henriques Correia[36], H. Herde[26], Y. Hernández Jiménez[33f], H. Herr[100], M. G. Herrmann[114], T. Herrmann[48], G. Herten[52], R. Hertenberger[114], L. Hervas[36], T. C. Herwig[136], G. G. Hesketh[95], N. P. Hessey[168a], H. Hibi[83], S. Higashino[82], E. Higón-Rodriguez[174], K. Hildebrand[37], J. C. Hill[32], K. K. Hill[29], K. H. Hiller[46], S. J. Hillier[21], M. Hils[48], I. Hinchliffe[18], F. Hinterkeuser[24], M. Hirose[132], S. Hirose[169], D. Hirschbuehl[182], B. Hiti[92], O. Hladik[140], J. Hobbs[155], R. Hobincu[27e], N. Hod[180], M. C. Hodgkinson[149], A. Hoecker[36], D. Hohn[52], D. Hohov[65], T. Holm[24], T. R. Holmes[37], M. Holzbock[115], L. B. A. H. Hommels[32], T. M. Hong[138], J. C. Honig[52], A. Hönle[115], B. H. Hooberman[173], W. H. Hopkins[6], Y. Horii[117], P. Horn[48], L. A. Horyn[37], S. Hou[158], A. Hoummada[35a], J. Howarth[57], J. Hoya[89], M. Hrabovsky[130], J. Hrivnac[65], A. Hrynevich[109], T. Hryn'ova[5], P. J. Hsu[64], S.-C. Hsu[148], Q. Hu[39], S. Hu[60c], Y. F. Hu[15a,15d,al], D. P. Huang[95], X. Huang[15c], Y. Huang[60a], Y. Huang[15a], Z. Hubacek[141], F. Hubaut[102], M. Huebner[24], F. Huegging[24], T. B. Huffman[134], M. Huhtinen[36], R. Hulsken[58], R. F. H. Hunter[34], N. Huseynov[80,aa], J. Huston[107], J. Huth[59], R. Hyneman[153], S. Hyrych[28a], G. Iacobucci[54], G. Iakovidis[29], I. Ibragimov[151], L. Iconomidou-Fayard[65], P. Iengo[36], R. Ignazzi[40], R. Iguchi[163], T. Iizawa[54], Y. Ikegami[82], M. Ikeno[82], N. Ilic[119,167,z], F. Iltzsche[48], H. Imam[35a],

G. Introzzi[71a,71b], M. Iodice[75a], K. Iordanidou[168a], V. Ippolito[73a,73b], M. F. Isacson[172], M. Ishino[163], W. Islam[129], C. Issever[19,46], S. Istin[160], J. M. Iturbe Ponce[63a], R. Iuppa[76a,76b], A. Ivina[180], J. M. Izen[43], V. Izzo[70a], P. Jacka[140], P. Jackson[1], R. M. Jacobs[46], B. P. Jaeger[152], V. Jain[2], G. Jäkel[182], K. B. Jakobi[100], K. Jakobs[52], T. Jakoubek[180], J. Jamieson[57], K. W. Janas[84a], R. Jansky[54], M. Janus[53], P. A. Janus[84a], G. Jarlskog[97], A. E. Jaspan[91], N. Javadov[80,aa], T. Javůrek[36], M. Javurkova[103], F. Jeanneau[144], L. Jeanty[131], J. Jejelava[159a], P. Jenni[52,c], N. Jeong[46], S. Jézéquel[5], J. Jia[155], Z. Jia[15c], H. Jiang[79], Y. Jiang[60a], Z. Jiang[153], S. Jiggins[52], F. A. Jimenez Morales[38], J. Jimenez Pena[115], S. Jin[15c], A. Jinaru[27b], O. Jinnouchi[165], H. Jivan[33f], P. Johansson[149], K. A. Johns[7], C. A. Johnson[66], E. Jones[178], R. W. L. Jones[90], S. D. Jones[156], T. J. Jones[91], J. Jovicevic[36], X. Ju[18], J. J. Junggeburth[115], A. Juste Rozas[14,v], A. Kaczmarska[85], M. Kado[73a,73b], H. Kagan[127], M. Kagan[153], A. Kahn[39], C. Kahra[100], T. Kaji[179], E. Kajomovitz[160], C. W. Kalderon[29], A. Kaluza[100], A. Kamenshchikov[123], M. Kaneda[163], N. J. Kang[145], S. Kang[79], Y. Kano[117], J. Kanzaki[82], L. S. Kaplan[181], D. Kar[33f], K. Karava[134], M. J. Kareem[168b], I. Karkanias[162], S. N. Karpov[80], Z. M. Karpova[80], V. Kartvelishvili[90], A. N. Karyukhin[123], E. Kasimi[162], A. Kastanas[45a,45b], C. Kato[60d], J. Katzy[46], K. Kawade[150], K. Kawagoe[88], T. Kawaguchi[117], T. Kawamoto[144], G. Kawamura[53], E. F. Kay[176], F. I. Kaya[170], S. Kazakos[14], V. F. Kazanin[122a,122b], J. M. Keaveney[33a], R. Keeler[176], J. S. Keller[34], E. Kellermann[97], D. Kelsey[156], J. J. Kempster[21], J. Kendrick[21], K. E. Kennedy[39], O. Kepka[140], S. Kersten[182], B. P. Kerševan[92], S. Ketabchi Haghighat[167], F. Khalil-Zada[13], M. Khandoga[144], A. Khanov[129], A. G. Kharlamov[122a,122b], T. Kharlamova[122a,122b], E. E. Khoda[175], T. J. Khoo[77], G. Khoriauli[177], E. Khramov[80], J. Khubua[159b], S. Kido[83], M. Kiehn[36], E. Kim[165], Y. K. Kim[37], N. Kimura[95], A. Kirchhoff[53], D. Kirchmeier[48], J. Kirk[143], A. E. Kiryunin[115], T. Kishimoto[163], D. P. Kisliuk[167], V. Kitali[46], C. Kitsaki[10], O. Kivernyk[24], T. Klapdor-Kleingrothaus[52], M. Klassen[61a], C. Klein[34], M. H. Klein[106], M. Klein[91], U. Klein[91], K. Kleinknecht[100], P. Klimek[36], A. Klimentov[29], F. Klimpel[36], T. Klingl[24], T. Klioutchnikova[36], F. F. Klitzner[114], P. Kluit[120], S. Kluth[115], E. Kneringer[77], E. B. F. G. Knoops[102], A. Knue[52], D. Kobayashi[88], M. Kobel[48], M. Kocian[153], T. Kodama[163], P. Kodys[142], D. M. Koeck[156], P. T. Koenig[24], T. Koffas[34], N. M. Köhler[36], M. Kolb[144], I. Koletsou[5], T. Komarek[130], T. Kondo[82], K. Köneke[52], A. X. Y. Kong[1], A. C. König[119], T. Kono[126], V. Konstantinides[95], N. Konstantinidis[95], B. Konya[97], R. Kopeliansky[66], S. Koperny[84a], K. Korcyl[85], K. Kordas[162], G. Koren[161], A. Korn[95], I. Korolkov[14], E. V. Korolkova[149], N. Korotkova[113], O. Kortner[115], S. Kortner[115], V. V. Kostyukhin[149,166], A. Kotsokechagia[65], A. Kotwal[49], A. Koulouris[10], A. Kourkoumeli-Charalampidi[71a,71b], C. Kourkoumelis[9], E. Kourlitis[6], V. Kouskoura[29], R. Kowalewski[176], W. Kozanecki[101], A. S. Kozhin[123], V. A. Kramarenko[113], G. Kramberger[92], D. Krasnopevtsev[60a], M. W. Krasny[135], A. Krasznahorkay[36], D. Krauss[115], J. A. Kremer[100], J. Kretzschmar[91], K. Kreul[19], P. Krieger[167], F. Krieter[114], S. Krishnamurthy[103], A. Krishnan[61b], M. Krivos[142], K. Krizka[18], K. Kroeninger[47], H. Kroha[115], J. Kroll[140], J. Kroll[136], K. S. Krowpman[107], U. Kruchonak[80], H. Krüger[24], N. Krumnack[79], M. C. Kruse[49], J. A. Krzysiak[85], A. Kubota[165], O. Kuchinskaia[166], S. Kuday[4b], D. Kuechler[46], J. T. Kuechler[46], S. Kuehn[36], T. Kuhl[46], V. Kukhtin[80], Y. Kulchitsky[108,ad], S. Kuleshov[146b], Y. P. Kulinich[173], M. Kuna[58], A. Kupco[140], T. Kupfer[47], O. Kuprash[52], H. Kurashige[83], L. L. Kurchaninov[168a], Y. A. Kurochkin[108], A. Kurova[112], M. G. Kurth[15a,15d], E. S. Kuwertz[36], M. Kuze[165], A. K. Kvam[148], J. Kvita[130], T. Kwan[104], C. Lacasta[174], F. Lacava[73a,73b], D. P. J. Lack[101], H. Lacker[19], D. Lacour[135], E. Ladygin[80], R. Lafaye[5], B. Laforge[135], T. Lagouri[146c], S. Lai[53], I. K. Lakomiec[84a], J. E. Lambert[128], S. Lammers[66], W. Lampl[7], C. Lampoudis[162], E. Lançon[29], U. Landgraf[52], M. P. J. Landon[93], V. S. Lang[52], J. C. Lange[53], R. J. Langenberg[103], A. J. Lankford[171], F. Lanni[29], K. Lantzsch[24], A. Lanza[71a], A. Lapertosa[55a,55b], J. F. Laporte[144], T. Lari[69a], F. Lasagni Manghi[23a,23b], M. Lassnig[36], V. Latonova[140], T. S. Lau[63a], A. Laudrain[100], A. Laurier[34], M. Lavorgna[70a,70b], S. D. Lawlor[94], M. Lazzaroni[69a,69b], B. Le[101], E. Le Guirriec[102], A. Lebedev[79], M. LeBlanc[7], T. LeCompte[6], F. Ledroit-Guillon[58], A. C. A. Lee[95], C. A. Lee[29], G. R. Lee[17], L. Lee[59], S. C. Lee[158], S. Lee[79], B. Lefebvre[168a], H. P. Lefebvre[94], M. Lefebvre[176], C. Leggett[18], K. Lehmann[152], N. Lehmann[20], G. Lehmann Miotto[36], W. A. Leight[46], A. Leisos[162,u], M. A. L. Leite[81c], C. E. Leitgeb[114], R. Leitner[142], K. J. C. Leney[42], T. Lenz[24], S. Leone[72a], C. Leonidopoulos[50], A. Leopold[135], C. Leroy[110], R. Les[107], C. G. Lester[32], M. Levchenko[137], J. Levêque[5], D. Levin[106], L. J. Levinson[180], D. J. Lewis[21], B. Li[15b], B. Li[106], C-Q. Li[60c,60d], F. Li[60c], H. Li[60a], H. Li[60b], J. Li[60c], K. Li[148], L. Li[60c], M. Li[15a,15d], Q. Y. Li[60a], S. Li[60c,60d], X. Li[46], Y. Li[46], Z. Li[60b], Z. Li[134], Z. Li[104], Z. Li[91], Z. Liang[15a], M. Liberatore[46], B. Liberti[74a], K. Lie[63c], S. Lim[29], C. Y. Lin[32], K. Lin[107], R. A. Linck[66], R. E. Lindley[7], J. H. Lindon[21], A. Linss[46], A. L. Lionti[54], E. Lipeles[136], A. Lipniacka[17], T. M. Liss[173,ai], A. Lister[175],

J. D. Little[8], B. Liu[79], B. X. Liu[152], H. B. Liu[29], J. B. Liu[60a], J. K. K. Liu[37], K. Liu[60c,60d], M. Liu[60a], M. Y. Liu[60a], P. Liu[15a], X. Liu[60a], Y. Liu[46], Y. Liu[15a,15d], Y. L. Liu[106], Y. W. Liu[60a], M. Livan[71a,71b], A. Lleres[58], J. Llorente Merino[152], S. L. Lloyd[93], C. Y. Lo[63b], E. M. Lobodzinska[46], P. Loch[7], S. Loffredo[74a,74b], T. Lohse[19], K. Lohwasser[149], M. Lokajicek[140], J. D. Long[173], R. E. Long[90], I. Longarini[73a,73b], L. Longo[36], I. Lopez Paz[101], A. Lopez Solis[149], J. Lorenz[114], N. Lorenzo Martinez[5], A. M. Lory[114], A. Lösle[52], X. Lou[45a,45b], X. Lou[15a], A. Lounis[65], J. Love[6], P. A. Love[90], J. J. Lozano Bahilo[174], M. Lu[60a], Y. J. Lu[64], H. J. Lubatti[148], C. Luci[73a,73b], F. L. Lucio Alves[15c], A. Lucotte[58], F. Luehring[66], I. Luise[155], L. Luminari[73a], B. Lund-Jensen[154], N. A. Luongo[131], M. S. Lutz[161], D. Lynn[29], H. Lyons[91], R. Lysak[140], E. Lytken[97], F. Lyu[15a], V. Lyubushkin[80], T. Lyubushkina[80], H. Ma[29], L. L. Ma[60b], Y. Ma[95], D. M. Mac Donell[176], G. Maccarrone[51], C. M. Macdonald[149], J. C. MacDonald[149], J. Machado Miguens[136], R. Madar[38], W. F. Mader[48], M. Madugoda Ralalage Don[129], N. Madysa[48], J. Maeda[83], T. Maeno[29], M. Maerker[48], V. Magerl[52], N. Magini[79], J. Magro[67a,67c,q], D. J. Mahon[39], C. Maidantchik[81b], A. Maio[139a,139b,139d], K. Maj[84a], O. Majersky[28a], S. Majewski[131], Y. Makida[82], N. Makovec[65], B. Malaescu[135], Pa. Malecki[85], V. P. Maleev[137], F. Malek[58], D. Malito[41a,41b], U. Mallik[78], C. Malone[32], S. Maltezos[10], S. Malyukov[80], J. Mamuzic[174], G. Mancini[51], J. P. Mandalia[93], I. Mandić[92], L. Manhaes de Andrade Filho[81a], I. M. Maniatis[162], J. Manjarres Ramos[48], K. H. Mankinen[97], A. Mann[114], A. Manousos[77], B. Mansoulie[144], I. Manthos[162], S. Manzoni[120], A. Marantis[162,u], G. Marceca[30], L. Marchese[134], G. Marchiori[135], M. Marcisovsky[140], L. Marcoccia[74a,74b], C. Marcon[97], M. Marjanovic[128], Z. Marshall[18], M. U. F. Martensson[172], S. Marti-Garcia[174], C. B. Martin[127], T. A. Martin[178], V. J. Martin[50], B. Martin dit Latour[17], L. Martinelli[75a,75b], M. Martinez[14,v], P. Martinez Agullo[174], V. I. Martinez Outschoorn[103], S. Martin-Haugh[143], V. S. Martoiu[27b], A. C. Martyniuk[95], A. Marzin[36], S. R. Maschek[115], L. Masetti[100], T. Mashimo[163], R. Mashinistov[111], J. Masik[101], A. L. Maslennikov[122a,122b], L. Massa[23a,23b], P. Massarotti[70a,70b], P. Mastrandrea[72a,72b], A. Mastroberardino[41a,41b], T. Masubuchi[163], D. Matakias[29], A. Matic[114], N. Matsuzawa[163], P. Mättig[24], J. Maurer[27b], B. Maček[92], D. A. Maximov[122a,122b], R. Mazini[158], I. Maznas[162], S. M. Mazza[145], J. P. Mc Gowan[104], S. P. Mc Kee[106], T. G. McCarthy[115], W. P. McCormack[18], E. F. McDonald[105], A. E. McDougall[120], J. A. Mcfayden[18], G. Mchedlidze[159b], M. A. McKay[42], K. D. McLean[176], S. J. McMahon[143], P. C. McNamara[105], C. J. McNicol[178], R. A. McPherson[176,z], J. E. Mdhluli[33f], Z. A. Meadows[103], S. Meehan[36], T. Megy[38], S. Mehlhase[114], A. Mehta[91], B. Meirose[43], D. Melini[160], B. R. Mellado Garcia[33f], J. D. Mellenthin[53], M. Melo[28a], F. Meloni[46], A. Melzer[24], E. D. Mendes Gouveia[139a,139e], A. M. Mendes Jacques Da Costa[21], H. Y. Meng[167], L. Meng[36], X. T. Meng[106], S. Menke[115], E. Meoni[41a,41b], S. Mergelmeyer[19], S. A. M. Merkt[138], C. Merlassino[134], P. Mermod[54,*], L. Merola[70a,70b], C. Meroni[69a], G. Merz[106], O. Meshkov[113,111], J. K. R. Meshreki[151], J. Metcalfe[6], A. S. Mete[6], C. Meyer[66], J-P. Meyer[144], M. Michetti[19], R. P. Middleton[143], L. Mijović[50], G. Mikenberg[180], M. Mikestikova[140], M. Mikuž[92], H. Mildner[149], A. Milic[167], C. D. Milke[42], D. W. Miller[37], L. S. Miller[34], A. Milov[180], D. A. Milstead[45a,45b], A. A. Minaenko[123], I. A. Minashvili[159b], L. Mince[57], A. I. Mincer[125], B. Mindur[84a], M. Mineev[80], Y. Minegishi[163], Y. Mino[86], L. M. Mir[14], M. Mironova[134], K. P. Mistry[136], T. Mitani[179], J. Mitrevski[114], V. A. Mitsou[174], M. Mittal[60c], O. Miu[167], A. Miucci[20], P. S. Miyagawa[93], A. Mizukami[82], J. U. Mjörnmark[97], T. Mkrtchyan[61a], M. Mlynarikova[121], T. Moa[45a,45b], S. Mobius[53], K. Mochizuki[110], P. Moder[46], P. Mogg[114], S. Mohapatra[39], R. Moles-Valls[24], K. Mönig[46], E. Monnier[102], A. Montalbano[152], J. Montejo Berlingen[36], M. Montella[95], F. Monticelli[89], S. Monzani[69a], N. Morange[65], A. L. Moreira De Carvalho[139a], D. Moreno[22a], M. Moreno Llácer[174], C. Moreno Martinez[14], P. Morettini[55b], M. Morgenstern[160], S. Morgenstern[48], D. Mori[152], M. Morii[59], M. Morinaga[179], V. Morisbak[133], A. K. Morley[36], G. Mornacchi[36], A. P. Morris[95], L. Morvaj[36], P. Moschovakos[36], B. Moser[120], M. Mosidze[159b], T. Moskalets[144], P. Moskvitina[119], J. Moss[31,m], E. J. W. Moyse[103], S. Muanza[102], J. Mueller[138], R. S. P. Mueller[114], D. Muenstermann[90], G. A. Mullier[97], D. P. Mungo[69a,69b], J. L. Munoz Martinez[14], F. J. Munoz Sanchez[101], P. Murin[28b], W. J. Murray[178,143], A. Murrone[69a,69b], J. M. Muse[128], M. Muškinja[18], C. Mwewa[33a], A. G. Myagkov[123,ae], A. A. Myers[138], G. Myers[66], J. Myers[131], M. Myska[141], B. P. Nachman[18], O. Nackenhorst[47], A.Nag Nag[48], K. Nagai[134], K. Nagano[82], Y. Nagasaka[62], J. L. Nagle[29], E. Nagy[102], A. M. Nairz[36], Y. Nakahama[117], K. Nakamura[82], T. Nakamura[163], H. Nanjo[132], F. Napolitano[61a], R. F. Naranjo Garcia[46], R. Narayan[42], I. Naryshkin[137], M. Naseri[34], T. Naumann[46], G. Navarro[22a], P. Y. Nechaeva[111], F. Nechansky[46], T. J. Neep[21], A. Negri[71a,71b], M. Negrini[23b], C. Nellist[119], C. Nelson[104], M. E. Nelson[45a,45b], S. Nemecek[140], M. Nessi[36,e], M. S. Neubauer[173], F. Neuhaus[100], M. Neumann[182], R. Newhouse[175], P. R. Newman[21], C. W. Ng[138],

Y. S. Ng[19], Y. W. Y. Ng[171], B. Ngair[35e], H. D. N. Nguyen[102], T. Nguyen Manh[110], E. Nibigira[38], R. B. Nickerson[134], R. Nicolaidou[144], D. S. Nielsen[40], J. Nielsen[145], M. Niemeyer[53], N. Nikiforou[11], V. Nikolaenko[123,ae], I. Nikolic-Audit[135], K. Nikolopoulos[21], P. Nilsson[29], H. R. Nindhito[54], A. Nisati[73a], N. Nishu[60c], R. Nisius[115], I. Nitsche[47], T. Nitta[179], T. Nobe[163], D. L. Noel[32], Y. Noguchi[86], I. Nomidis[135], M. A. Nomura[29], M. Nordberg[36], J. Novak[92], T. Novak[92], O. Novgorodova[48], R. Novotny[118], L. Nozka[130], K. Ntekas[171], E. Nurse[95], F. G. Oakham[34,aj], J. Ocariz[135], A. Ochi[83], I. Ochoa[139a], J. P. Ochoa-Ricoux[146a], K. O'Connor[26], S. Oda[88], S. Odaka[82], S. Oerdek[53], A. Ogrodnik[84a], A. Oh[101], C. C. Ohm[154], H. Oide[165], R. Oishi[163], M. L. Ojeda[167], H. Okawa[169], Y. Okazaki[86], M. W. O'Keefe[91], Y. Okumura[163], A. Olariu[27b], L. F. Oleiro Seabra[139a], S. A. Olivares Pino[146a], D. Oliveira Damazio[29], J. L. Oliver[1], M. J. R. Olsson[171], A. Olszewski[85], J. Olszowska[85], Ö. O. Öncel[24], D. C. O'Neil[152], A. P. O'neill[134], A. Onofre[139a,139e], P. U. E. Onyisi[11], H. Oppen[133], R. G. Oreamuno Madriz[121], M. J. Oreglia[37], G. E. Orellana[89], D. Orestano[75a,75b], N. Orlando[14], R. S. Orr[167], V. O'Shea[57], R. Ospanov[60a], G. Otero y Garzon[30], H. Otono[88], P. S. Ott[61a], G. J. Ottino[18], M. Ouchrif[35d], J. Ouellette[29], F. Ould-Saada[133], A. Ouraou[144,*], Q. Ouyang[15a], M. Owen[57], R. E. Owen[143], V. E. Ozcan[12c], N. Ozturk[8], J. Pacalt[130], H. A. Pacey[32], K. Pachal[49], A. Pacheco Pages[14], C. Padilla Aranda[14], S. Pagan Griso[18], G. Palacino[66], S. Palazzo[50], S. Palestini[36], M. Palka[84b], P. Palni[84a], C. E. Pandini[54], J. G. Panduro Vazquez[94], P. Pani[46], G. Panizzo[67a,67c], L. Paolozzi[54], C. Papadatos[110], K. Papageorgiou[9,g], S. Parajuli[42], A. Paramonov[6], C. Paraskevopoulos[10], D. Paredes Hernandez[63b], S. R. Paredes Saenz[134], B. Parida[180], T. H. Park[167], A. J. Parker[31], M. A. Parker[32], F. Parodi[55a,55b], E. W. Parrish[121], J. A. Parsons[39], U. Parzefall[52], L. Pascual Dominguez[135], V. R. Pascuzzi[18], J. M. P. Pasner[145], F. Pasquali[120], E. Pasqualucci[73a], S. Passaggio[55b], F. Pastore[94], P. Pasuwan[45a,45b], S. Pataraia[100], J. R. Pater[101], A. Pathak[181,i], J. Patton[91], T. Pauly[36], J. Pearkes[153], M. Pedersen[133], L. Pedraza Diaz[119], R. Pedro[139a], T. Peiffer[53], S. V. Peleganchuk[122a,122b], O. Penc[140], C. Peng[63b], H. Peng[60a], B. S. Peralva[81a], M. M. Perego[65], A. P. Pereira Peixoto[139a], L. Pereira Sanchez[45a,45b], D. V. Perepelitsa[29], E. Perez Codina[168a], L. Perini[69a,69b], H. Pernegger[36], S. Perrella[36], A. Perrevoort[120], K. Peters[46], R. F. Y. Peters[101], B. A. Petersen[36], T. C. Petersen[40], E. Petit[102], V. Petousis[141], C. Petridou[162], F. Petrucci[75a,75b], M. Pettee[183], N. E. Pettersson[103], K. Petukhova[142], A. Peyaud[144], R. Pezoa[146d], L. Pezzotti[71a,71b], T. Pham[105], P. W. Phillips[143], M. W. Phipps[173], G. Piacquadio[155], E. Pianori[18], A. Picazio[103], R. H. Pickles[101], R. Piegaia[30], D. Pietreanu[27b], J. E. Pilcher[37], A. D. Pilkington[101], M. Pinamonti[67a,67c], J. L. Pinfold[3], C. Pitman Donaldson[95], M. Pitt[161], L. Pizzimento[74a,74b], A. Pizzini[120], M.-A. Pleier[29], V. Plesanovs[52], V. Pleskot[142], E. Plotnikova[80], P. Podberezko[122a,122b], R. Poettgen[97], R. Poggi[54], L. Poggioli[135], I. Pogrebnyak[107], D. Pohl[24], I. Pokharel[53], G. Polesello[71a], A. Poley[152,168a], A. Policicchio[73a,73b], R. Polifka[142], A. Polini[23b], C. S. Pollard[46], V. Polychronakos[29], D. Ponomarenko[112], L. Pontecorvo[36], S. Popa[27a], G. A. Popeneciu[27d], L. Portales[5], D. M. Portillo Quintero[58], S. Pospisil[141], K. Potamianos[46], I. N. Potrap[80], C. J. Potter[32], H. Potti[11], T. Poulsen[97], J. Poveda[174], T. D. Powell[149], G. Pownall[46], M. E. Pozo Astigarraga[36], A. Prades Ibanez[174], P. Pralavorio[102], M. M. Prapa[44], S. Prell[79], D. Price[101], M. Primavera[68a], M. L. Proffitt[148], N. Proklova[112], K. Prokofiev[63c], F. Prokoshin[80], S. Protopopescu[29], J. Proudfoot[6], M. Przybycien[84a], D. Pudzha[137], A. Puri[173], P. Puzo[65], D. Pyatiizbyantseva[112], J. Qian[106], Y. Qin[101], A. Quadt[53], M. Queitsch-Maitland[36], G. Rabanal Bolanos[59], M. Racko[28a], F. Ragusa[69a,69b], G. Rahal[98], J. A. Raine[54], S. Rajagopalan[29], A. Ramirez Morales[93], K. Ran[15a,15d], D. F. Rassloff[61a], D. M. Rauch[46], F. Rauscher[114], S. Rave[100], B. Ravina[57], I. Ravinovich[180], J. H. Rawling[101], M. Raymond[36], A. L. Read[133], N. P. Readioff[149], M. Reale[68a,68b], D. M. Rebuzzi[71a,71b], G. Redlinger[29], K. Reeves[43], D. Reikher[161], A. Reiss[100], A. Rej[151], C. Rembser[36], A. Renardi[46], M. Renda[27b], M. B. Rendel[115], A. G. Rennie[57], S. Resconi[69a], E. D. Resseguie[18], S. Rettie[95], B. Reynolds[127], E. Reynolds[21], O. L. Rezanova[122a,122b], P. Reznicek[142], E. Ricci[76a,76b], R. Richter[115], S. Richter[46], E. Richter-Was[84b], M. Ridel[135], P. Rieck[115], O. Rifki[46], M. Rijssenbeek[155], A. Rimoldi[71a,71b], M. Rimoldi[46], L. Rinaldi[23b], T. T. Rinn[173], G. Ripellino[154], I. Riu[14], P. Rivadeneira[46], J. C. Rivera Vergara[176], F. Rizatdinova[129], E. Rizvi[93], C. Rizzi[36], S. H. Robertson[104,z], M. Robin[46], D. Robinson[32], C. M. Robles Gajardo[146d], M. Robles Manzano[100], A. Robson[57], A. Rocchi[74a,74b], C. Roda[72a,72b], S. Rodriguez Bosca[174], A. Rodriguez Rodriguez[52], A. M. Rodríguez Vera[168b], S. Roe[36], J. Roggel[182], O. Røhne[133], R. Röhrig[115], R. A. Rojas[146d], B. Roland[52], C. P. A. Roland[66], J. Roloff[29], A. Romaniouk[112], M. Romano[23a,23b], N. Rompotis[91], M. Ronzani[125], L. Roos[135], S. Rosati[73a], G. Rosin[103], B. J. Rosser[136], E. Rossi[46], E. Rossi[75a,75b], E. Rossi[70a,70b], L. P. Rossi[55b], L. Rossini[46], R. Rosten[14], M. Rotaru[27b], B. Rottler[52], D. Rousseau[65], G. Rovelli[71a,71b], A. Roy[11], D. Roy[33f], A. Rozanov[102],

Y. Rozen[160], X. Ruan[33f], T. A. Ruggeri[1], F. Rühr[52], A. Ruiz-Martinez[174], A. Rummler[36], Z. Rurikova[52], N. A. Rusakovich[80], H. L. Russell[104], L. Rustige[38,47], J. P. Rutherfoord[7], E. M. Rüttinger[149], M. Rybar[142], G. Rybkin[65], E. B. Rye[133], A. Ryzhov[123], J. A. Sabater Iglesias[46], P. Sabatini[174], L. Sabetta[73a,73b], S. Sacerdoti[65], H.F-W. Sadrozinski[145], R. Sadykov[80], F. Safai Tehrani[73a], B. Safarzadeh Samani[156], M. Safdari[153], P. Saha[121], S. Saha[104], M. Sahinsoy[115], A. Sahu[182], M. Saimpert[36], M. Saito[163], T. Saito[163], H. Sakamoto[163], D. Salamani[54], G. Salamanna[75a,75b], A. Salnikov[153], J. Salt[174], A. Salvador Salas[14], D. Salvatore[41a,41b], F. Salvatore[156], A. Salvucci[63a], A. Salzburger[36], J. Samarati[36], D. Sammel[52], D. Sampsonidis[162], D. Sampsonidou[60c,60d], J. Sánchez[174], A. Sanchez Pineda[67a,36,67c], H. Sandaker[133], C. O. Sander[46], I. G. Sanderswood[90], M. Sandhoff[182], C. Sandoval[22b], D. P. C. Sankey[143], M. Sannino[55a,55b], Y. Sano[117], A. Sansoni[51], C. Santoni[38], H. Santos[139a,139b], S. N. Santpur[18], A. Santra[174], K. A. Saoucha[149], A. Sapronov[80], J. G. Saraiva[139a,139d], O. Sasaki[82], K. Sato[169], F. Sauerburger[52], E. Sauvan[5], P. Savard[167,aj], R. Sawada[163], C. Sawyer[143], L. Sawyer[96], I. Sayago Galvan[174], C. Sbarra[23b], A. Sbrizzi[67a,67c], T. Scanlon[95], J. Schaarschmidt[148], P. Schacht[115], D. Schaefer[37], L. Schaefer[136], U. Schäfer[100], A. C. Schaffer[65], D. Schaile[114], R. D. Schamberger[155], E. Schanet[114], C. Scharf[19], N. Scharmberg[101], V. A. Schegelsky[137], D. Scheirich[142], F. Schenck[19], M. Schernau[171], C. Schiavi[55a,55b], L. K. Schildgen[24], Z. M. Schillaci[26], E. J. Schioppa[68a,68b], M. Schioppa[41a,41b], K. E. Schleicher[52], S. Schlenker[36], K. R. Schmidt-Sommerfeld[115], K. Schmieden[100], C. Schmitt[100], S. Schmitt[46], L. Schoeffel[144], A. Schoening[61b], P. G. Scholer[52], E. Schopf[134], M. Schott[100], J. F. P. Schouwenberg[119], J. Schovancova[36], S. Schramm[54], F. Schroeder[182], A. Schulte[100], H-C. Schultz-Coulon[61a], M. Schumacher[52], B. A. Schumm[145], Ph. Schune[144], A. Schwartzman[153], T. A. Schwarz[106], Ph. Schwemling[144], R. Schwienhorst[107], A. Sciandra[145], G. Sciolla[26], F. Scuri[72a], F. Scutti[105], L. M. Scyboz[115], C. D. Sebastiani[91], K. Sedlaczek[47], P. Seema[19], S. C. Seidel[118], A. Seiden[145], B. D. Seidlitz[29], T. Seiss[37], C. Seitz[46], J. M. Seixas[81b], G. Sekhniaidze[70a], S. J. Sekula[42], N. Semprini-Cesari[23a,23b], S. Sen[49], C. Serfon[29], L. Serin[65], L. Serkin[67a,67b], M. Sessa[60a], H. Severini[128], S. Sevova[153], F. Sforza[55a,55b], A. Sfyrla[54], E. Shabalina[53], J. D. Shahinian[136], N. W. Shaikh[45a,45b], D. Shaked Renous[180], L. Y. Shan[15a], M. Shapiro[18], A. Sharma[36], A. S. Sharma[1], P. B. Shatalov[124], K. Shaw[156], S. M. Shaw[101], M. Shehade[180], Y. Shen[128], A. D. Sherman[25], P. Sherwood[95], L. Shi[95], C. O. Shimmin[183], Y. Shimogama[179], M. Shimojima[116], J. D. Shinner[94], I. P. J. Shipsey[134], S. Shirabe[165], M. Shiyakova[80,x], J. Shlomi[180], A. Shmeleva[111], M. J. Shochet[37], J. Shojaii[105], D. R. Shope[154], S. Shrestha[127], E. M. Shrif[33f], M. J. Shroff[176], E. Shulga[180], P. Sicho[140], A. M. Sickles[173], E. Sideras Haddad[33f], O. Sidiropoulou[36], A. Sidoti[23a,23b], F. Siegert[48], Dj. Sijacki[16], M.Jr. Silva[181], M. V. Silva Oliveira[36], S. B. Silverstein[45a], S. Simion[65], R. Simoniello[100], C. J. Simpson-allsop[21], S. Simsek[12b], P. Sinervo[167], V. Sinetckii[113], S. Singh[152], M. Sioli[23a,23b], I. Siral[131], S. Yu. Sivoklokov[113], J. Sjölin[45a,45b], A. Skaf[53], E. Skorda[97], P. Skubic[128], M. Slawinska[85], K. Sliwa[170], V. Smakhtin[180], B. H. Smart[143], J. Smiesko[28b], N. Smirnov[112], S. Yu. Smirnov[112], Y. Smirnov[112], L. N. Smirnova[113,r], O. Smirnova[97], E. A. Smith[37], H. A. Smith[134], M. Smizanska[90], K. Smolek[141], A. Smykiewicz[85], A. A. Snesarev[111], H. L. Snoek[120], I. M. Snyder[131], S. Snyder[29], R. Sobie[176,z], A. Soffer[161], A. Søgaard[50], F. Sohns[53], C. A. Solans Sanchez[36], E. Yu. Soldatov[112], U. Soldevila[174], A. A. Solodkov[123], A. Soloshenko[80], O. V. Solovyanov[123], V. Solovyev[137], P. Sommer[149], H. Son[170], A. Sonay[14], W. Song[143], W. Y. Song[168b], A. Sopczak[141], A. L. Sopio[95], F. Sopkova[28b], S. Sottocornola[71a,71b], R. Soualah[67a,67c], A. M. Soukharev[122a,122b], D. South[46], S. Spagnolo[68a,68b], M. Spalla[115], M. Spangenberg[178], F. Spanò[94], D. Sperlich[52], T. M. Spieker[61a], G. Spigo[36], M. Spina[156], D. P. Spiteri[57], M. Spousta[142], A. Stabile[69a,69b], B. L. Stamas[121], R. Stamen[61a], M. Stamenkovic[120], A. Stampekis[21], E. Stanecka[85], B. Stanislaus[134], M. M. Stanitzki[46], M. Stankaityte[134], B. Stapf[120], E. A. Starchenko[123], G. H. Stark[145], J. Stark[58], P. Staroba[140], P. Starovoitov[61a], S. Stärz[104], R. Staszewski[85], G. Stavropoulos[44], M. Stegler[46], P. Steinberg[29], A. L. Steinhebel[131], B. Stelzer[152,168a], H. J. Stelzer[138], O. Stelzer-Chilton[168a], H. Stenzel[56], T. J. Stevenson[156], G. A. Stewart[36], M. C. Stockton[36], G. Stoicea[27b], M. Stolarski[139a], S. Stonjek[115], A. Straessner[48], J. Strandberg[154], S. Strandberg[45a,45b], M. Strauss[128], T. Strebler[102], P. Strizenec[28b], R. Ströhmer[177], D. M. Strom[131], R. Stroynowski[42], A. Strubig[45a,45b], S. A. Stucci[29], B. Stugu[17], J. Stupak[128], N. A. Styles[46], D. Su[153], W. Su[60d,148,60c], X. Su[60a], N. B. Suarez[138], V. V. Sulin[111], M. J. Sullivan[91], D. M. S. Sultan[54], S. Sultansoy[4c], T. Sumida[86], S. Sun[106], X. Sun[101], C. J. E. Suster[157], M. R. Sutton[156], S. Suzuki[82], M. Svatos[140], M. Swiatlowski[168a], S. P. Swift[2], T. Swirski[177], A. Sydorenko[100], I. Sykora[28a], M. Sykora[142], T. Sykora[142], D. Ta[100], K. Tackmann[46,w], J. Taenzer[161], A. Taffard[171], R. Tafirout[168a], E. Tagiev[123], R. H. M. Taibah[135], R. Takashima[87], K. Takeda[83], T. Takeshita[150],

E. P. Takeva[50], Y. Takubo[82], M. Talby[102], A. A. Talyshev[122a,122b], K. C. Tam[63b], N. M. Tamir[161], J. Tanaka[163],
R. Tanaka[65], S. Tapia Araya[173], S. Tapprogge[100], A. Tarek Abouelfadl Mohamed[107], S. Tarem[160],
K. Tariq[60b], G. Tarna[27b,d], G. F. Tartarelli[69a], P. Tas[142], M. Tasevsky[140], E. Tassi[41a,41b], G. Tateno[163],
A. Tavares Delgado[139a], Y. Tayalati[35e], A. J. Taylor[50], G. N. Taylor[105], W. Taylor[168b], H. Teagle[91], A. S. Tee[90],
R. Teixeira De Lima[153], P. Teixeira-Dias[94], H. Ten Kate[36], J. J. Teoh[120], K. Terashi[163], J. Terron[99],
S. Terzo[14], M. Testa[51], R. J. Teuscher[167,z], S. J. Thais[183], N. Themistokleous[50], T. Theveneaux-Pelzer[19],
D. W. Thomas[94], J. P. Thomas[21], E. A. Thompson[46], P. D. Thompson[21], E. Thomson[136], E. J. Thorpe[93],
V. O. Tikhomirov[111,af], Yu. A. Tikhonov[122a,122b], S. Timoshenko[112], P. Tipton[183], S. Tisserant[102],
K. Todome[23a,23b], S. Todorova-Nova[142], S. Todt[48], J. Tojo[88], S. Tokár[28a], K. Tokushuku[82], E. Tolley[127],
R. Tombs[32], K. G. Tomiwa[33f], M. Tomoto[82,117], L. Tompkins[153], P. Tornambe[103], E. Torrence[131],
H. Torres[48], E. Torró Pastor[174], M. Toscani[30], C. Tosciri[134], J. Toth[102,y], D. R. Tovey[149], A. Traeet[17],
C. J. Treado[125], T. Trefzger[177], F. Tresoldi[156], A. Tricoli[29], I. M. Trigger[168a], S. Trincaz-Duvoid[135],
D. A. Trischuk[175], W. Trischuk[167], B. Trocmé[58], A. Trofymov[65], C. Troncon[69a], F. Trovato[156], L. Truong[33c],
M. Trzebinski[85], A. Trzupek[85], F. Tsai[46], J. C.-L. Tseng[134], P. V. Tsiareshka[108,ad], A. Tsirigotis[162,u],
V. Tsiskaridze[155], E. G. Tskhadadze[159a], M. Tsopoulou[162], I. I. Tsukerman[124], V. Tsulaia[18], S. Tsuno[82],
D. Tsybychev[155], Y. Tu[63b], A. Tudorache[27b], V. Tudorache[27b], A. N. Tuna[36], S. Turchikhin[80],
D. Turgeman[180], I. Turk Cakir[4b,s], R. J. Turner[21], R. Turra[69a], P. M. Tuts[39], S. Tzamarias[162], E. Tzovara[100],
K. Uchida[163], F. Ukegawa[169], G. Unal[36], M. Unal[11], A. Undrus[29], G. Unel[171], F. C. Ungaro[105],
Y. Unno[82], K. Uno[163], J. Urban[28b], P. Urquijo[105], G. Usai[8], Z. Uysal[12d], V. Vacek[141], B. Vachon[104],
K. O. H. Vadla[133], T. Vafeiadis[36], A. Vaidya[95], C. Valderanis[114], E. Valdes Santurio[45a,45b], M. Valente[168a],
S. Valentinetti[23a,23b], A. Valero[174], L. Valéry[46], R. A. Vallance[21], A. Vallier[36], J. A. Valls Ferrer[174],
T. R. Van Daalen[14], P. Van Gemmeren[6], S. Van Stroud[95], I. Van Vulpen[120], M. Vanadia[74a,74b], W. Vandelli[36],
M. Vandenbroucke[144], E. R. Vandewall[129], D. Vannicola[73a,73b], R. Vari[73a], E. W. Varnes[7], C. Varni[55a,55b],
T. Varol[158], D. Varouchas[65], K. E. Varvell[157], M. E. Vasile[27b], G. A. Vasquez[176], F. Vazeille[38],
D. Vazquez Furelos[14], T. Vazquez Schroeder[36], J. Veatch[53], V. Vecchio[101], M. J. Veen[120], L. M. Veloce[167],
F. Veloso[139a,139c], S. Veneziano[73a], A. Ventura[68a,68b], A. Verbytskyi[115], V. Vercesi[71a], M. Verducci[72a,72b],
C. M. Vergel Infante[79], C. Vergis[24], W. Verkerke[120], A. T. Vermeulen[120], J. C. Vermeulen[120], C. Vernieri[153],
P. J. Verschuuren[94], M. C. Vetterli[152,aj], N. Viaux Maira[146d], T. Vickey[149], O. E. Vickey Boeriu[149],
G. H. A. Viehhauser[134], L. Vigani[61b], M. Villa[23a,23b], M. Villaplana Perez[174], E. M. Villhauer[50], E. Vilucchi[51],
M. G. Vincter[34], G. S. Virdee[21], A. Vishwakarma[50], C. Vittori[23a,23b], I. Vivarelli[156], M. Vogel[182],
P. Vokac[141], J. Von Ahnen[46], S. E. von Buddenbrock[33f], E. Von Toerne[24], V. Vorobel[142], K. Vorobev[112],
M. Vos[174], J. H. Vossebeld[91], M. Vozak[101], N. Vranjes[16], M. Vranjes Milosavljevic[16], V. Vrba[141,*],
M. Vreeswijk[120], N. K. Vu[102], R. Vuillermet[36], I. Vukotic[37], S. Wada[169], P. Wagner[24], W. Wagner[182],
J. Wagner-Kuhr[114], S. Wahdan[182], H. Wahlberg[89], R. Wakasa[169], V. M. Walbrecht[115], J. Walder[143],
R. Walker[114], S. D. Walker[94], W. Walkowiak[151], V. Wallangen[45a,45b], A. M. Wang[59], A. Z. Tang[181],
C. Wang[60a], C. Wang[60c], H. Wang[18], H. Wang[3], J. Wang[63a], P. Wang[42], Q. Wang[128], R.-J. Wang[100],
R. Wang[60a], R. Wang[6], S. M. Wang[158], W. T. Wang[60a], W. Wang[15c], W. X. Wang[60a], Y. Wang[60a],
Z. Wang[106], C. Wanotayaroj[46], A. Warburton[104], C. P. Ward[32], R. J. Ward[21], N. Warrack[57], A. T. Watson[21],
M. F. Watson[21], G. Watts[148], B. M. Waugh[95], A. F. Webb[11], C. Weber[29], M. S. Weber[20], S. A. Weber[34],
S. M. Weber[61a], Y. Wei[134], A. R. Weidberg[134], J. Weingarten[47], M. Weirich[100], C. Weiser[52],
P. S. Wells[36], T. Wenaus[29], B. Wendland[47], T. Wengler[36], S. Wenig[36], N. Wermes[24], M. Wessels[61a],
T. D. Weston[20], K. Whalen[131], A. M. Wharton[90], A. S. White[106], A. White[8], M. J. White[1], D. Whiteson[171],
B. W. Whitmore[90], W. Wiedenmann[181], C. Wiel[48], M. Wielers[143], N. Wieseotte[100], C. Wiglesworth[40],
L. A. M. Wiik-Fuchs[52], H. G. Wilkens[36], L. J. Wilkins[94], D. M. Williams[39], H. H. Williams[136], S. Williams[32],
S. Willocq[103], P. J. Windischhofer[134], I. Wingerter-Seez[5], E. Winkels[156], F. Winklmeier[131], B. T. Winter[52],
M. Wittgen[153], M. Wobisch[96], A. Wolf[100], R. Wölker[134], J. Wollrath[52], M. W. Wolter[85], H. Wolters[139a,139c],
V. W. S. Wong[175], A. F. Wongel[46], N. L. Woods[145], S. D. Worm[46], B. K. Wosiek[85], K. W. Woźniak[85],
K. Wraight[57], S. L. Wu[181], X. Wu[54], Y. Wu[60a], J. Wuerzinger[134], T. R. Wyatt[101], B. M. Wynne[50],
S. Xella[40], J. Xiang[63c], X. Xiao[106], X. Xie[60a], I. Xiotidis[156], D. Xu[15a], H. Xu[60a], H. Xu[60a], L. Xu[29],
R. Xu[136], T. Xu[144], W. Xu[106], Y. Xu[15b], Z. Xu[60b], Z. Xu[153], B. Yabsley[157], S. Yacoob[33a], D. P. Yallup[95],
N. Yamaguchi[88], Y. Yamaguchi[165], A. Yamamoto[82], M. Yamatani[163], T. Yamazaki[163], Y. Yamazaki[83],
J. Yan[60c], Z. Yan[25], H. J. Yang[60c,60d], H. T. Yang[18], S. Yang[60a], T. Yang[63c], X. Yang[60a], X. Yang[58,60b],
Y. Yang[163], Z. Yang[60a,106], W-M. Yao[18], Y. C. Yap[46], H. Ye[15c], J. Ye[42], S. Ye[29], I. Yeletskikh[80],

M. R. Yexley[90], E. Yigitbasi[25], P. Yin[39], K. Yorita[179], K. Yoshihara[79], C. J. S. Young[36], C. Young[153], J. Yu[79], R. Yuan[60b,h], X. Yue[61a], M. Zaazoua[35e], B. Zabinski[85], G. Zacharis[10], E. Zaffaroni[54], J. Zahreddine[135], A. M. Zaitsev[123,ae], T. Zakareishvili[159b], N. Zakharchuk[34], S. Zambito[36], D. Zanzi[36], S. V. Zeißner[47], C. Zeitnitz[182], G. Zemaityte[134], J. C. Zeng[173], O. Zenin[123], T. Ženiš[28a], D. Zerwas[65], M. Zgubič[134], B. Zhang[15c], D. F. Zhang[15b], G. Zhang[15b], J. Zhang[6], K. Zhang[15a], L. Zhang[15c], L. Zhang[60a], M. Zhang[173], R. Zhang[181], S. Zhang[106], X. Zhang[60c], X. Zhang[60b], Y. Zhang[15a,15d], Z. Zhang[63a], Z. Zhang[65], P. Zhao[49], Y. Zhao[145], Z. Zhao[60a], A. Zhemchugov[80], Z. Zheng[106], D. Zhong[173], B. Zhou[106], C. Zhou[181], H. Zhou[7], M. Zhou[155], N. Zhou[60c], Y. Zhou[7], C. G. Zhu[60b], C. Zhu[15a,15d], H. L. Zhu[60a], H. Zhu[15a], J. Zhu[106], Y. Zhu[60a], X. Zhuang[15a], K. Zhukov[111], V. Zhulanov[122a,122b], D. Zieminska[66], N. I. Zimine[80], S. Zimmermann[52,*], Z. Zinonos[115], M. Ziolkowski[151], L. Živković[16], G. Zobernig[181], A. Zoccoli[23a,23b], K. Zoch[53], T. G. Zorbas[149], R. Zou[37], L. Zwalinski[36]

1 Department of Physics, University of Adelaide, Adelaide, Australia

2 Physics Department, SUNY Albany, Albany, NY, USA

3 Department of Physics, University of Alberta, Edmonton, AB, Canada

4 (a)Department of Physics, Ankara University, Ankara, Turkey; (b)Application and Research Center for Advanced Studies, Istanbul Aydin University, Istanbul, Turkey; (c)Division of Physics, TOBB University of Economics and Technology, Ankara, Turkey

5 LAPP, Univ. Savoie Mont Blanc, CNRS/IN2P3, Annecy , France

6 High Energy Physics Division, Argonne National Laboratory, Argonne, IL, USA

7 Department of Physics, University of Arizona, Tucson, AZ, USA

8 Department of Physics, University of Texas at Arlington, Arlington, TX, USA

9 Physics Department, National and Kapodistrian University of Athens, Athens, Greece

10 Physics Department, National Technical University of Athens, Zografou, Greece

11 Department of Physics, University of Texas at Austin, Austin, TX, USA

12 (a)Faculty of Engineering and Natural Sciences, Bahcesehir University, Istanbul, Turkey; (b)Faculty of Engineering and Natural Sciences, Istanbul Bilgi University, Istanbul, Turkey; (c)Department of Physics, Bogazici University, Istanbul, Turkey; (d)Department of Physics Engineering, Gaziantep University, Gaziantep, Turkey

13 Institute of Physics, Azerbaijan Academy of Sciences, Baku, Azerbaijan

14 Institut de Física d'Altes Energies (IFAE), Barcelona Institute of Science and Technology, Barcelona, Spain

15 (a)Institute of High Energy Physics, Chinese Academy of Sciences, Beijing, China; (b)Physics Department, Tsinghua University, Beijing, China; (c)Department of Physics, Nanjing University, Nanjing, China; (d)University of Chinese Academy of Science (UCAS), Beijing, China

16 Institute of Physics, University of Belgrade, Belgrade, Serbia

17 Department for Physics and Technology, University of Bergen, Bergen, Norway

18 Physics Division, Lawrence Berkeley National Laboratory and University of California, Berkeley, CA, USA

19 Institut für Physik, Humboldt Universität zu Berlin, Berlin, Germany

20 Albert Einstein Center for Fundamental Physics and Laboratory for High Energy Physics, University of Bern, Bern, Switzerland

21 School of Physics and Astronomy, University of Birmingham, Birmingham, UK

22 (a)Facultad de Ciencias y Centro de Investigaciónes, Universidad Antonio Nariño, Bogotá, Colombia; (b)Departamento de Física, Universidad Nacional de Colombia, Bogotá, Colombia

23 (a)Dipartimento di Fisica, INFN Bologna and Universita' di Bologna, Bologna, Italy; (b)INFN Sezione di Bologna, Bologna, Italy

24 Physikalisches Institut, Universität Bonn, Bonn, Germany

25 Department of Physics, Boston University, Boston, MA, USA

26 Department of Physics, Brandeis University, Waltham, MA, USA

27 (a)Transilvania University of Brasov, Brasov, Romania; (b)Horia Hulubei National Institute of Physics and Nuclear Engineering, Bucharest, Romania; (c)Department of Physics, Alexandru Ioan Cuza University of Iasi, Iasi, Romania; (d)Physics Department, National Institute for Research and Development of Isotopic and Molecular Technologies, Cluj-Napoca, Romania; (e)University Politehnica Bucharest, Bucharest, Romania; (f)West University in Timisoara, Timisoara, Romania

28 (a)Faculty of Mathematics, Physics and Informatics, Comenius University, Bratislava, Slovakia; (b)Department of Subnuclear Physics, Institute of Experimental Physics of the Slovak Academy of Sciences, Kosice, Slovak Republic

29 Physics Department, Brookhaven National Laboratory, Upton, NY, USA

30 Departamento de Física, Universidad de Buenos Aires, Buenos Aires, Argentina

31 California State University, Long Beach, CA, USA

32 Cavendish Laboratory, University of Cambridge, Cambridge, UK

33 (a)Department of Physics, University of Cape Town, Cape Town, South Africa; (b)iThemba Labs, Western Cape, Cape Town, South Africa; (c)Department of Mechanical Engineering Science, University of Johannesburg, Johannesburg, South Africa; (d)National Institute of Physics, University of the Philippines Diliman, Quezon City, Philippines; (e)Department of Physics, University of South Africa, Pretoria, South Africa; (f)School of Physics, University of the Witwatersrand, Johannesburg, South Africa

34 Department of Physics, Carleton University, Ottawa, ON, Canada

35 (a)Faculté des Sciences Ain Chock, Réseau Universitaire de Physique des Hautes Energies-Université Hassan II, Casablanca, Morocco; (b)Faculté des Sciences, Université Ibn-Tofail, Kenitra, Morocco; (c)Faculté des Sciences Semlalia, Université Cadi Ayyad, LPHEA-Marrakech, Marrakech, Morocco; (d)LPMR, Faculté des Sciences, Université Mohamed Premier, Oujda, Morocco; (e)Faculté des sciences, Université Mohammed V, Rabat, Morocco

36 CERN, Geneva, Switzerland

37 Enrico Fermi Institute, University of Chicago, Chicago, IL, USA

38 LPC, Université Clermont Auvergne, CNRS/IN2P3, Clermont-Ferrand, France

39 Nevis Laboratory, Columbia University, Irvington, NY, USA

40 Niels Bohr Institute, University of Copenhagen, Copenhagen, Denmark

41 (a)Dipartimento di Fisica, Università della Calabria, Rende, Italy; (b)INFN Gruppo Collegato di Cosenza, Laboratori Nazionali di Frascati, Frascati, Italy

42 Physics Department, Southern Methodist University, Dallas, TX, USA

43 Physics Department, University of Texas at Dallas, Richardson, TX, USA

44 National Centre for Scientific Research "Demokritos", Agia Paraskevi, Greece

45 (a)Department of Physics, Stockholm University, Stockholm, Sweden; (b)Oskar Klein Centre, Stockholm, Sweden

46 Deutsches Elektronen-Synchrotron DESY, Hamburg and Zeuthen, Germany

47 Lehrstuhl für Experimentelle Physik IV, Technische Universität Dortmund, Dortmund, Germany

48 Institut für Kern- und Teilchenphysik, Technische Universität Dresden, Dresden, Germany

49 Department of Physics, Duke University, Durham, NC, USA

50 SUPA-School of Physics and Astronomy, University of Edinburgh, Edinburgh, UK

51 INFN e Laboratori Nazionali di Frascati, Frascati, Italy

52 Physikalisches Institut, Albert-Ludwigs-Universität Freiburg, Freiburg, Germany

53 II. Physikalisches Institut, Georg-August-Universität Göttingen, Göttingen, Germany

54 Département de Physique Nucléaire et Corpusculaire, Université de Genève, Geneve, Switzerland

55 (a)Dipartimento di Fisica, Università di Genova, Genoa, Italy; (b)INFN Sezione di Genova, Genoa, Italy

56 II. Physikalisches Institut, Justus-Liebig-Universität Giessen, Giessen, Germany

57 SUPA-School of Physics and Astronomy, University of Glasgow, Glasgow, UK

58 LPSC, Université Grenoble Alpes, CNRS/IN2P3, Grenoble INP, Grenoble, France

59 Laboratory for Particle Physics and Cosmology, Harvard University, Cambridge, MA, USA

60 (a)Department of Modern Physics and State Key Laboratory of Particle Detection and Electronics, University of Science and Technology of China, Hefei, China; (b)Institute of Frontier and Interdisciplinary Science and Key Laboratory of Particle Physics and Particle Irradiation (MOE), Shandong University, Qingdao, China; (c)School of Physics and Astronomy, Shanghai Jiao Tong University, Key Laboratory for Particle Astrophysics and Cosmology (MOE), SKLPPC, Shanghai, China; (d)Tsung-Dao Lee Institute, Shanghai, China

61 (a)Kirchhoff-Institut für Physik, Ruprecht-Karls-Universität Heidelberg, Heidelberg, Germany; (b)Physikalisches Institut, Ruprecht-Karls-Universität Heidelberg, Heidelberg, Germany

62 Faculty of Applied Information Science, Hiroshima Institute of Technology, Hiroshima, Japan

63 (a)Department of Physics, Chinese University of Hong Kong, Hong Kong, Shatin, NT, China; (b)Department of Physics, University of Hong Kong, Hong Kong, China; (c)Department of Physics and Institute for Advanced Study, Hong Kong University of Science and Technology, Clear Water Bay, Kowloon, Hong Kong, China

64 Department of Physics, National Tsing Hua University, Hsinchu, Taiwan

65 IJCLab, Université Paris-Saclay, CNRS/IN2P3, 91405 Orsay, France

66 Department of Physics, Indiana University, Bloomington, IN, USA

67 (a)INFN Gruppo Collegato di Udine, Sezione di Trieste, Udine, Italy; (b)ICTP, Trieste, Italy; (c)Dipartimento Politecnico di Ingegneria e Architettura, Università di Udine, Udine, Italy

68 (a)INFN Sezione di Lecce, Lecce, Italy; (b)Dipartimento di Matematica e Fisica, Università del Salento, Lecce, Italy

69 (a)INFN Sezione di Milano, Milan, Italy; (b)Dipartimento di Fisica, Università di Milano, Milan, Italy

70 (a)INFN Sezione di Napoli, Naples, Italy; (b)Dipartimento di Fisica, Università di Napoli, Naples, Italy

71 (a)INFN Sezione di Pavia, Pavia, Italy; (b)Dipartimento di Fisica, Università di Pavia, Pavia, Italy

72 (a)INFN Sezione di Pisa, Pisa, Italy; (b)Dipartimento di Fisica E. Fermi, Università di Pisa, Pisa, Italy

73 (a)INFN Sezione di Roma, Rome, Italy; (b)Dipartimento di Fisica, Sapienza Università di Roma, Rome, Italy

74 (a)INFN Sezione di Roma Tor Vergata, Rome, Italy; (b)Dipartimento di Fisica, Università di Roma Tor Vergata, Rome, Italy

75 (a)INFN Sezione di Roma Tre, Rome, Italy; (b)Dipartimento di Matematica e Fisica, Università Roma Tre, Rome, Italy

76 (a)INFN-TIFPA, Trento, Italy; (b)Università degli Studi di Trento, Trento, Italy

77 Institut für Astro- und Teilchenphysik, Leopold-Franzens-Universität, Innsbruck, Austria

78 University of Iowa, Iowa City, IA, USA

79 Department of Physics and Astronomy, Iowa State University, Ames, IA, USA

80 Joint Institute for Nuclear Research, Dubna, Russia

81 (a)Departamento de Engenharia Elétrica, Universidade Federal de Juiz de Fora (UFJF), Juiz de Fora, Brazil; (b)Universidade Federal do Rio De Janeiro COPPE/EE/IF, Rio de Janeiro, Brazil; (c)Instituto de Física, Universidade de São Paulo, São Paulo, Brazil

82 KEK, High Energy Accelerator Research Organization, Tsukuba, Japan

83 Graduate School of Science, Kobe University, Kobe, Japan

84 (a)Faculty of Physics and Applied Computer Science, AGH University of Science and Technology, Kraków, Poland; (b)Marian Smoluchowski Institute of Physics, Jagiellonian University, Kraków, Poland

85 Institute of Nuclear Physics Polish Academy of Sciences, Kraków, Poland

86 Faculty of Science, Kyoto University, Kyoto, Japan

87 Kyoto University of Education, Kyoto, Japan

88 Research Center for Advanced Particle Physics and Department of Physics, Kyushu University, Fukuoka , Japan

89 Instituto de Física La Plata, Universidad Nacional de La Plata and CONICET, La Plata, Argentina

90 Physics Department, Lancaster University, Lancaster, UK

91 Oliver Lodge Laboratory, University of Liverpool, Liverpool, UK

92 Department of Experimental Particle Physics, Jožef Stefan Institute and Department of Physics, University of Ljubljana, Ljubljana, Slovenia

93 School of Physics and Astronomy, Queen Mary University of London, London, UK

94 Department of Physics, Royal Holloway University of London, Egham, UK

95 Department of Physics and Astronomy, University College London, London, UK

96 Louisiana Tech University, Ruston, LA, USA

97 Fysiska institutionen, Lunds universitet, Lund, Sweden

98 Centre de Calcul de l'Institut National de Physique Nucléaire et de Physique des Particules (IN2P3), Villeurbanne, France

99 Departamento de Física Teorica C-15 and CIAFF, Universidad Autónoma de Madrid, Madrid, Spain

100 Institut für Physik, Universität Mainz, Mainz, Germany

101 School of Physics and Astronomy, University of Manchester, Manchester, UK

102 CPPM, Aix-Marseille Université, CNRS/IN2P3, Marseille, France

103 Department of Physics, University of Massachusetts, Amherst, MA, USA

104 Department of Physics, McGill University, Montreal, QC, Canada

105 School of Physics, University of Melbourne, Victoria, Australia

106 Department of Physics, University of Michigan, Ann Arbor, MI, USA

107 Department of Physics and Astronomy, Michigan State University, East Lansing, MI, USA

108 B.I. Stepanov Institute of Physics, National Academy of Sciences of Belarus, Minsk, Belarus

109 Research Institute for Nuclear Problems of Byelorussian State University, Minsk, Belarus

110 Group of Particle Physics, University of Montreal, Montreal, QC, Canada

[111] P.N. Lebedev Physical Institute of the Russian Academy of Sciences, Moscow, Russia

[112] National Research Nuclear University MEPhI, Moscow, Russia

[113] D.V. Skobeltsyn Institute of Nuclear Physics, M.V. Lomonosov Moscow State University, Moscow, Russia

[114] Fakultät für Physik, Ludwig-Maximilians-Universität München, Munich, Germany

[115] Max-Planck-Institut für Physik (Werner-Heisenberg-Institut), Munich, Germany

[116] Nagasaki Institute of Applied Science, Nagasaki, Japan

[117] Graduate School of Science and Kobayashi-Maskawa Institute, Nagoya University, Nagoya, Japan

[118] Department of Physics and Astronomy, University of New Mexico, Albuquerque, NM, USA

[119] Institute for Mathematics, Astrophysics and Particle Physics, Radboud University/Nikhef, Nijmegen, The Netherlands

[120] Nikhef National Institute for Subatomic Physics and University of Amsterdam, Amsterdam, The Netherlands

[121] Department of Physics, Northern Illinois University, DeKalb, IL, USA

[122] [a]Budker Institute of Nuclear Physics and NSU, SB RAS, Novosibirsk, Russia; [b]Novosibirsk State University Novosibirsk, Novosibirsk, Russia

[123] Institute for High Energy Physics of the National Research Centre Kurchatov Institute, Protvino, Russia

[124] Institute for Theoretical and Experimental Physics named by A.I. Alikhanov of National Research Centre "Kurchatov Institute", Moscow, Russia

[125] Department of Physics, New York University, New York, NY, USA

[126] Ochanomizu University, Otsuka, Bunkyo-ku, Tokyo, Japan

[127] Ohio State University, Columbus, OH, USA

[128] Homer L. Dodge Department of Physics and Astronomy, University of Oklahoma, Norman, OK, USA

[129] Department of Physics, Oklahoma State University, Stillwater, OK, USA

[130] Palacký University, Joint Laboratory of Optics, Olomouc, Czech Republic

[131] Institute for Fundamental Science, University of Oregon, Eugene, OR, USA

[132] Graduate School of Science, Osaka University, Osaka, Japan

[133] Department of Physics, University of Oslo, Oslo, Norway

[134] Department of Physics, Oxford University, Oxford, UK

[135] LPNHE, Sorbonne Université, Université de Paris, CNRS/IN2P3, Paris, France

[136] Department of Physics, University of Pennsylvania, Philadelphia, PA, USA

[137] Konstantinov Nuclear Physics Institute of National Research Centre "Kurchatov Institute", PNPI, St. Petersburg, Russia

[138] Department of Physics and Astronomy, University of Pittsburgh, Pittsburgh, PA, USA

[139] [a]Laboratório de Instrumentação e Física Experimental de Partículas-LIP, Lisbon, Portugal; [b]Departamento de Física, Faculdade de Ciências, Universidade de Lisboa, Lisbon, Portugal; [c]Departamento de Física, Universidade de Coimbra, Coimbra, Portugal; [d]Centro de Física Nuclear da Universidade de Lisboa, Lisbon, Portugal; [e]Departamento de Física, Universidade do Minho, Braga, Portugal; [f]Departamento de Física Teórica y del Cosmos, Universidad de Granada, Granada, Spain; [g]Dep Física and CEFITEC of Faculdade de Ciências e Tecnologia, Universidade Nova de Lisboa, Caparica, Portugal; [h]Instituto Superior Técnico, Universidade de Lisboa, Lisbon, Portugal

[140] Institute of Physics of the Czech Academy of Sciences, Prague, Czech Republic

[141] Czech Technical University in Prague, Prague, Czech Republic

[142] Charles University, Faculty of Mathematics and Physics, Prague, Czech Republic

[143] Particle Physics Department, Rutherford Appleton Laboratory, Didcot, UK

[144] IRFU, CEA, Université Paris-Saclay, Gif-sur-Yvette, France

[145] Santa Cruz Institute for Particle Physics, University of California Santa Cruz, Santa Cruz, CA, USA

[146] [a]Departamento de Física, Pontificia Universidad Católica de Chile, Santiago, Chile; [b]Universidad Andres Bello, Department of Physics, Santiago, Chile; [c]Instituto de Alta Investigación, Universidad de Tarapacá, Arica, Chile; [d]Departamento de Física, Universidad Técnica Federico Santa María, Valparaiso, Chile

[147] Universidade Federal de São João del Rei (UFSJ), São João del Rei, Brazil

[148] Department of Physics, University of Washington, Seattle, WA, USA

[149] Department of Physics and Astronomy, University of Sheffield, Sheffield, UK

[150] Department of Physics, Shinshu University, Nagano, Japan

[151] Department Physik, Universität Siegen, Siegen, Germany

[152] Department of Physics, Simon Fraser University, Burnaby, BC, Canada

[153] SLAC National Accelerator Laboratory, Stanford, CA, USA

[154] Department of Physics, Royal Institute of Technology, Stockholm, Sweden

[155] Departments of Physics and Astronomy, Stony Brook University, Stony Brook, NY, USA

[156] Department of Physics and Astronomy, University of Sussex, Brighton, UK

[157] School of Physics, University of Sydney, Sydney, Australia

[158] Institute of Physics, Academia Sinica, Taipei, Taiwan

[159] (a)E. Andronikashvili Institute of Physics, Iv. Javakhishvili Tbilisi State University, Tbilisi, Georgia; (b)High Energy Physics Institute, Tbilisi State University, Tbilisi, Georgia

[160] Department of Physics, Technion, Israel Institute of Technology, Haifa, Israel

[161] Raymond and Beverly Sackler School of Physics and Astronomy, Tel Aviv University, Tel Aviv, Israel

[162] Department of Physics, Aristotle University of Thessaloniki, Thessaloniki, Greece

[163] International Center for Elementary Particle Physics and Department of Physics, University of Tokyo, Tokyo, Japan

[164] Graduate School of Science and Technology, Tokyo Metropolitan University, Tokyo, Japan

[165] Department of Physics, Tokyo Institute of Technology, Tokyo, Japan

[166] Tomsk State University, Tomsk, Russia

[167] Department of Physics, University of Toronto, Toronto, ON, Canada

[168] (a)TRIUMF, Vancouver, BC, Canada; (b)Department of Physics and Astronomy, York University, Toronto, ON, Canada

[169] Division of Physics and Tomonaga Center for the History of the Universe, Faculty of Pure and Applied Sciences, University of Tsukuba, Tsukuba, Japan

[170] Department of Physics and Astronomy, Tufts University, Medford, MA, USA

[171] Department of Physics and Astronomy, University of California Irvine, Irvine, CA, USA

[172] Department of Physics and Astronomy, University of Uppsala, Uppsala, Sweden

[173] Department of Physics, University of Illinois, Urbana, IL, USA

[174] Instituto de Física Corpuscular (IFIC), Centro Mixto Universidad de Valencia-CSIC, Valencia, Spain

[175] Department of Physics, University of British Columbia, Vancouver, BC, Canada

[176] Department of Physics and Astronomy, University of Victoria, Victoria, BC, Canada

[177] Fakultät für Physik und Astronomie, Julius-Maximilians-Universität Würzburg, Würzburg, Germany

[178] Department of Physics, University of Warwick, Coventry, UK

[179] Waseda University, Tokyo, Japan

[180] Department of Particle Physics and Astrophysics, Weizmann Institute of Science, Rehovot, Israel

[181] Department of Physics, University of Wisconsin, Madison, WI, USA

[182] Fakultät für Mathematik und Naturwissenschaften, Fachgruppe Physik, Bergische Universität Wuppertal, Wuppertal, Germany

[183] Department of Physics, Yale University, New Haven, CT, USA

[a] Also at Borough of Manhattan Community College, City University of New York, New York, NY, USA

[b] Also at Centro Studi e Ricerche Enrico Fermi, Rome, Italy

[c] Also at CERN, Geneva, Switzerland

[d] Also at CPPM, Aix-Marseille Université, CNRS/IN2P3, Marseille, France

[e] Also at Département de Physique Nucléaire et Corpusculaire, Université de Genève, Geneve, Switzerland

[f] Also at Departament de Fisica de la Universitat Autonoma de Barcelona, Barcelona, Spain

[g] Also at Department of Financial and Management Engineering, University of the Aegean, Chios, Greece

[h] Also at Department of Physics and Astronomy, Michigan State University, East Lansing, MI, USA

[i] Also at Department of Physics and Astronomy, University of Louisville, Louisville, KY, USA

[j] Also at Department of Physics, Ben Gurion University of the Negev, Beer Sheva, Israel

[k] Also at Department of Physics, California State University, East Bay, USA

[l] Also at Department of Physics, California State University, Fresno, USA

[m] Also at Department of Physics, California State University, Sacramento, USA

[n] Also at Department of Physics, King's College London, London, UK

[o] Also at Department of Physics, St. Petersburg State Polytechnical University, St. Petersburg, Russia

[p] Also at Department of Physics, University of Fribourg, Fribourg, Switzerland

[q] Also at Dipartimento di Matematica, Informatica e Fisica, Università di Udine, Udine, Italy

[r] Also at Faculty of Physics, M.V. Lomonosov Moscow State University, Moscow, Russia

[s] Also at Giresun University, Faculty of Engineering, Giresun, Turkey

[t] Also at Graduate School of Science, Osaka University, Osaka, Japan

[u] Also at Hellenic Open University, Patras, Greece

[v] Also at Institucio Catalana de Recerca i Estudis Avancats, ICREA, Barcelona, Spain

[w] Also at Institut für Experimentalphysik, Universität Hamburg, Hamburg, Germany

[x] Also at Institute for Nuclear Research and Nuclear Energy (INRNE) of the Bulgarian Academy of Sciences, Sofia, Bulgaria

[y] Also at Institute for Particle and Nuclear Physics, Wigner Research Centre for Physics, Budapest, Hungary

[z] Also at Institute of Particle Physics (IPP), Ottawa, Canada

[aa] Also at Institute of Physics, Azerbaijan Academy of Sciences, Baku, Azerbaijan

[ab] Also at Instituto de Fisica Teorica, IFT-UAM/CSIC, Madrid, Spain

[ac] Also at Department of Physics, Istanbul University, Istanbul, Turkey

[ad] Also at Joint Institute for Nuclear Research, Dubna, Russia

[ae] Also at Moscow Institute of Physics and Technology State University, Dolgoprudny, Russia

[af] Also at National Research Nuclear University MEPhI, Moscow, Russia

[ag] Also at Physics Department, An-Najah National University, Nablus, Palestine

[ah] Also at Physikalisches Institut, Albert-Ludwigs-Universität Freiburg, Freiburg, Germany

[ai] Also at The City College of New York, New York, NY, USA

[aj] Also at TRIUMF, Vancouver, BC, Canada

[ak] Also at Universita di Napoli Parthenope, Naples, Italy

[al] Also at University of Chinese Academy of Sciences (UCAS), Beijing, China

[*] Deceased